

Nordic Master Programme in Innovative and Sustainable Energy Engineering

Experimental Assessment of the Thermal Performance of Two Different Photovoltaic/Thermal Collectors

Ellen Louise Nicholson

© 2025

This work is licensed under a [Creative Commons](https://creativecommons.org/licenses/by-nc-sa/4.0/) “Attribution-NonCommercial-ShareAlike 4.0 International” license.



Author Ellen Louise Nicholson

Title Experimental Assessment of the Thermal Performance of Two Different Photovoltaic/Thermal Collectors

Degree programme Nordic Master Programme in Innovative and Sustainable Energy Engineering

Major Energy Systems

Supervisor Prof. Olli Himanen

Advisor Mr. Francisco Beltran (MSc)

Date 4 June 2024

Number of pages 79+6

Language English

Abstract

In Nordic countries, interest is growing in the use of photovoltaic/thermal (PVT) collectors as sources for borehole regeneration in ground source heat pump systems. A PVT collector is a combination of a photovoltaic (PV) panel and a solar thermal collector (STC), allowing for the simultaneous generation of electricity and heat as the STC cools the PV. By setting the temperature of the working fluid under the ambient temperature, heat gains can also be observed at times of no irradiance, improving the thermal performance (TP) of the system. To optimise heat exchange between the working fluid and the ambient, fins are added to the back of the PVT absorber to increase the heat exchange surface area.

This study compares the TP of two prototype box-channel PVT collectors, assessing the impact of fins in low temperature operating conditions. The two PVT collectors are tested simultaneously at an outdoor testing facility at KTH Royal Institute of Technology in Stockholm, Sweden. The outdoor environment allows for the analysis of a variety of weather conditions, such as solar irradiance, wind speed and wind direction. The impact of different working fluid flow rates and roof installations on the TP are also evaluated. Quantifying the impacts of these different conditions will show whether an increase in TP due to the fins justifies their additional cost. To obtain thermal performance coefficients, the equation for modelled thermal power of a STC presented in ISO 9806:2017 is simplified. These coefficients serve as key performance indicators to compare the TP of the two PVTs under the conditions studied.

The results show that increasing irradiance and wind speeds improve the TP of the PVTs. However, it was observed that the same increase in either irradiance or wind speed does not result in the same improvement in specific thermal power under all operating conditions. An optimum flow rate of 0.021 kg/s/m^2 was identified. Additionally, it was found that fins do improve the TP of the PVT collectors. Improvements in specific thermal power, when compared to the PVT with no fins, as large as 16% were observed, at a flow rate of 0.028 kg/s/m^2 . When the airflow around the PVTs was restricted, through the addition of roof installations, the improvement in specific thermal power dropped to 6 or 7% depending on the roof installation.

Keywords Photovoltaic-thermal Collector, Heat Pump, Thermal Performance, Fins, Experimental Analysis, Cold Climate

Acknowledgements

I would like to sincerely thank Francisco Beltran for the day-to-day supervision of the thesis project and all the guidance provided throughout. I would like to thank Olli Himanen for his helpful input at the start of the thesis project, ensuring that I had a clear structure to follow for the remained of the project. I would also like to thank Valentin Delachaux and Mohamad Ali Jaafar for their support and interest throughout the thesis project. Finally, I would like to thank Alonso Conejos for his help conducting the experimental assessment of the two PVT collector prototypes.

Stockholm, 4 June 2024

Ellen L. Nicholson

Contents

Abstract	3
Acknowledgements	4
Contents	5
Abbreviations	8
List of Figures	12
List of Tables	14
1 Introduction	15
1.1 Objectives and Research Questions	16
1.2 Scope	17
1.3 Report Structure	17
2 Literature Review	18
2.1 PVT Collector Designs	18
2.1.1 Absorber Designs	18
2.1.2 Glazing	19
2.1.3 Insulation	19
2.1.4 Fins	19
2.1.5 PVT Performance	20
2.2 Factors Affecting PVT Operation	20
2.2.1 Mass Flow Rate	21
2.2.2 Irradiance	22
2.2.3 Ambient Temperature	22
2.2.4 Wind	22
2.2.5 Roof Installations	23
2.2.6 Condensation, Frost and Rain	23
2.3 Previous PVT and GSHP Integration Research	23
3 Methodology	25
3.1 Testing Rig and Equipment	25
3.1.1 Testing Rig	25
3.1.1.1 Heat Pump	26
3.1.1.2 Heat Meters	26
3.1.2 PVT Collectors	26
3.2 Experiments	28
3.2.1 Flow Rates	28
3.2.2 Roof Installations	29
3.3 Data Analysis	29

3.3.1	Filters	30
3.3.2	Key Performance Indicators	31
3.3.3	Calculation of the KPIs	31
3.4	Model	33
3.4.1	Geometry	33
3.4.2	Boundary Conditions	34
3.4.3	Mesh	34
3.4.4	Convective Heat Transfer Coefficient	36
3.4.5	Thermal Power	36
4	Results	37
4.1	Low Flow Rate	37
4.1.1	Impact of Irradiance	38
4.1.1.1	Finned vs. Non-finned	39
4.1.2	Impact of Wind	40
4.1.2.1	Different Wind Speeds	40
4.1.2.2	Finned vs. Non-finned	41
4.1.2.3	Different Wind Directions	42
4.2	Impact of Different Roof Installations	43
4.2.1	Side Panels	45
4.2.1.1	Impact of Irradiance and Wind Speed	45
4.2.1.2	Impact of Wind Direction	46
4.2.2	Back Panel	48
4.2.2.1	Impact of Irradiance and Wind Speed	48
4.2.2.2	Impact of Wind Direction	49
4.2.3	Back and Side Panels	50
4.2.3.1	Impact of Irradiance and Wind Speed	51
4.3	Medium Flow Rate	51
4.3.1	Impact of Irradiance	52
4.3.2	Impact of Wind Speeds	52
4.3.3	Impact of Wind Direction	54
4.4	High Flow Rate	54
4.4.1	Impact of Irradiance	55
4.4.2	Impact of Wind Speed	56
4.4.3	Impact of Wind Direction	57
4.5	Model Results	57
4.5.1	Convective Heat Transfer Coefficients	58
4.5.2	Thermal Power Degradation	59
5	Discussions	62
5.1	Comparison of the PVT Collectors	62
5.2	Different Operating Conditions	63
5.2.1	Changing Flow Rates	63
5.2.2	Different Roof Installations	66
5.3	Finned vs. Non-Finned	69

5.4	Non-Uniform Flow Rate Distribution	70
5.5	Comparability of Results	70
5.6	Uncertainties	70
6	Conclusions	72
	References	75
	Appendices	80
A	Ambient conditions	80
B	Coefficients	82
C	Graphs	85

Abbreviations

CFD	Computational fluid dynamics
EU	European Union
F-PVT	Finned photovoltaic thermal collector
GSHP	Ground source heat pump
HP	Heat pump
IRENA	International Renewable Energy Agency
ISO	International Organization for Standardization
KPI	Key Performance Indicator
KTH	Kungliga Tekniska högskolan
NF-PVT	Non-finned photovoltaic thermal collector
PV	Photovoltaic
PVT	Photovoltaic thermal
ST	Sheet-and-Tube
STC	Solar Thermal Collector
TP	Thermal performance

List of Figures

1	Cross section of a typical PVT collector.	16
2	Visual representation of the structure of the report.	17
3	Cross section of different absorbed designs from [1]. (Left) Sheet-and-tube absorber. (Middle) Roll bond absorber. (Right) Box channel absorber.	18
4	System Diagram of the PVT testing facility at KTH.	25
5	Heat pump used in the experiments with the cold and hot storage tanks.	26
6	PVT Testing Array at KTH.	27
7	Left) The back of the finned PVT with the vertical fins visible. Right) Back of the non-finned PVT with the box-channel aluminium absorber visible.	27
8	Right) Example of a side panel attached to the PVT. Left) Example of a back panel attached to the PVT.	29
9	Monthly mean fluid temperature profiles for a range of annual average mean fluid temperatures [2].	32
10	(TOP) Cross section view of two of the absorber channels and the PV layer on top. Each channel consists of multiple micro-channels, highlighted by the red square. (Bottom) Side view of the PVT. Graphics are not to scale and only serve as a visual explanation aid.	33
11	The skewness factor of the micro-channel mesh at the inlet boundary as well as in the center of the micro-channel.	35
12	Regression lines for different irradiance levels for the NF-PVT plotted over the obtained data. The data is colour-coded with respect to the irradiance level of each data point. The coefficients used in the calculation can be found in Table 8.	39
13	Regression lines for different irradiance levels for the F-PVT plotted over the obtained data. The data is colour-coded with respect to the irradiance level of each data point. The coefficients used in the calculation can be found in Table 8.	40
14	Comparison between NF-PVT and F-PVT at different irradiance levels.	41
15	Regression lines for different wind levels at two different irradiance values for both the NF-PVT and the F-PVT. The coefficients used in the calculation can be found in Table 8.	42
16	Raw data measured of the NF-PVT on the 21 of May 2024, to justify the removal of time dependent data points.	44
17	Impact of time-restricted filtering on the NF-PVT during operation with side panels. The coefficients used for the regressions can be found in time-restricted regression line can be found in Table 10 while the coefficients to calculate the overall regression lines can be found in Appendix B in Table B2.	45

18	The regression lines for both the NF-PVT and the F-PVT at two different irradiance levels, comparing the impact of wind speed when the side panels were attached. The coefficients used for the regression lines can be found in Table 10.	47
19	Comparison between NF-PVT and F-PVT at different irradiance levels for the medium flow rate.	52
20	The impact of different wind speed on the specific thermal power output of the NF-PVT at the medium flow rate and two different irradiance levels.	53
21	Comparison between NF-PVT and F-PVT at different irradiance levels for the high flow rate.	55
22	Comparison between NF-PVT and F-PVT at different wind levels for the high flow rate.	56
23	The impact of changing flow rates on the convective heat transfer coefficient of the micro-channel at three different irradiance levels and a constant temperature difference of 10 °C.	59
24	The impact of changing flow rates on the convective heat transfer coefficient of the micro-channel at three different temperature differences and a constant irradiance level of 500 W/m ²	60
25	Comparison of the power degradation for the six scenarios at zero irradiance, for three difference temperature differences between ambient and fluid inlet temperature.	60
26	Comparison of the power degradation for the six scenarios at an irradiance of 500 W/m ² , for three difference temperature differences between ambient and fluid inlet temperature.	61
27	Comparison of the power degradation for the six scenarios at an irradiance of 1000 W/m ² , for three difference temperature differences between ambient and fluid inlet temperature.	61
28	Left) Thermal image of the NF-PVT. Right) Thermal Image of the F-PVT.	62
29	The regression lines of the NF-PVT at the three tested flow rates, comparing the impact of changing irradiance.	63
30	The regression lines of the F-PVT at the three tested flow rates, comparing the impact of changing irradiance level.	64
31	The regression lines of the NF-PVT at the three tested flow rates, comparing the impact of changing wind speed.	65
32	The regression lines of the NF-PVT with the different roof installations, comparing the impact of changing irradiance level.	67
33	The regression lines of the NF-PVT with the different roof installations, comparing the impact of changing wind speed.	68
C1	Regression lines for different wind directions at two different irradiance values for the NF-PVT, at a low flow rate.	85
C2	Regression lines for different wind directions at two different irradiance values for the F-PVT, at a low flow rate.	86

C3	Impact of filtering on the side panels data set for the F-PVT. The coefficients for the regression lines can be found in Tables 10 and B2, for the time restricted and overall regression lines.	86
C4	Regressions lines for both the NF-PVT and the F-PVT at different irradiance levels, considering the case when the side panels were attached. The coefficients used for the regressions can be found in Table 10.	87
C5	Impact of filtering on the roof data set for the NF-PVT. The coefficients for the regression lines can be found in Tables 12 and B4, for the time restricted and overall regression lines.	87
C6	Impact of filtering on the roof data set for the F-PVT. The coefficients for the regression lines can be found in Tables 12 and B4, for the time restricted and overall regression lines.	88
C7	Regressions lines for both the NF-PVT and the F-PVT at different irradiance levels, considering the case when the roof was attached. The coefficients used for the regressions can be found in Table 12.	88
C8	The regression lines for both the NF-PVT and the F-PVT at two different irradiance levels, comparing the impact of wind speed when the roof was attached. The coefficients used for the regression lines can be found in Table 12.	89
C9	Impact of filtering on the data set with the roof and side panels present for the NF-PVT. The coefficients for the regression lines can be found in Tables 14 and B6, for the time restricted and overall regression lines.	90
C10	Impact of filtering on the data set with the roof and side panels present for the F-PVT. The coefficients for the regression lines can be found in Tables 14 and B6, for the time restricted and overall regression lines.	90
C11	Regressions lines for both the NF-PVT and the F-PVT at different irradiance levels, considering the case when both the side panels and the roof were attached. The coefficients used for the regressions can be found in Table 14.	91
C12	The regression lines for both the NF-PVT and the F-PVT at two different irradiance levels, comparing the impact of wind speed when both the side panels and the roof were attached. The coefficients used for the regression lines can be found in Table 14.	92
C13	The data collected for NF-PVT at the medium flow rate, colour coded to the irradiance level which they represent.	93
C14	The data collected for F-PVT at the medium flow rate, colour coded to the irradiance level which they represent.	93
C15	The data collected for NF-PVT at the high flow rate, colour coded to the irradiance level which they represent.	94
C16	The data collected for F-PVT at the high flow rate, colour coded to the irradiance level which they represent.	94
C17	The regression lines of the F-PVT at the three tested flow rates, comparing the impact of changing wind speed.	95

C18	The regression lines of the F-PVT with the different roof installations, comparing the impact of changing irradiance level.	95
C19	The regression lines of the F-PVT with the different roof installations, comparing the impact of changing wind speed.	96

List of Tables

1	Variables of Equation 2 for the modelled steady-state specific power of a PVT collector from ISO 9806:2017.	21
2	Ambient conditions over evaluation period	28
3	KPIs to quantify the thermal performance of the PVT collectors.	31
4	Model boundary conditions.	34
5	Boundary conditions of for the mesh refinement study.	35
6	Different flow rate scenarios for the multi-channel COMSOL model.	36
7	Result classifications.	37
8	KPIs of the NF-PVT and F-PVT with a low flow rate.	38
9	Wind dependence coefficients of the NF-PVT and F-PVT with a low flow rate.	42
10	KPIs of the NF-PVT and F-PVT with a low flow rate and side panels.	46
11	Wind dependence coefficients of the NF-PVT and F-PVT with a low flow rate and side panels.	46
12	KPIs of the NF-PVT and F-PVT with a low flow rate and a roof.	48
13	Wind dependence coefficients of the NF-PVT and F-PVT with a low flow rate and a back panel.	49
14	KPIs of the NF-PVT and F-PVT with a low flow rate, a roof and side panels.	50
15	KPIs of the NF-PVT and F-PVT with a medium flow rate.	51
16	Wind dependence coefficients of the NF-PVT and F-PVT with a medium flow rate.	54
17	KPIs of the NF-PVT and F-PVT with a high flow rate.	55
18	Coefficients of the NF-PVT and F-PVT for different wind directions at a high flow rate.	57
19	Comparison of the numerically modelled and NF-PVT regression of specific thermal power output under different ambient conditions.	58
20	The first two columns present a comparison of the annual thermal energy output of the NF-PVT and F-PVT at different flow rates to the low flow rate, respectively. The last column compares the F-PVT to the NF-PVT as the respective flow rate.	66
21	Comparison of the baseline coefficients to those of the three different roof installations for both the NF-PVT and the F-PVT.	67
22	The first two columns present a comparison of the annual thermal energy output of the NF-PVT and F-PVT with different roof installation types to the low flow rate baseline, respectively. The last column compares the F-PVT to the NF-PVT as the respective roof installations.	69
A1	Average ambient and operational conditions for the low flow rate data sets.	80
A2	Average ambient and operational conditions for side panel data sets.	80
A3	Average ambient and operational conditions for roof data sets.	80

A4	Average ambient and operational conditions for roof and side panels data sets.	81
A5	Average ambient and operational conditions for the medium flow rate data sets.	81
A6	Average ambient and operational conditions for the high flow rate data sets.	81
B1	Wind dependence coefficients of the NF-PVT and F-PVT with a low flow rate.	82
B2	KPIs of the NF-PVT and F-PVT with a low flow rate and side panels for all the data point collected.	82
B3	Wind dependence coefficients of the NF-PVT and F-PVT with side panels.	82
B4	KPIs of the NF-PVT and F-PVT with a low flow rate and a roof for all the data point collected.	83
B5	Wind dependence coefficients of the NF-PVT and F-PVT with a roof.	83
B6	KPIs of the NF-PVT and F-PVT with a low flow rate, roof and side panels for all the data point collected.	83
B7	Wind dependence coefficients of the NF-PVT and F-PVT with a roof and side panels.	83
B8	Wind dependence coefficients of the NF-PVT and F-PVT with a medium flow rate.	83
B9	Wind dependence coefficients of the NF-PVT and F-PVT with a high flow rate.	84

1 Introduction

As mean global temperatures keep rising, due to increased human-induced carbon dioxide emissions, the effects of climate change are becoming ever more apparent [3]. In order to try and mitigate the effects of the climate crisis, many national as well as international efforts are underway. These include the 151 existing national net-zero targets [4] as well as international agreements, such as the Paris Agreement or European Climate Law. One of the key focuses of these efforts is the so-called energy transition, moving away from fossil fuel generation to carbon-neutral technologies. According to IRENA, the transition needs to occur by 2050 to prevent mean global temperatures rising past 1.5 °C over pre-industrialisation levels [5]. This leads to the need for a continued, massive and rapid scale up of renewable energies, such as wind and solar.

The use of these renewable energy sources for electricity generation world-wide was reported at 30% (excluding bioenergy) in 2022 however, the use of renewable energy in heat is only 11.4% [6]. Because the heating sector constitutes the largest energy end use, close to half of the final energy consumption worldwide, it is imperative to increase the share of renewable energy in this sector [6]. In the European Union (EU), around 60% of heating demand comes from space and water heating in buildings [7]. Therefore, the implementation of a carbon neutral heating solution in buildings would greatly decrease the emissions of the heating sector.

One of the central technologies for decarbonising heating in buildings is the heat pump (HP) [8]. As part of the European Green Deal, the European Commission published the RePowerEU plan which outlines the EU's aim to double the rate at which individual HPs are deployed [9]. However, it has been acknowledged that HPs cannot be used as a stand-alone replacement for gas boilers [10]. This is in part due to the strain HPs place on electricity demand resulting in the need for both enhanced production and distribution capacity as well as greater renewable penetration in electricity generation [10].

Through the implementation of an integrated system comprising a rooftop photovoltaic (PV) module with a HP, the issues related to the electricity demand lessen. Nevertheless, this solution is not very efficient due to both the daily as well as seasonal variability of solar energy. This is especially important in high latitude areas, such as the Nordics where the mismatch of PV production and heat demand is the greatest. To maximise the high production of PV in the summer in these regions, these systems can be integrated with seasonal thermal storage [11]. A typical seasonal thermal storage mechanism in the Nordic countries is the use of boreholes [12]. This leads to the implementation of photovoltaic/thermal (PVT) and ground source heat pump (GSHP) systems for borehole regeneration. Additionally, Sommerfeldt and Madani (2018) found that the main benefit of adding PVTs to GSHP systems is the reduced borehole length and spacing [12].

A photovoltaic/thermal collector is the combination of a PV panel with a solar thermal collector, together PVT. Figure 1 shows the typical construction of a PVT collector, with a thermal absorber mechanically attached to the back of a PV panel.

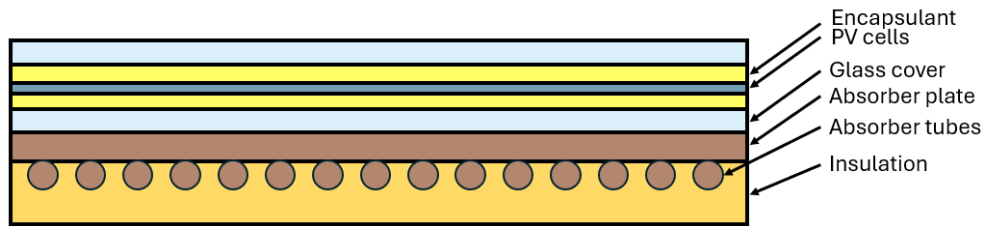


Figure 1: Cross section of a typical PVT collector.

The benefit of this dual module is that a PVT collector can simultaneously produce electricity and heat, so increasing the energy gained per unit area [13] compared to individual PV panels or solar thermal collectors. Furthermore, because the thermal collector removes heat from the back of the PV panel, it has been demonstrated that the electrical efficiency of the PVT increases [14].

With part of the EU's Fit For 55 package focusing on making building more efficient [15] the integration of PVT into buildings is of increasing interest [16]. This is because when used in buildings, PVT can produce heat and electrical energy [17]. However, the implementation of building integrated PVT (BiPVT) is still in the development phase [17] and faces several bottlenecks to wide scale adoption. These include the higher cost of production as well as installation of PVT collectors compared to PV or solar thermal systems, reducing the economic viability of the PVT system [16]. Additionally, the lack of public awareness and product standardisation and certification further hinder implementation of BiPVT systems [16].

To help alleviate the impact of these bottlenecks, further research into the system integration of both BiPVT and PVT with GSHPs needs to be conducted. This will allow for the optimisation of the design resulting in lower costs as well as increased standardisation. Research will also increase the collective knowledge on how the system operates, in turn increasing the confidence stakeholders have in the system. This will result in more certifications and warranties allowing for the systems to be commercialised.

1.1 Objectives and Research Questions

As interest in series integration of PVTs with a GSHP increases, so does the interest in the thermal performance of PVTs in this configuration. This is because the PVT acts as both a heat source for the HP and a source to regenerate the boreholes during the summer months. Furthermore, when the PVT is run under low temperature operating conditions, meaning the temperature of the inlet fluid is lower than ambient air temperature, the PVT can absorb heat from both the PV panel as well as the surrounding air. Therefore, this study focuses on quantifying the thermal output of two box-channel PVT collector prototypes under low temperature operating conditions. The difference between the two prototypes is the presence of fins on the absorber of one of the collectors, meant to enhance its heat exchange capabilities with the ambient. Therefore, the objective is to quantify the impact of these fins on the thermal

operation of a PVT collector under low operating temperatures and in a wide range of weather conditions. To fulfil this objective, the report will strive to answer the following research questions:

1. How do varying ambient conditions, such as wind and solar irradiance, affect the thermal output of the finned and non-finned designs?
2. How do varying mass flow rates of the working fluid impact the thermal performance of the finned and non-finned designs?
3. How do different types of roof installations affect the performance of the finned and non-finned designs?

1.2 Scope

The scope of the report is limited to the thermal operation of a low temperature PVT collector. The definition of low temperature in this report refers to inlet temperature to the PVT between -5°C and 10°C . The ambient weather conditions of the experiment will be typical dynamic outdoor conditions for the period of February to May in Stockholm, Sweden. As the focus of the report is the thermal operation, the electrical component generated by the PVT will not be discussed in detail. When answering Research Question 2, weather conditions consisting of snow and frost formation will not be considered, limiting the scope to different ambient temperatures, irradiance levels and wind speeds.

1.3 Report Structure

In order to answer the posed research questions the following structure will be observed: Section 2 will give a literature review of different factors affecting PVT performance as well as the effect these factors have on that performance; Section 3 will provide a detailed methodology for both the numerical and empirical parts of the study along with how the data analysis will be conducted; Section 4 will present the results of the study; Section 5 will discuss the results with Section 6 summarising the study and outlining the main conclusions. This structure is visually presented in Figure 2.

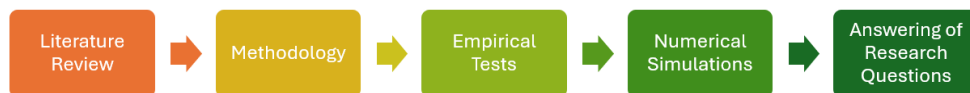


Figure 2: Visual representation of the structure of the report.

2 Literature Review

2.1 PVT Collector Designs

PVT absorber designs can be broadly classified by the type of working fluid they use for heat exchange, namely water-based and air type absorbers. However, it has been found that water-based PVT systems can operate at higher thermal efficiencies, due to the better thermal properties of water compared to air [1]. Furthermore, as the tested PVTs in this study use a water-based solution as their working fluid, the following literature review will focus on water-based PVT collectors. Four more broad classification categories can be defined [13]. These include the geometric design of the absorber as well as if the PVT is glazed, insulated or has fins attached to the absorber. These features will be discussed in following subsections.

2.1.1 Absorber Designs

Many different designs of flat plate absorbers, as seen in Figure 3, have been tested in the pursuit of optimising the thermal energy gained. One of the most common designs found in both literature and the commercial market is a sheet-and-tube (ST) absorber [18]. In this design the absorber consists of a metal plate with soldered circular tubes running in parallel down the length of the absorber [1]. The advantages of this design include the low cost and ease of manufacturing, however the small contact surface area and imperfect bonding between the working fluid tubes and the absorber plate reduces the thermal performance due to a smaller area for heat exchange [1].

A design that allows for the increased contact between the PV panel and working fluid while maintaining the manufacturing ease is the roll bond design [1]. This design has channels for the working fluid integrated into the absorber. A disadvantage of the roll bond design is the large pressure drop experienced in the absorber [19]. It has been shown that this larger pressure drop hinders thermal performance due to its impact on the flow distribution, creating an uneven-flow distribution in the absorber, as well as resulting in a higher required pumping power to circulate the working fluid [20].

Another design which increases the surface area available for heat transfer between the PV panel and the working fluid is the box channel design. This is because in this design the fluid is flowing through the entire absorber plate thus maximising the surface area available for heat transfer [1]. This leads to box channel absorbers thermally outperforming ST absorbers [18]. However, because of special connections

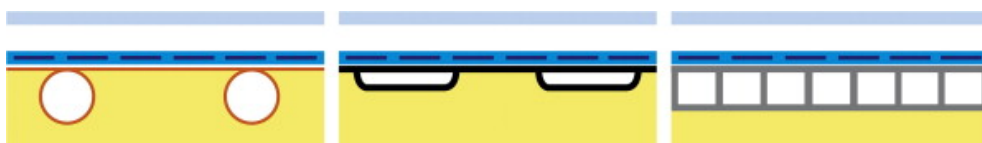


Figure 3: Cross section of different absorber designs from [1]. (Left) Sheet-and-tube absorber. (Middle) Roll bond absorber. (Right) Box channel absorber.

between the absorber plate and the inlet/outlet manifolds, the box channel design can be more expensive to manufacture than the two other designs mentioned above [1].

2.1.2 Glazing

One feature of the commercially available PVT panels is glazing [21]. Glazing consists of placing a glass layer above the PV module in order to reduce the thermal losses to the ambient air through radiation from the top of the PV module. It has been shown that glazing significantly improves the thermal efficiency of PVT modules [21]. Therefore when the system is being optimised for thermal performance, for example for domestic hot water or space heating, glazing is a desired feature [21]. However, it has also been shown that adding a glazing layer to the PV module decreases the electrical efficiency of the module by about 20% [22]. This is because the additional glass layer increases the absorption losses incurred as a result of reflection [22] and increases the PV module surface temperature, further decreasing the electrical output [23].

Due to the high thermal losses of unglazed PVT collectors, they are limited to low temperature applications where the heat loss is limited [24]. They are therefore ideal for integration with GSHP and borehole regeneration applications [25].

2.1.3 Insulation

Much like glazing, insulation serves to reduce heat losses from the PVT absorber to the environment [1]. Because of the reduced thermal losses, the outlet temperature of the working fluid is also increased [1]. However, when operating at low ambient temperatures the increased outlet fluid temperature may lead to a positive difference between the fluid and ambient temperature, leading to heat loss to the ambient rather than heat gains. It is therefore beneficial to use uninsulated PVT modules as this enables heat exchange between higher ambient air and the lower working fluid temperature [26].

2.1.4 Fins

With the increased interest of integrating PVT with GSHP, fins have begun to appear on commercially available PVTs [27]. This is because fins enable greater heat exchange between the working fluid and ambient air, by increasing the heat transfer area between the two [28].

Giovanetti et. al. (2019) concluded that while the fins increase the heat transfer coefficient of the collector compared to non-finned designs, they also increased the sensitivity of the collector to specific environmental conditions [28]. This finding coincides with the findings of Beltran et. al. (2023), who through a validated numerical model found that the addition of fins increases the collector U-value [2]. In the concurrent empirical tests, the two finned designs displayed the highest thermal loss coefficients [27]. Lämmle and Munz (2022) summarised that the improvement of

convective heat gains caused by the addition of fins was of particular importance during periods of low irradiance, such as nighttime as well as winter operation [29].

However, the implementation of fins to increase the U-value comes with trade-offs. These include the higher cost of the PVT absorber due to increased material use as well as increased difficulty in manufacturing [27]. It is therefore necessary to fully understand the impact of the fins on the thermal operation to ensure that this trade-off is beneficial.

2.1.5 PVT Performance

In an outdoor testing environment, Beltran et. al. (2024) tested different PVT absorber designs and analysed the resulting zero-loss efficiency along with the relative specific thermal cost [27]. They found that a sheet-and-tube absorber design had a zero-loss efficiency of 41% while the finned sheet and tube absorber has a zero-loss efficiency of 43%. This shows that the fins increase the thermal performance of the PVT, however they also increased the relative specific thermal cost of the PVT collector by roughly 15%.

Similarly, a box-channel design displayed a zero-loss efficiency of 49%, higher than that of the sheet-and-tube design, along with a relative specific cost roughly 20% higher than the sheet-and-tube design. This study further highlights the trade-off between thermal efficiency and component cost.

2.2 Factors Affecting PVT Operation

In 2017 the International Organisation for Standardisation (ISO) published the ISO 9806:2017 standard regarding the testing methods for solar thermal collectors (STC) [30]. In this standard they presented equations that can be used to model, and so describe, the extracted power from a collector in steady state. Equation 1 describes the useful power extracted from a STC:

$$\dot{Q} = \dot{m}c_p\Delta T, \quad (1)$$

where \dot{Q} is the thermal power, \dot{m} is the mass flow rate of the working fluid, c_p is the specific heat capacity of the working fluid at its mean temperature and ΔT is the temperature difference between fluid inlet and outlet temperature of working fluid. From this equation it is possible to see that the power extracted depends on the mass flow rate. This will be discussed below.

To model the thermal power extracted from a STC operating in a steady-state the ISO standard presented Equation 2:

$$\dot{Q} = A_G \left[\begin{array}{l} \eta_0 G - a_1 (T_m - T_a) - a_2 (T_m - T_a)^2 - a_3 u' (T_m - T_a) + \\ a_4 (E_L - \sigma T_{sky}^4) - a_6 u' G - a_7 u' (E_L - \sigma T_{sky}^4) - a_8 (T_m - T_a)^4 \end{array} \right], \quad (2)$$

where variable descriptions are given in Table 1. From this equation it is possible to see that the thermal power gained depends not only on the mass flow rate but also

Table 1: Variables of Equation 2 for the modelled steady-state specific power of a PVT collector from ISO 9806:2017.

Symbol	Variable	Unit
A_G	Area of the collector	m^2
η_0	Zero-loss efficiency	-
G	Hemispherical solar irradiance	W/m^2
a_1	Heat loss coefficient	$W/(m^2 \cdot K)$
T_m	Mean working fluid temperature	$^{\circ}C$
T_a	Ambient air temperature	$^{\circ}C$
a_2	Temperature dependence of a_1	$W/(m^2 \cdot K^2)$
a_3	Wind speed dependence of a_1	$J/(m^3 \cdot K)$
u'	Reduced wind speed $u' = u - 3m/s$	m/s
a_4	Sky temperature dependence of a_1	-
E_L	Longwave irradiance	W/m^2
T_{sky}	Sky Temperature	$^{\circ}C$
a_5	Effective thermal capacity	$J/(m^2 \cdot K)$
a_6	Wind speed dependence of η_0	s/m
a_7	Wind speed dependence of infrared radiation exchange	$W/(m^2 \cdot K^4)$
a_8	Radiation loss	$W/(m^2 \cdot K^4)$

on various ambient conditions. These include irradiance, ambient temperature as well as wind speed, which will be discussed in further detail below.

2.2.1 Mass Flow Rate

As shown above, the mass flow rate affects the thermal power of a PVT collector [30]. This is because the flow rate of the working fluid of a PVT collector will have an impact on the rate of heat exchange between the PV panel and the working fluid, affecting the thermal performance of the collector [14]. Because of this, the ISO standard recommends testing STC at a mass flow rate of 0.02 kg/s m^2 [30]. However, this has not been optimised for PVT collectors, nor for operation at low temperatures.

The optimal flow rates for PVT operation reported in literature form a large range [14] showing that the optimal flow rate depends heavily on both PVT collector design as well as operating conditions [1]. However, it has been found that, in warm climates, increasing mass flow rate increases thermal efficiency [31][32]. A previous study performed at the KTH testing facility found that during nighttime operation mass flow rates had a negligible impact on thermal performance and during daytime operation an optimal flow rate was found [33]. This flow rate corresponded to a rate at which a balance between incoming solar irradiation warming up the PV panel and the working fluid cooling it down was found.

2.2.2 Irradiance

While low temperature PVT collectors utilise the ambient air to increase their thermal performance during periods of low to no irradiance, the main purpose of the PVT absorber is to collect heat as solar irradiance warms up the PV panel. Abdul-Ganiyu et. al. (2021) found that thermal efficiency of the PVT collector was directly proportional to the irradiance received by the collector [31]. While this result was obtained in a warm climate, Eskola (2023) also observed an increase in zero-loss efficiency of the tested PVT collectors as irradiance increased in a cold climate [33]. However, the impact of the irradiance on the heat loss coefficient depended on the flow rate used [33].

2.2.3 Ambient Temperature

The difference between ambient temperature and the temperature of the working fluid of the PVT determines the extent of the heat gains experienced by the working fluid. When ambient temperature is lower than that of the working fluid, the working fluid is losing heat. Therefore, in this scenario a low heat loss coefficient would be desirable to ensure the least amount of heat loss to the ambient. However, when the ambient temperature is higher than that of the working fluid, as is the case in low temperature operation, the opposite is true. In this case a high heat loss coefficient means that a large amount of heat is being provided to the working fluid by the ambient, increasing the thermal performance of the PVT.

2.2.4 Wind

The presence of wind has an effect on the thermal performance of the PVT due to the disturbance of the air around the collector. Chhugani et. al. (2020) found that a reduction of wind velocity and turbulence behind a PVT collector significantly reduced the heat loss coefficient, leading to less heat exchange between the ambient air and the PVT working fluid [34]. Therefore, higher wind speeds are desired for increased heat exchange between the ambient air and the PVT working fluid in low operating conditions. However, increased wind speeds will also serve to cool down the front of the PV panel, meaning that there is less heat available to be absorbed by the working fluid. It has been observed that the significance of wind on the thermal output of the PVT decreases as irradiance increases [33]. In the same set of experiments, a similar observation was made for increased mass flow rates.

When fins are added to the back of the PVT absorber, the wind direction as well as the wind speed becomes an important factor affecting the thermal output [34]. In their experimental set up, Giovannetti et. al. (2019) evaluated the impact of wind direction on the performance a finned PVT panel [28]. They found that the wind-dependence coefficients of the thermal performance were much higher when the wind was flowing parallel to the fins compared to when the wind direction was perpendicular to the fins. In their outdoor testing, with variable wind directions, the coefficients fell in the range of the these two extremes.

2.2.5 Roof Installations

The impact of different roof installations on the thermal performance of the PVT are not known. However, the roof installations may serve to shelter the absorber from wind. This has been found to hinder heat transfer. A previous study showed that a single PVT panel is more affected by wind than a larger collector array due to self-shielding [28]. This self shielding results in a restricted air flow around the absorber and so hinders heat transfer at the inner collectors in the array.

2.2.6 Condensation, Frost and Rain

While not analysed further in this report, it is important to understand the effect of these phenomenon as well as under which conditions they occur. This will enable easy filtering of these phenomenon from the obtained results later on in the report.

Condensation occurs when the surface temperature of the PVT absorber falls below the dew point, but stays above the frost point [35]. It has been shown that condensation improves the heat gains of the working fluid from the ambient [34][36][37]. Frost on the other hand, which occurs when the surface temperature falls below the frost point, hinders the convective gains from ambient air [28][34]. However, frost formation, rather than the presence of ice, can lead to heat gains in the system [33][37]. These heat gains were observed to be larger than the heat losses observed during the defrosting process [33].

As discussed in Bunea et. al. (2015) there is a non-negligible amount of heat exchanged between the PVT collector and rainwater. However, as the temperature of the rainwater is difficult to quantify, the extent of the impact of rain on the thermal output of PVT collectors has yet to be verified [37].

2.3 Previous PVT and GSHP Integration Research

As highlighted above, the electrical efficiency of a PVT is highest at lower PV cell temperatures. However, when considering the thermal output, higher output temperatures of the PVT module result in higher heat usability [31]. This issue can be resolved when integrating the PVT with a GSHP, as the operating temperature are also low. Schmidt et. al. (2018) found that the use of a PVT array as the single source for a solar HP was a promising concept for heat delivery in a residential building [38].

Somerfeldt and Madani (2019) conducted a techno-economic analysis of PVT plus GSHP systems for multi-family housing and found that under nominal conditions the use of a PV plus GSHP was more economic. However, if the design of the borehole field is compromised, the PVT plus GSHP system becomes a more interesting option. This is also the case when an old GSHP is due for replacement with a HP with a higher Seasonal coefficient of performance [39].

Chhugani et. al. (2020) performed Hardware-in-the-Loop experiments with a PVT collector as the sole source of a HP. They achieved good system efficiency and concluded that the system can be used as an alternative to an air-source HP [40].

Lämmle and Munz (2022) showed that the integration of a finned PVT as a sole source for a HP achieved a seasonal performance factor higher than that of an air-source HP but lower than a brine- source HP [29].

As current research shows, there is significant potential to improve the design of PVT collectors for optimal GSHP integration [2]. It has also been highlighted that outdoor experiments on PVT collectors is essential to understand their behaviour and so be able to optimise their performance [28].

3 Methodology

3.1 Testing Rig and Equipment

Previous research has suggested that the integration of PVT with GSHP is a suitable option to increase the penetration of PVT and GSHP in multi-family housing, avoiding the spacing issue as well as providing borehole regeneration and green electricity [26]. To obtain data for the operation of this system, the thermal performance of PVT collectors needs to be analysed.

3.1.1 Testing Rig

To answer the posed research questions empirical data is used. The experiments are conducted on an outdoor test rig, located on the rooftop of the Energy Technology Laboratory at KTH Royal Institute of Technology in Stockholm, Sweden.

As seen in the system diagram in Figure 4, the test rig consists of two south-facing PVT collectors, at a tilt of 45°, connected to a cold fluid storage tank. The two PVT collectors are able to run simultaneously with both electricity and thermal output being monitored by micro-inverters and heat meters, respectively. The electricity produced is recorded every five minutes while the parameters needed to calculate the thermal output, namely inlet/outlet working fluid temperatures and mass flow rate, are stored every 60 seconds.

A reference cell as well as a weather station are located next to the two PVT collectors. The reference cell measures the global irradiance in the plane of the PVT collectors while the weather station monitors the local ambient weather conditions, such as temperature, wind speed, wind direction, relative humidity and dew point. Data from these sources is recorded every 60 seconds.

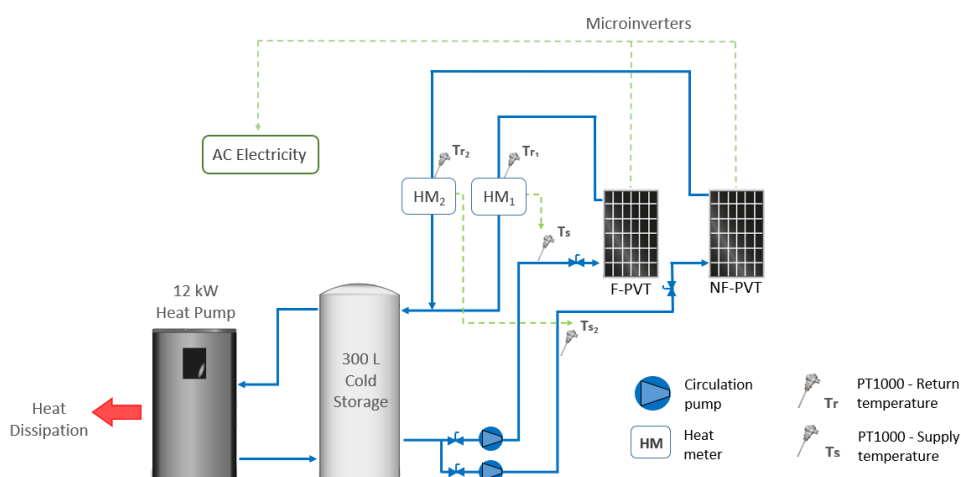


Figure 4: System Diagram of the PVT testing facility at KTH.

3.1.1.1 Heat Pump

To be able to provide cold working fluid to the inlet of the PVT collectors, the working fluid in the 300L cold fluid storage tank needs to be continuously cooled. This is achieved by connecting the tank to a Thermia variable-speed HP with an operational power of 3 to 12 kW. Even at peak summer temperatures and irradiance the HP can provide temperatures as low as -5°C . The working fluid is a 25/75 volumetric mixture of ethylene glycol and water, hereafter referred to as brine. The heat from the HP is dissipated by a 10 kW air-water heat exchanger. The set up can be seen in Figure 5.



Figure 5: Heat pump used in the experiments with the cold and hot storage tanks.

3.1.1.2 Heat Meters

To measure the inlet/outlet temperatures as well as the flow rate of the working fluid, each pipe has an electromagnetic heat meter with PT1000 temperature sensors (2Flow AB). The heat meters do not obstruct the pipe, so do not block the flow of the liquid meaning there is no resultant pressure loss. The heat meters can provide a flow rate measurement within $\pm 0.5\%$ of the actual flow rate, and can measure rates above $0.08\text{ m}^3/\text{h}$. The flow rate is manually adjusted by changing the pumping power of the circulation pumps. The accuracy of the temperature measurement is $\pm 0.15^{\circ}\text{C}$ in the range of -30 to $+175^{\circ}\text{C}$. The heat meters can also detect temperature differences of between 3 to 70°C . The heat meters are located 20 meters away from the PVT collectors and heat gains from the pipes are subtracted when calculating the PVT collector thermal output. This is explained in detail below.

3.1.2 PVT Collectors

The PVT collectors being tested are both unglazed and uninsulated. This is because while the report does not focus on the electrical output of the PVT collectors, it is still the main desired output of the real system. The thermal energy gained through the

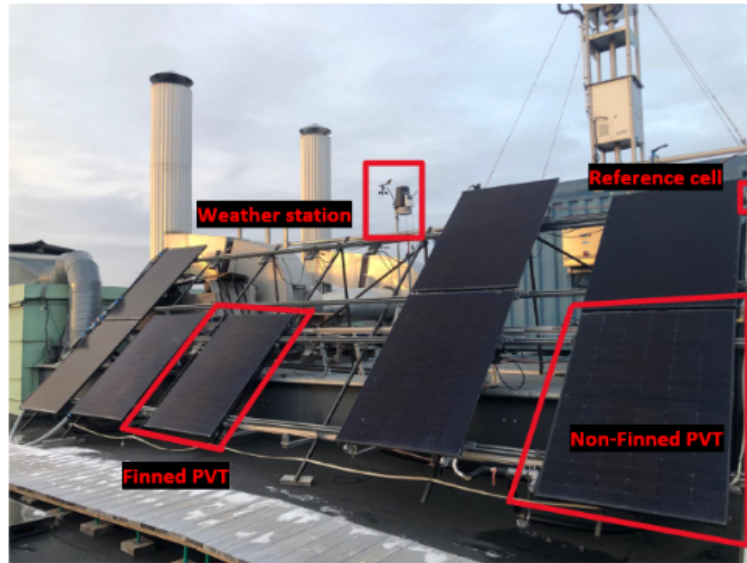


Figure 6: PVT Testing Array at KTH.



Figure 7: Left) The back of the finned PVT with the vertical fins visible. Right) Back of the non-finned PVT with the box-channel aluminium absorber visible.

absorber is therefore an additional energy source, that would otherwise be dissipated to the environment. Instead of this outcome, the thermal energy is used as a heat source for bore hole regeneration, and in this case a heat source for the HP. The PVT module is uninsulated due to the operation occurring at low temperatures. As defined above, these temperatures are lower than the ambient temperature and so heat from the environment can also be absorbed by the thermal exchanger to generate additional thermal energy. This is not possible if the PVT collector is insulated.

Figure 6 shows the test rig array with the two PVT collectors being tested. Both collectors have a surface area of 1.95 m^2 . The two collectors are identical with the exception of the presence of vertical fins on one of the absorbers, as seen on the left of Figure 7. This PVT will henceforth be referred to as the F-PVT. The fins serve to

maximise the heat exchange area with ambient air.

The absorber design utilised is a harp shaped aluminium box-channel, as seen on the right of Figure 7. This image also corresponds to the non-finned PVT, further referred to as NF-PVT. The absorber consists of a long horizontal header tube connected to 19 flat box-channel sections. These are separated by an air gap, creating a larger area for heat exchange with the ambient.

3.2 Experiments

The experiments performed for data collection occurred in spring 2024 in outdoor dynamic ambient conditions. As each experimental operating condition is run for several days, the thermal performance can be analysed in a variety of ambient conditions, namely differing wind speeds and directions, ambient temperatures and irradiances. The range of ambient conditions observed is presented in Table 2. This data was used to help answer Research Question 1.

Table 2: Ambient conditions over evaluation period

Condition	Unit	Minimum	Maximum
Irradiance	W/m ²	0	1225
Wind Speed	m/s	0	10.4
Ambient Temperature	°C	-7.4	28

As there were numerous disruptions during the testing period, such as unsuitable weather conditions, HP malfunctions, errors in measuring data and other experiments, the data presented in this study corresponds to a period of about 14 days. While the testing period occurred over 3 months, March to May of 2024, much of the data was suitable for analysis as it did not fit the required criteria for the study and so was filtered out. This filtering is further explained below.

3.2.1 Flow Rates

To answer Research Question 2, the PVT collectors are operated under a range of different brine flow rates. The manufacturer of the PVT collector prototypes recommended a brine flow rate of 100 l/h per PVT collector. This converts to a volumetric flow rate of approximately 50 l/h/m². Due to the limits of the measurement equipment this flow rate is placed as the bottom of tested range, resulting in an experimental range of roughly 50 to 100 l/h/m², or 0.014 to 0.028 kg/s/m² respectively. To further validate the use of this range, the ISO recommended flow rate of 0.02 kg/s/m² of collector area for testing of solar thermal collectors lies within the chosen range [30].

To further study the impact of changing flow rates, a numerical model is used to analyse the impact on thermal performance of a non-uniform flow distribution through the absorber. This analysis will be conducted at the baseline flow rate of 100 l/h.

3.2.2 Roof Installations

To analyse the impact of different types of roof installations and so answer Research Question 3, three different scenarios are studied.

The first scenario includes the addition of side panels to the PVTs. The side panels, made out of corrugated black plastic, are attached perpendicularly to both sides of the PVT as seen in right of Figure 8. This was done to try to minimise the impact of wind and so the location of the two PVT collectors on the test rig.

The second scenario includes the addition of a back panel attached at a distance of 14.5 cm behind the back of the PVT absorber. The back panel is attached at the same tilt as the PVT and can be seen on the left of Figure 8.



Figure 8: Right) Example of a side panel attached to the PVT. Left) Example of a back panel attached to the PVT.

The third scenario includes both the addition of the side panels and the back panel. For all three scenarios a constant volumetric flow rate of 100 l/h is used, as this was used as the baseline in this study. The effect of the different ambient weather conditions is also studied in these scenarios.

3.3 Data Analysis

The primary result of the experiments is the the measured thermal power, \dot{Q} [W], absorbed from the PVT collectors. This is calculated using Equation 3.

$$\dot{Q} = \dot{V} \rho c_p (T_{out} - T_{in}), \quad (3)$$

where \dot{V} is the volume flow rate, ρ is the density, c_p is the specific heat capacity of the brine and T_{out} and T_{in} are the outlet and inlet temperatures of the brine, respectively. To be able to compare the results of this study to other literature, this measured power is divided by the area of the PVT collectors to obtain a specific thermal power output, \dot{q} [W/m²].

To have accurate data on the thermal gains of the absorber, the heat gains in the pipes between the absorber and the point of measurement need to be subtracted. This is done using the thermal resistivity, R , of the pipe. To obtain the thermal resistivity of the pipe Equation 4 is used:

$$R = \frac{\Delta x}{Ak}, \quad (4)$$

where Δx is the thickness of the pipe, A is the cross-sectional area and k is the thermal conductance of the insulation. For our case, $\Delta x = 0.15$ mm, $A = 804$ mm² and $k = 0.0227$ W/(mK). Once the thermal resistance of the pipe has been found, heat gains from both the inlet and outlet pipe are calculated and subtracted from the measured thermal power, \dot{Q} .

3.3.1 Filters

With the aim to improve reliability of the results, the data was filtered before being used to calculate the thermal performance coefficients. The first level of filtering removed data points when unwanted weather phenomenon, such as rain, condensation or frost, occurred. While the presence of rain was detected by the testing facilities weather station, it was not always possible to visually verify the presence of condensation or frost. Therefore, in addition to the visual observations, the following assumptions were used to determine the presence of condensation or frost:

- condensation is present if any area of the absorber has a temperature between 0°C and the dew point temperature,
- frost is present if any area of the absorber has a temperature below 0°C and the dew point temperatures, and
- condensation and frost is present if condensation or frost, respectively, have been present in the last hour.

The second level of filtering removed data points where the inlet temperature as well as the flow rates of the two PVT absorbers were not equal. This is done to ensure that the thermal performance of the two PVTs can be directly compared. Furthermore, data points where the inlet temperature was larger than the ambient were removed in order to study the thermal performance of low temperature operation. Upon initial analysis of the results, a further temperature filter was added. This filter ensured that the mean fluid temperature of brine was at least 1 °C lower than the ambient temperature. This eliminated data points where there was low heat exchange between the the ambient and the fluid, reducing the uncertainty in the results. For a similar reason, data points where the measured power was lower than 10 W were also removed.

To minimise the impacts of the time dependence of heat exchange on the results, moving averages of the inlet and outlet temperature as well as irradiance were taken. This helped smooth out rapid changes in the operating conditions which would not be reflected in the power output due to the system not being able to reach a steady-state

instantaneously as the rapid changes took place. This method of filtering the data was validated against the removal of data where rapid changes in operating conditions took place and it was found that the results were within operational uncertainty.

3.3.2 Key Performance Indicators

To facilitate the analysis of the thermal performance of the PVT collectors, different key performance indicators (KPI) are defined. These include the calculated annual thermal energy output as well as the zero-loss efficiency and the heat loss coefficient with their wind speed dependencies. These KPIs can be found in Table 3.

Table 3: KPIs to quantify the thermal performance of the PVT collectors.

KPI	Symbol	Unit
Annual Thermal Energy	q	kWh/m ² /yr
Zero-loss efficiency	η_0	-
Wind speed dependence of η_0	a_6	s/m
Heat loss coefficient	a_1	W/m ² ·K
Wind speed dependence of a_1	a_3	J/m ³ ·K

To compare the thermal outputs of the two PVT's under the different conditions the annual thermal energy output is used. The annual thermal energy output, is the sum of the energy outputs of the PVT calculated over a typical meteorological year.

The zero-loss efficiency, η_0 , gives the efficiency of the collector at converting incident solar irradiation into heat after the production of electricity at the PV layer. As it is an efficiency, the value can range from 0-1, where 0 means that no solar irradiance is converted to heat and 1 means that all the solar irradiance is converted to heat.

The wind speed dependence of the zero-loss efficiency, a_6 , indicates how large of an impact wind velocity has on the PVT absorber's ability to exchange heat with the ambient. The higher the value of a_6 , the larger sensitivity of the collector to variations in wind speed.

The heat loss coefficient, a_1 , represents the PVT's rate of heat exchange with the ambient. If heat is being lost to the ambient by the PVT, then a smaller a_1 is desired to minimise the heat losses. However, if heat is being gained from the environment, then a larger value of a_1 is desired to maximise heat gains.

The wind speed dependence of the heat loss coefficient, a_3 , quantifies the impact of the wind speed on the rate of heat exchange of the PVT. The higher the value of a_3 , the larger an impact wind has on the heat exchange rate.

3.3.3 Calculation of the KPIs

The annual thermal energy output is calculated based on coefficients obtained from Equation 5 below, hourly weather data for a typical meteorological year in Stockholm and the monthly mean fluid temperature. The method used is the same as the one described by Beltran et. al. (2024) [27]. The weather data corresponds to Meteonorm 8

[41] while the monthly mean fluid temperature is taken from Sommerfeldt and Madani's (2019) TRNSYS simulation of an integrated PVT and GSHP [39]. As seen in Figure 9, the monthly mean fluid temperatures were calculated for annual average mean fluid temperatures between 0 to 20 °C. However, as the annual average mean fluid temperature for Stockholm is 5 °C, this was used to calculate the presented results [39].

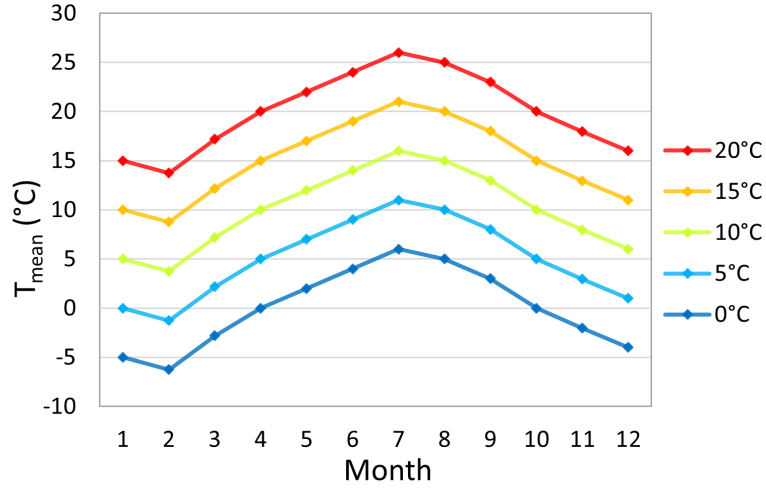


Figure 9: Monthly mean fluid temperature profiles for a range of annual average mean fluid temperatures [2].

To obtain the rest of the chosen KPIs, a multivariable linear regression is used to calculate the modelled thermal power. As seen above, the ISO 9806:2017 standard provides Equation 2 to model the thermal power of a STC under steady-state test conditions [30]. However, due to restrictions imposed by available measurement equipment, terms including the sky temperature or infrared radiation exchange are not considered in this study. Additionally, the a_2 term is also not considered as it would make the regression a polynomial one, increasing the complexity of the analysis. In the ISO standard, reduced wind speed is used in favour of actual wind speed. However, as the majority of wind conditions in the experiments took place at wind speeds under 3 m/s, this study will consider actual wind speed when calculating the KPIs. Furthermore, as per the ISO standard, for an unglazed flat plate collector, the radiation losses are zero [30]. Therefore, Equation 2 is simplified to the following:

$$\dot{q} = \eta_0 G - a_1 (T_m - T_a) - a_3 u (T_m - T_a) - a_6 u G. \quad (5)$$

As per the instructions in the ISO 9806:2017 standard, if the regression outputs a negative coefficient, that coefficient is set to zero and the regression is re-calculated [30].

To quantify how well the modelled thermal power matches the measured data, the coefficient of determination of the regression was calculated.

3.4 Model

To study the impact of the temperature distribution along the absorber of the PVT in more detail a three-dimensional numerical model of the absorber is developed in COMSOL Multiphysics, hereafter referred to as COMSOL. The model is used to investigate the convective heat transfer coefficient between the fluid and the aluminium absorber under different conditions. Then the thermal power output is calculated and validated against experimental data as well as other literature. The validated model results are then used to investigate the degradation of the thermal power when there is an uneven flow rate distribution within the PVT absorber.

The COMSOL model is set up in steady-state conditions using two physics interfaces: the laminar flow interface, as the fluid flow through the absorber is assumed to be laminar, and the heat transfer in solids and fluids interface. These two are coupled through non-isothermal flow coupling, meaning that fluid properties are dependent on temperature. In addition to these built-in COMSOL settings, certain assumptions are also implemented:

- Ambient temperature and air velocity are uniform around the absorber [42][43],
- All radiation exchanges are neglected [18][43][44],
- Thermal losses at the edge of the PVT are negligible [43][44] and
- Solid material properties are independent of temperature [42].

3.4.1 Geometry

A sketch of the geometry of the modelled PVT collector can be seen in Figure 10. The absorber is made out of aluminium and consists of different channels, with each channel being made up by a number of micro-channels. Furthermore, a harp shape for

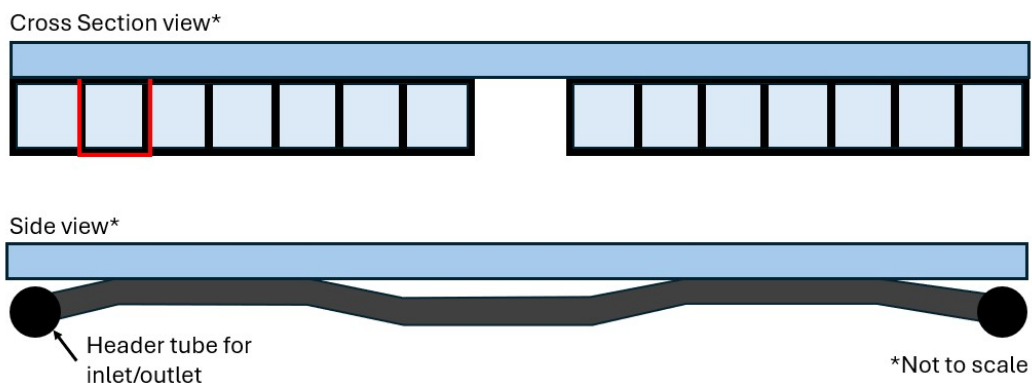


Figure 10: (TOP) Cross section view of two of the absorber channels and the PV layer on top. Each channel consists of multiple micro-channels, highlighted by the red square. (Bottom) Side view of the PVT. Graphics are not to scale and only serve as a visual explanation aid.

the absorber is utilised to allow for the electrical equipment in the middle of the PV panel as well as the header tubes at the top and bottom of the absorber.

When modelling, a single micro-channel, highlighted by the red square in Figure 10, is constructed with water used as the fluid. This is a valid approach to simplifying the COMSOL model as the fluid properties of water are very similar to that of the brine. The micro-channel is tilted at a 45° to match the testing rig with the fluid inlet at the bottom of the micro-channel. This is done to minimise the turbulence caused by the buoyancy of the warm fluid as it rises. It is assumed that every micro-channel behaves the same and so by modelling only one, a greater model accuracy can be achieved using less computational power. A range of flow rates, presented in Table 4, are simulated in the micro-channel to investigate the effect of flow rate on the heat transfer coefficient.

3.4.2 Boundary Conditions

For the COMSOL model to work, specific boundary conditions are defined. Because the main aim of the model is to determine the thermal power output under different operating conditions, Table 4 gives the ranges of varied boundary conditions. The flow rate quoted in Table 4 corresponds to the equivalent flow rate of the whole collector rather than the actual flow rate through the micro-channel. This is done to ease understanding of the different flow rates used.

Table 4: Model boundary conditions.

Parameter	Unit	Range
Fluid Flow Rate	l/h	70 to 130
Fluid Inlet Temperature	°C	-5, 0, 5
Ambient Temperature	°C	10
Irradiance	W/m ²	0, 500, 1,000

As mentioned above, the fluid flow through the micro-channel is assumed to be laminar. This is further verified by the calculation of the Reynold's number to ensure that for at all the tested flow rates, the flow remains laminar. A static pressure of 0 Pa is defined at the outlet of the micro-channel, with the inlet pressure being monitored to obtain the pressure drop through the micro-channel.

3.4.3 Mesh

For COMSOL to solve the model, the geometry first needs to be divided into a mesh. The mesh used is a free quadrangular mesh, applied to the inlet surface of the micro-channel. This mesh is then swept from inlet to the outlet of the micro-channel. To increase the accuracy of the model, boundary layers are added to the liquid domain. There is a trade-off between model accuracy and computation time with increasing mesh elements, so to choose the number of mesh elements used to run the model a mesh refinement study is conducted.

Table 5: Boundary conditions of for the mesh refinement study.

Boundary Condition	Unit	Micro-channel
Flow Rate	l/h	100
Fluid Inlet Temperature	°C	0
Ambient Temperature	°C	10
Irradiance	W/m ²	500

For the micro-channel geometry, the boundary conditions used for the mesh refinement study are shown in Table 5. In this case, the convective heat transfer coefficient stayed constant at a value of 4389 W/(m²K) irrespective of the number of mesh elements used. Up to a total of 276700 mesh elements were tested. Now that the final mesh has been chosen, the mesh quality is checked. This is done by inspecting the skewness factor of each element in the mesh. COMSOL provides the skewness factor on a scale from 0 to 1, with 1 denoting the highest quality. According to Gothäll (2017), the minimum recommended element quality, or skewness factor, is 0.1. Figure 11 provides a visual representation of the mesh element quality in the micro-channel, with the minimum skewness factor being 0.442, satisfying the mesh quality condition.

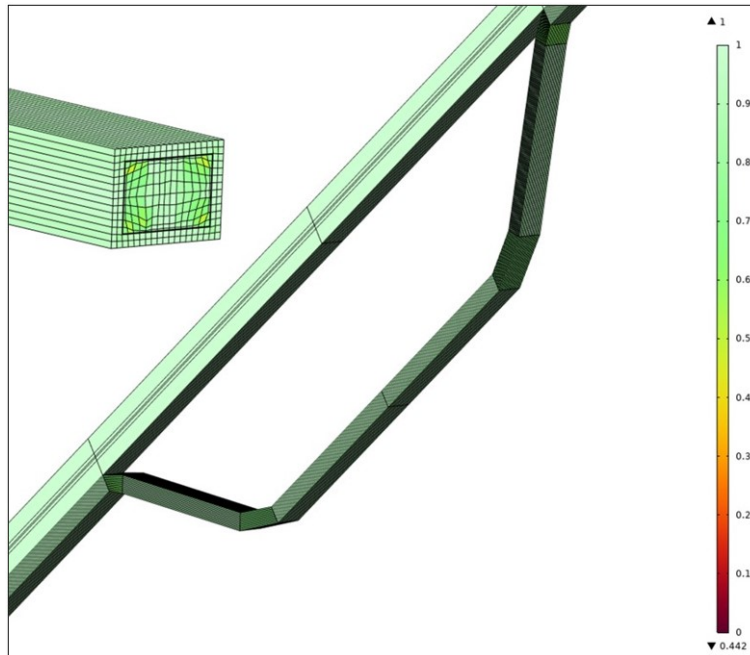


Figure 11: The skewness factor of the micro-channel mesh at the inlet boundary as well as in the center of the micro-channel.

3.4.4 Convective Heat Transfer Coefficient

The convective heat transfer coefficient quantifies how well heat is conducted from a material to a liquid and is given by Equation 6:

$$h = \frac{q}{A\Delta T}, \quad (6)$$

where h is the convective heat transfer coefficient, q is the heat flux, A is the area and ΔT is the temperature difference between the two areas through which heat is being transferred. The heat flux can also be further defined by Equation 7:

$$q = \dot{m}c_p\Delta T, \quad (7)$$

where \dot{m} is the mass flow rate, c_p is the specific heat capacity of the fluid and ΔT is the temperature difference of the fluid at the outlet and inlet. By combining Equations 6 and 7 it is possible to calculate the heat transfer coefficient from the results obtained from the COMSOL model.

3.4.5 Thermal Power

To quantify the degradation of the thermal power output, assuming a non-uniform mass flow distribution, different scenarios are studied. These scenarios are created by calculating the overall specific power output of 4 independent channels with different flow rates. These scenarios are presented in Table 6 and represent different degrees of non-uniformity in the mass flow. The results of these scenarios will be compared to a baseline with a uniform mass flow for all four channels and repeated for different combinations ambient conditions presented in Table 4. This will allow for the study of how a non-uniform mass flow is affected by different ambient conditions which impact the specific power output of a PVT.

Table 6: Different flow rate scenarios for the multi-channel COMSOL model.

Scenario	Channel 1	Channel 2	Channel 3	Channel 4
1	baseline	+10%	baseline	-10%
2	baseline	+10%	+10%	-20%
3	baseline	-10%	-10%	+20%
4	baseline	-10%	-20%	+30%
5	baseline	+10%	+20%	-30%
6	baseline	+30%	baseline	-30%

4 Results

In the Results section, results of all the different experiments will be presented. For each experiment, the impact of ambient conditions will be discussed, answering research question 1. Because one of the overarching aims of this study has been to compare the impact fins have on the thermal performance of a PVT, the NF-PVT and F-PVT will also be compared for every experiment. To aid the presentation of the results all results corresponding to the NF-PVT will be in blue and the F-PVT will be in orange. This is done for ease of visual comparison in the presented Figures.

When analysing the experimental results, classifications of ambient as well as operational conditions were used. The conditions classified are flow rate, irradiance level and wind speed. These classifications can be seen in Table 7. The effect of wind direction has also been studied, with the following classification: North corresponds to wind directions from north-west to north-east, East corresponds to wind directions from north-east to south-east, South corresponds to wind directions from south-east to south-west, and West corresponds to wind directions from south-west to north-west. These wind direction classifications were chosen to show the wind coming directly at the front of the PVT (North), towards the back of the PVT (South) and from the sides of the PVT (East and West). Furthermore, the impact of different roof installations was also analysed.

Table 7: Result classifications.

Classification	Flow rate [m ³ /h]	Irradiance [W/m ²]	Wind speed [m/s]
Zero	-	0	-
Low	0.1	0-200	<1
Medium	0.15	-	1-2
High	0.2	>200	>2

In the following sections, the presented coefficients are all positive because the data collected corresponds to low temperature operation. Therefore, all terms with $T_m - T_a$ will be negative, converting Equation 5 into the following:

$$\dot{q} = \eta_0 G + a_1 (T_a - T_m) + a_3 u (T_a - T_m) - a_6 u G. \quad (8)$$

Therefore, for the remainder of this report a positive heat loss coefficient corresponds to a heat gain rather than a heat loss.

4.1 Low Flow Rate

Once unwanted weather conditions had been filtered out along with observed outliers, data corresponding to the low flow rate consisted of 3,408 data points. This corresponds to approximately 57 hours of operational time. The ambient conditions over this period can be seen in Appendix A. Table 8 presents the calculated KPIs.

Table 8: KPIs of the NF-PVT and F-PVT with a low flow rate.

KPI	NF-PVT	F-PVT
Annual Thermal Energy	2070	2161
η_0	0.423	0.506
a_1	38.460	34.105
a_3	3.001	4.251
a_6	0.000	0.000
R^2	0.94	0.92

As expected the F-PVT generates more thermal energy annually than the NF-PVT, by roughly 4%. This can be attributed to the F-PVT's higher zero-loss efficiency. While it is expected that the zero-loss efficiency of the two panels should be quite similar, upon inspection of the two PVTs it was found that for the NF-PVT thermal contact between the absorber and the back of the PV panel is much worse than that of the F-PVT. This is further addressed in Section 5 below.

The heat loss coefficient, a_1 , of the F-PVT is lower than that of the NF-PVT. This indicated that for the F-PVT there is less heat transfer between the brine and the ambient than for the NF-PVT. This result contradicts the expectation as the fins should serve to increase heat transfer with the ambient. However, considering the experimental set up, the F-PVT is placed in a location much more protected from wind than the NF-PVT, possibly hindering efficient heat transfer. Additionally, as mentioned above, the imperfect contact between the absorber and the PV panel in the NF-PVT results in more of the absorber being exposed to ambient air, increasing heat transfer with the ambient. This will be further discussed in Section 5 below.

Despite this, the wind dependence of the heat loss coefficient, a_3 , of the F-PVT is higher than that of the NF-PVT because of the fins as expected [34].

4.1.1 Impact of Irradiance

To study the impact irradiance has on the thermal performance of the PVTs, the obtained coefficients were used to plot regression lines for different irradiance levels. In these regression lines, the value of the wind speed has been set to 1 m/s so that the impact of irradiance can be isolated. The value of the wind has been set to 1 m/s in all specific thermal power calculations unless specified otherwise for ease of comparison.

Figures 12 and 13 show how irradiance affects the specific thermal power output of the NF-PVT and F-PVT respectively. As expected for both PVTs [31], as the irradiance increases, so does the specific thermal power output. This is because as irradiance increases, there is more solar energy available to be converted into thermal energy by the absorber. Additionally, increasing irradiance levels usually also correspond to increases in ambient temperature, meaning that is probably a larger temperature difference between the brine temperature and the ambient. This larger temperature difference allows the absorber to absorb more of the ambient heat further increasing

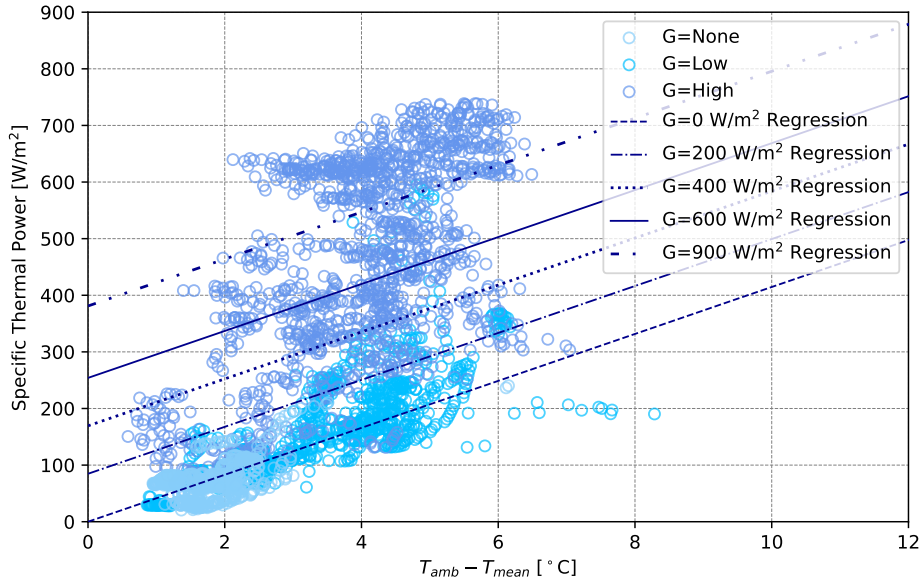


Figure 12: Regression lines for different irradiance levels for the NF-PVT plotted over the obtained data. The data is colour-coded with respect to the irradiance level of each data point. The coefficients used in the calculation can be found in Table 8.

the specific thermal power output.

4.1.1.1 *Finned vs. Non-finned*

When considering the NF-PVT it was found that a 200 W/m^2 increase in irradiance resulted in an 85 W/m^2 increase in specific thermal power of the regression irrespective of the temperature difference between the ambient and the mean brine temperatures. For the F-PVT, this increase was calculated to be 101 W/m^2 .

In Figure 14 a comparison between the NF-PVT and the F-PVT at different irradiance levels can be seen. At zero-irradiance, the regression for the F-PVT consistently lies under the regression for the NF-PVT with the discrepancy between the two increasing as the temperature difference increases. This is because of the significantly higher a_1 of the NF-PVT, see Table 8. At a non-zero irradiance, the F-PVT outperforms the NF-PVT at smaller temperature differences, while the opposite is true at high temperature differences. This is because at higher irradiances, the majority of the thermal energy gained by the brine is from cooling the PV panel rather than from heat exchange with the ambient. Therefore, the higher zero-loss efficiency of the F-PVT is the key contributor to the specific thermal power output. At these higher irradiances, the heat exchange with the ambient only becomes relevant at larger temperature differences, meaning the effect of the higher a_1 of the NF-PVT can be observed. As the irradiance level increases, the temperature difference at which the NF-PVT begins to outperform the F-PVT increases, because increasingly larger

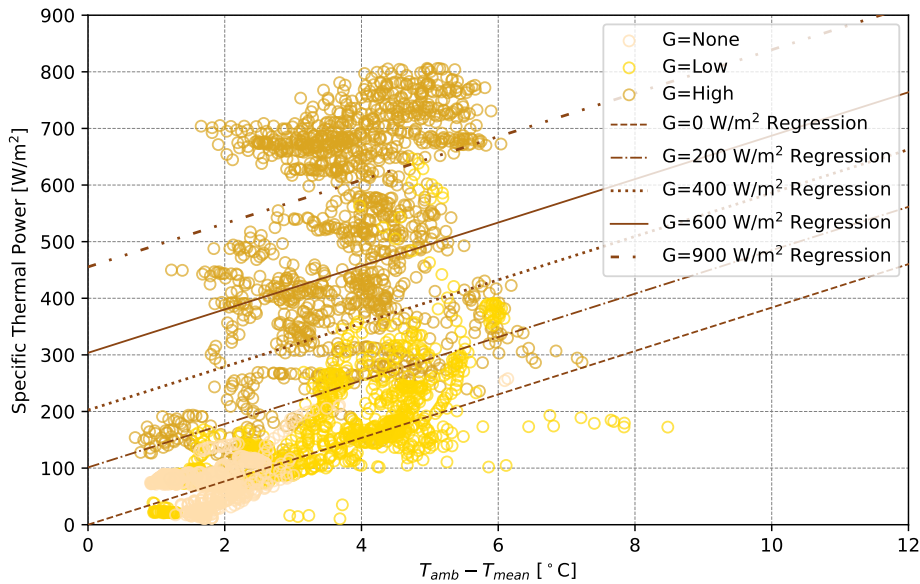


Figure 13: Regression lines for different irradiance levels for the F-PVT plotted over the obtained data. The data is colour-coded with respect to the irradiance level of each data point. The coefficients used in the calculation can be found in Table 8.

temperature differences are needed to observe the impact of the higher a_1 coefficient.

4.1.2 Impact of Wind

Similarly as for when the impact of irradiance was studied, the impact of different wind conditions, wind speed and direction, were investigated. When looking at the wind speed, all different wind directions were considered as limited amounts of data restricted further filtering by wind direction.

4.1.2.1 Different Wind Speeds

The impact of wind speed was studied at two different irradiance levels. This was done by setting the value of irradiance to either zero or 400 W/m^2 in Equation 8 when calculating the regression lines. As seen in Figure 15, at the low flow rate, increasing wind speeds increased specific thermal power output of the PVTs. It can also be seen that as the difference between the ambient and mean fluid temperatures increases, the positive impact of wind is larger. This result is expected [34], as the increasing wind speed creates a larger airflow around the PVT, enabling for more effective heat transfer from the ambient.

It was also observed that as irradiance increased, the positive impact of increasing wind speed decreased. This can be seen when comparing the impact of wind speed at the two chosen irradiance levels. At zero irradiance and a temperature difference of $4 \text{ }^\circ\text{C}$, increasing wind speed from 0.5 m/s to 3 m/s resulted in a 19% and 29%

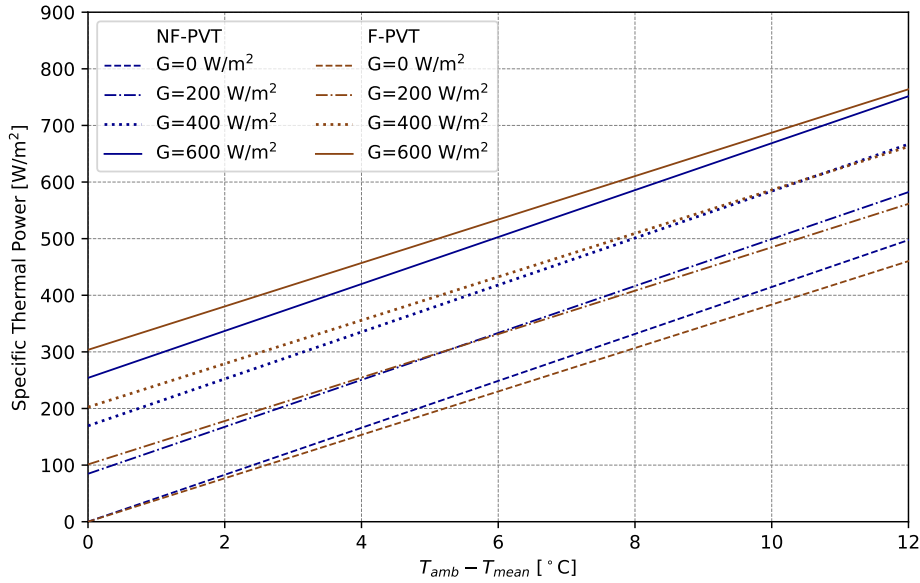


Figure 14: Comparison between NF-PVT and F-PVT at different irradiance levels.

increase in specific thermal power of the regression, for the NF-PVT and F-PVT respectively. In contrast, at an irradiance level of 400 W/m^2 and with the same temperature difference, the increase was only 9% and 12%, respectively. These results also confirm Eskola's (2023) result that as irradiance increases the impact of increasing wind speed decreases [33].

4.1.2.2 Finned vs. Non-finned

From Figure 15, it can also be seen that at zero irradiance the NF-PVT outperforms the F-PVT. However, as wind speed increases the difference between the two decreases. This shows that the F-PVT is more sensitive to changing wind speeds, with higher wind speeds being more beneficial to the thermal performance of the F-PVT than that of the NF-PVT. This can be seen by the higher a_3 of the F-PVT compared to the NF-PVT in Table 8.

At an irradiance level of 400 W/m^2 , the F-PVT thermally outperforms the NF-PVT at low temperature differences. Similarly to the impact of increasing irradiance, at higher temperature differences the NF-PVT begins to outperform the F-PVT, with the intersect temperature increasing as wind speed increases. The reasoning here is the same as the one given for this phenomenon happening with increasing irradiance: as irradiance increases the significance of the zero-loss efficiency and a_3 is greater than that of a_1 coefficient at low temperature differences, while at high temperature differences the impact of a_1 dominates.

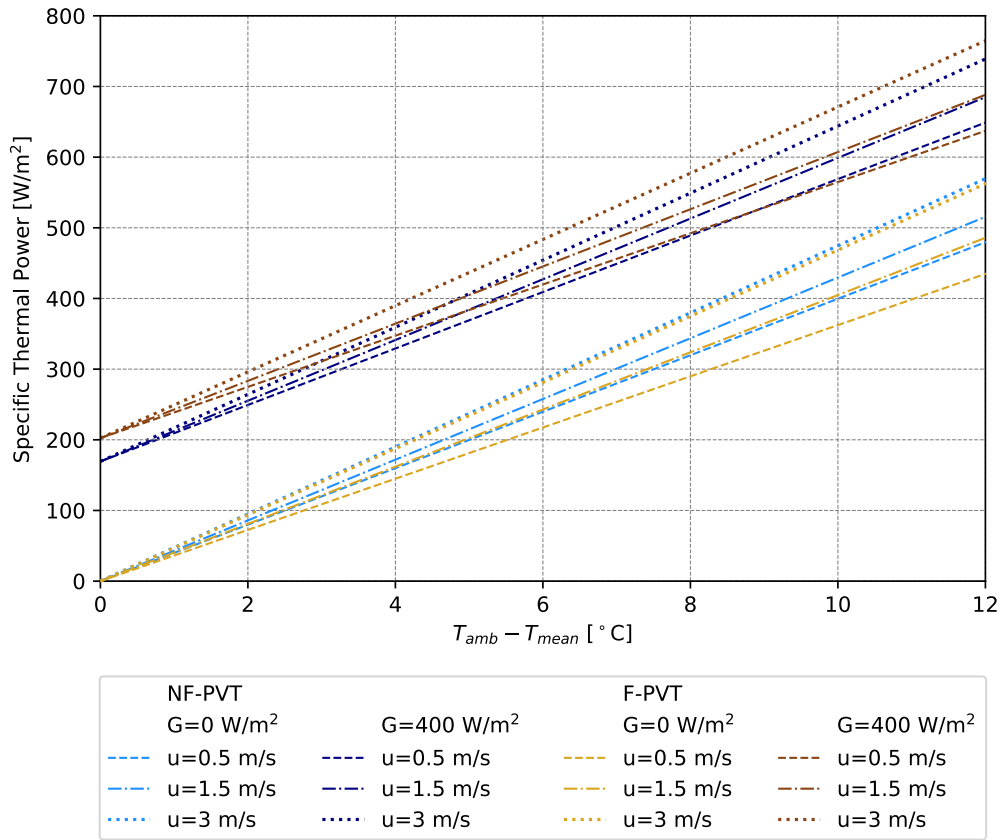


Figure 15: Regression lines for different wind levels at two different irradiance values for both the NF-PVT and the F-PVT. The coefficients used in the calculation can be found in Table 8.

4.1.2.3 Different Wind Directions

By filtering the data set by wind direction and recalculating the KPIs, the impact of the incident direction of the wind on the PVTs was studied. Table 9 gives the wind dependence for the heat loss coefficient and of the zero-loss efficiency of both the NF-PVT and F-PVT.

Table 9: Wind dependence coefficients of the NF-PVT and F-PVT with a low flow rate.

Wind Direction	NF-PVT			F-PVT		
	a_1	a_3	a_6	a_1	a_3	a_6
North	48.097	0.011	0.022	44.143	2.564	0.049
East	38.260	2.898	0.000	33.128	3.249	0.000
South	35.846	2.144	0.000	31.666	2.608	0.000
West	47.752	0.321	0.000	45.470	2.061	0.000

Similarly to the overall coefficients presented in Table 8, the a_1 of the F-PVT is lower than that of the NF-PVT at all wind directions while the a_3 is higher. The a_6 coefficient is also higher for the F-PVT when considering a north wind direction, towards the front of the PV panel. For the remaining wind directions a_6 was zero for both PVTs.

The results also show that both PVTs are more strongly affected by the wind when it is blowing east, across the back of the PVT, or south, towards the back of the PVT. This can be seen by the higher a_3 for the south and east wind directions. This can be explained by the fact that when the wind is blowing in these directions the PVTs are more sheltered, seen by the lower a_1 , and so only small variations in wind speed are actually experienced by the PVTs. This then results in the regression overestimating a_3 .

4.2 Impact of Different Roof Installations

To try and understand the impacts of different types of roof installations on the thermal performance of the PVTs, three different scenarios were tried. These included the addition of side panels and a back panel individually as well as both present.

When selecting the data points used to calculate the coefficients from Equation 5, instead of using all the collected data, the data was restricted by the time at which it was collected, see Figure 17. This was done to isolate data points where the sun was to either side of the PVT's, warming up the side panels, or reflecting off the back panel, providing additional heat to the absorber. As the impact of these phenomenon is not known, to study the steady-state impact of the roof installation these isolated data points were removed. Furthermore, when collecting data during days with a higher ambient temperature with a cloudless sky, the time-dependence of heat transfer was observed. As seen in Figure 16, during these days, between the times of 4:30 am and 7 am, as the ambient temperature was quite high while the mean fluid temperature was relatively low. This leads to a high observed temperature difference. However, as irradiance is very low at this time, only small heat gains from the ambient are measured as the PV panel has not had the chance to heat up yet. This leads to low power outputs at high temperature differences which lowers the specific thermal power output of the calculated regression at high temperature differences. While this is something that is observed during ordinary operation, to quantify the effect of the type of roof installation a more steady-state operation is desired as mentioned above.

The impact of the changing irradiance conditions as well as wind speed was studied for the different roof installation types. It was found that the roof installations did not affect the general impact of the increasing irradiance or wind speed on the specific power of the PVTs as the trends observed were the same as for the baseline. Any differences to the baseline will be further discussed in Section 5 after the presentation of the results.

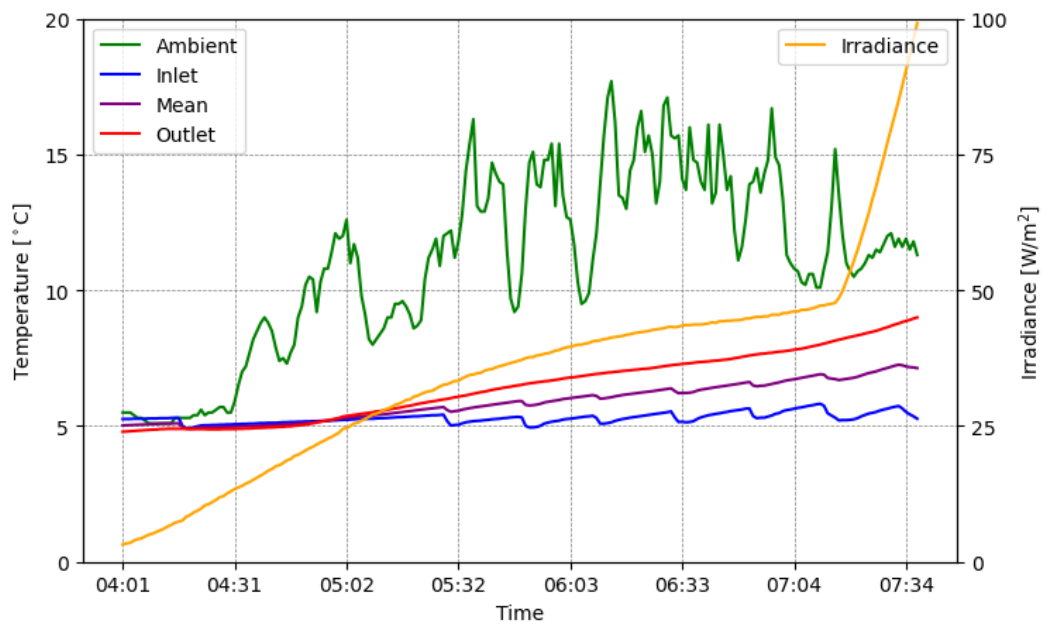


Figure 16: Raw data measured of the NF-PVT on the 21 of May 2024, to justify the removal of time dependent data points.

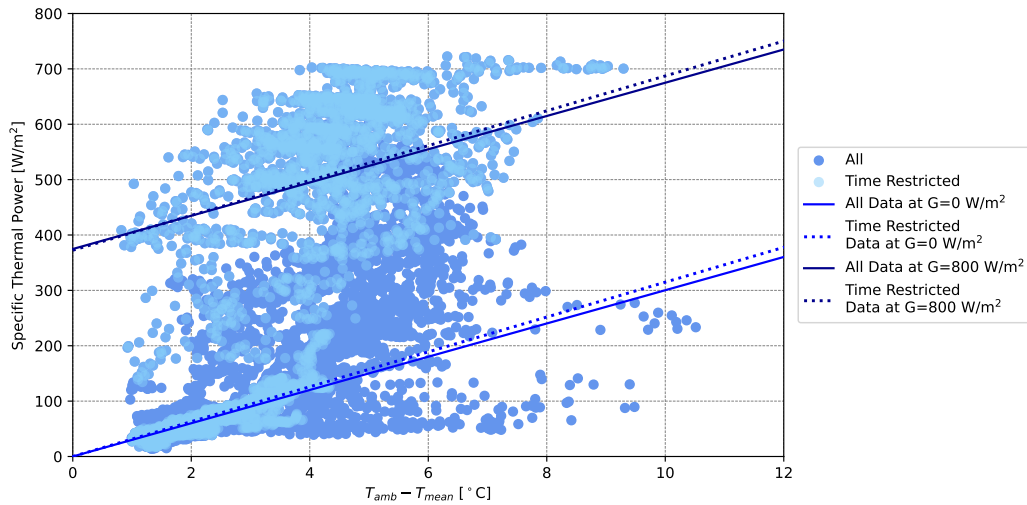


Figure 17: Impact of time-restricted filtering on the NF-PVT during operation with side panels. The coefficients used for the regressions can be found in time-restricted regression line can be found in Table 10 while the coefficients to calculate the overall regression lines can be found in Appendix B in Table B2.

4.2.1 Side Panels

The impact of the above-mentioned time restricted filtering can be seen in Figure 17 for the NF-PVT. At zero irradiance, the time-restricted regression always overestimates the specific thermal power output with respect to the overall regression, obtained using all available data points. For the NF-PVT the overestimate is 5%. At an irradiance level of 800 W/m^2 , the time-restricted regression first slightly underestimates the specific thermal power of the overall regression at low temperature difference and then gradually overestimates it at high temperature differences. However at a temperature difference of $10 \text{ }^\circ\text{C}$, the time-restricted data set overestimates the overall regression by less than 2%. The same trend can be seen for the F-PVT, however the overestimate is 8% and 2%. Figure C3 for the F-PVT can be found in Appendix C. Nevertheless, for the majority of the observed conditions the two regression lines give very similar outputs.

The time-restricted data corresponds to 3,362 data points, translating to approximately 56 hours of operation and the ambient conditions over this period can be found in Appendix A. In Table 10, the time-restricted coefficients can be seen. Similarly to the baseline coefficients, the F-PVT displays a higher zero-loss efficiency resulting in a approximately 6% higher annual thermal energy output. The NF-PVT again has a higher a_1 while the F-PVT has higher wind speed dependencies.

4.2.1.1 Impact of Irradiance and Wind Speed

When side panels were present, a 200 W/m^2 increase in irradiance on the NF-PVT resulted in a 93 W/m^2 increase in specific thermal power of the regression irrespective

Table 10: KPIs of the NF-PVT and F-PVT with a low flow rate and side panels.

KPI	NF-PVT	F-PVT
Annual Thermal Energy	1906	2016
η_0	0.478	0.562
a_1	26.708	21.626
a_3	4.773	6.493
a_6	0.012	0.016
R^2	0.97	0.97

of the temperature difference between the ambient and the mean brine temperatures. For the F-PVT, this increase was calculated to be 109 W/m^2 . Figure C4 in Appendix C shows how the regression for the NF-PVT compares to the F-PVT at different irradiance levels. The trends observed are the same as in the low flow rate case.

In terms of the impact of wind, at zero-irradiance, the NF-PVT experienced a 41% increase in specific thermal power of the regression when the wind speed increased from 0.5 m/s to 3 m/s. For the F-PVT this increase was 65%. At an irradiance level of 400 W/m^2 and a temperature difference of $4 \text{ }^\circ\text{C}$, this increase was only 12% and 15% for the NF-PVT and F-PVT respectively. When comparing how the NF-PVT and F-PVT behave under different wind speeds, the trends observed are the same as for the low flow rate. However, as seen in Figure 18, at an irradiance level of 400 W/m^2 and at a really small temperature difference lower wind speeds lead to higher specific thermal power outputs than high wind speeds, for both PVTs.

4.2.1.2 Impact of Wind Direction

Because the side panels restrict the wind blowing across the back of the absorber, east and west, but create a wind channel if the wind is blowing perpendicularly to the PVT, south and north, the impact of wind direction was studied. The coefficients for the different wind directions can be seen in Table 11. When filtering by wind direction it was found that during the observed time period, the wind direction was north for less than 50 non-consecutive minutes and so this direction was not considered in the analysis.

Table 11: Wind dependence coefficients of the NF-PVT and F-PVT with a low flow rate and side panels.

Wind Direction	NF-PVT			F-PVT		
	a_1	a_3	a_6	a_1	a_3	a_6
North	-	-	-	-	-	-
East	25.097	3.815	0.000	18.241	4.769	0.000
South	28.373	2.979	0.000	25.097	4.114	0.000
West	20.778	14.690	0.097	22.587	14.785	0.107

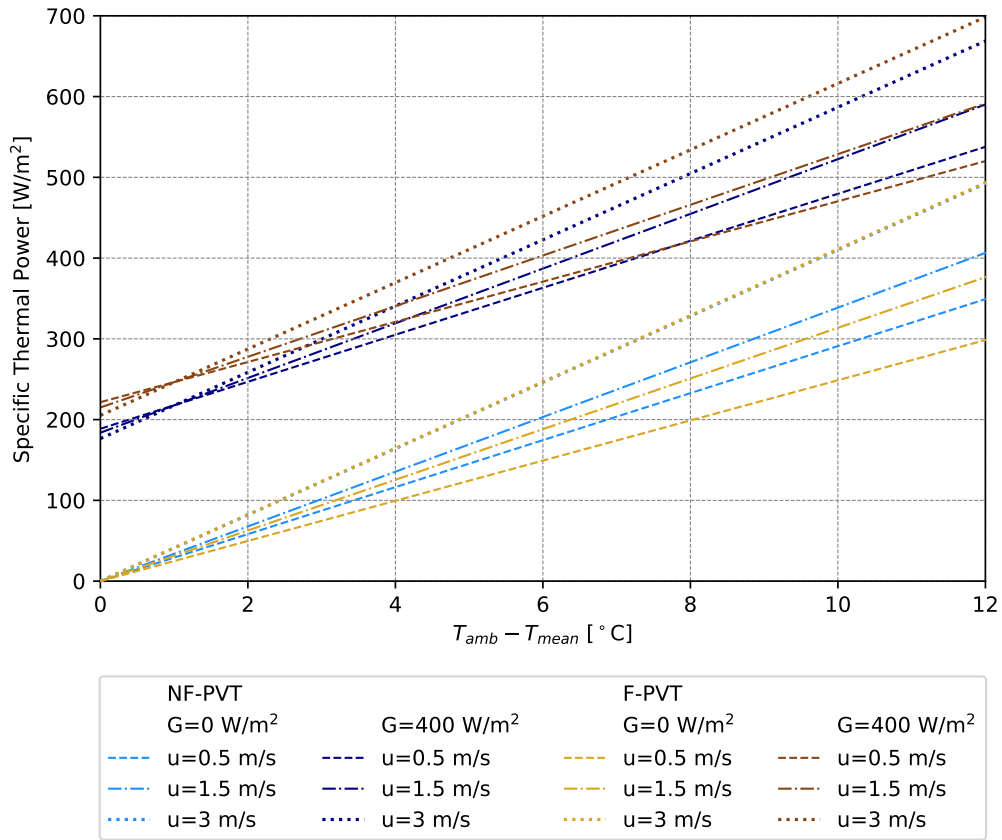


Figure 18: The regression lines for both the NF-PVT and the F-PVT at two different irradiance levels, comparing the impact of wind speed when the side panels were attached. The coefficients used for the regression lines can be found in Table 10.

With the side panels, despite the PVTs being sheltered from wind blowing south, the wind direction was parallel to the fins, resulting in an increased a_1 compared to the east and west blowing winds. This is in line with what is expected from literature [28].

As evidenced by all the previously presented results, the increased a_3 of the F-PVT shows that the fins increase the wind dependence of the absorber.

The large observed difference between the east and west coefficients, which were expected to be the same as in both cases the wind is blowing perpendicular to the fins, can be explained by the use of different data set when recalculating the wind direction coefficients. As seen in Table A2 in Appendix A, all observed ambient conditions are significantly lower when considering the east wind direction compared to the west. This will skew the results of both regressions to describe the average conditions experienced.

4.2.2 Back Panel

The time-restricted filtering for the data collected when there was a roof attached behind the PVT had a similar impact on the coefficients as for when the side panels were attached. However, considering the back panel data, the overestimate, with respect to the overall regression, at zero irradiance was 14% and 27% respectively for the NF-PVT and F-PVT. For the NF-PVT at an irradiance level of 800 W/m^2 , for low temperature differences the time-restricted regression underestimates the specific thermal power output of the overall regression, with the underestimate being at 4% lower at a temperature difference of 2°C . At a temperature difference of 10°C the overestimate is just under 2%. For the F-PVT, at 800 W/m^2 the under- and overestimates were 5% and 3% respectively. These larger discrepancies come from the fact that when the back panel was present there were more data points recorded with a low power at higher temperature differences. This skews the regression towards calculating a low power output at high temperature differences. This can be seen in Figures C5 and C6 in Appendix C. However, to keep the comparison between the data sets fair the filtering parameters were maintained.

The time-restricted data set contains 3,201 data points corresponding to approximately 53 hours of operational data. The ambient conditions over this period are given in Appendix A. Table 12 shows the time-restricted coefficients for both the NF-PVT and the F-PVT. The overall coefficients of the entire data set can be found in Appendix B in Table B4.

Table 12: KPIs of the NF-PVT and F-PVT with a low flow rate and a roof.

KPI	NF-PVT	F-PVT
Annual Thermal Energy	1723	1840
η_0	0.488	0.554
a_1	29.857	28.197
a_3	2.041	3.224
a_6	0.004	0.014
R^2	0.96	0.96

As with both cases before, the F-PVT has a higher annual thermal energy output than the NF-PVT. In the case of the back panel, the annual thermal energy output of the F-PVT is 7% higher. The other calculated KPIs follow the previously observed trends: F-PVT has a higher zero-loss efficiency, NF-PVT has a higher a_1 and the F-PVT has a higher a_3 and a_6 .

4.2.2.1 Impact of Irradiance and Wind Speed

For the back panel, a 200 W/m^2 increase in irradiance for the NF-PVT resulted in a 97 W/m^2 increase in specific thermal power of the regression irrespective of the temperature difference between the ambient and the mean brine temperatures. For the F-PVT, this increase was calculated to be 107 W/m^2 . Figure C7 in Appendix C, shows

the calculated regression lines for both PVTs, displaying the same trends as for both the low flow rate and the side panel experiments.

In terms of the impact of wind, at zero-irradiance, the NF-PVT experienced a 17% increase in specific thermal power of the regression when the wind speed increased from 0.5 m/s to 3 m/s. For the F-PVT this increase was 27%. At an irradiance level of 400 W/m² and a temperature difference of 4 °C the increase in specific thermal power was only 5% for both PVTs, considering the same increase in wind speed. Figure C8 in Appendix C compares the regression lines for the two PVTs at different wind speeds. The trends observed are the same as explained before for the low flow rate and side panels.

4.2.2.2 Impact of Wind Direction

Like with the side panels, the back panel will create a wind-channel, however unlike the side panels the back panel will create a wind channel no matter the direction of the wind. To quantify the impact of wind direction on the PVT with a back panel, the data was filtered by wind direction and the coefficients recalculated. The coefficients for the different wind directions can be seen in Table 13.

Table 13: Wind dependence coefficients of the NF-PVT and F-PVT with a low flow rate and a back panel.

Wind Direction	NF-PVT			F-PVT		
	a_1	a_3	a_6	a_1	a_3	a_6
North	-	-	-	-	-	-
East	27.919	4.441	0.000	21.687	4.194	0.000
South	30.418	1.733	0.000	29.322	2.355	0.002
West	25.710	3.213	0.000	25.545	3.676	0.001

Similarly to the results of the side panels, there were insufficient data point recorded for the wind blowing north. Additionally, the a_1 of both PVTs is highest for south blowing wind. This supports the conclusion that the creation of the wind channel aids in increasing the heat transfer with the ambient. However, as here the wind channel is for all wind directions it can be seen that when the wind is blowing parallel to the direction of the fins, it is more beneficial for heat transfer than when the wind is blowing perpendicular to the fins. This is because when the wind is blowing perpendicular to the fins, the outer fins act as shields sheltering the inner fins from the impact of the wind.

When the wind is blowing west, the two heat transfer coefficients are almost equal. As the NF-PVT is more exposed to west blowing winds than the F-PVT, it can be concluded that the fins do aid in heat transfer. This can be deduced because if the fins did not help with heat transfer the a_1 of the F-PVT would be much lower than that of the NF-PVT.

In contrast, for the east direction wind, the F-PVT is much more sheltered than from the west blowing winds. Therefore, despite the theoretical positive impact of

the fins, there is not enough wind incident on the absorber for them to affect the heat exchange. As the NF-PVT is more exposed to the east blowing wind, the a_1 of the NF-PVT is much higher than the F-PVT in this case.

The differences in the calculated a_3 coefficients for the different wind directions can be explained by the use of different data sets. For the east direction, the a_3 coefficients of the two PVTs fall within statistical uncertainty of each other, while in the south and west direction the impact of the fins can be seen in the higher a_3 of the F-PVT.

4.2.3 Back and Side Panels

When the back and side panels were added, the time-restricted data affected the coefficients following the same trend as for when they were added individually. For the NF-PVT, at zero irradiance, the time-restricted data overestimated the specific thermal power of the overall regression by 4%. For the same conditions when considering the F-PVT the overestimate is 18%. At an irradiance level of 800 W/m^2 and a temperature difference of $2 \text{ }^\circ\text{C}$, for the NF-PVT the underestimate of the specific thermal power of the overall regression is only 1% while for the F-PVT it is 2%. At the same irradiance level but at a temperature difference of $10 \text{ }^\circ\text{C}$ the specific thermal power was overestimated by 1% for the NF-PVT and 3% for the F-PVT. For the case of the NF-PVT, Figure C9 in Appendix C shows that the two regression lines give very similar specific thermal power outputs at all observed conditions. However for the F-PVT, seen in Figure C10, the difference in the specific thermal power outputs is larger. Nonetheless, to ensure comparability the filtering was applied to both data sets.

A total of 2,158 data points were collected for the PVTs with both the side panels and the roof attached. This is equal to roughly 36 hours of operation time and the ambient conditions can be seen in Appendix A. The coefficients calculated from this data set can be found in Table 14, along with the other KPIs.

Table 14: KPIs of the NF-PVT and F-PVT with a low flow rate, a roof and side panels.

KPI	NF-PVT	F-PVT
Annual Thermal Energy	1528	1451
η_0	0.507	0.560
a_1	21.899	21.382
a_3	2.786	1.943
a_6	0.015	0.019
R^2	0.97	0.97

With this roof installation the F-PVT performs worse than the NF-PVT in terms of annual thermal energy output. The F-PVT experiences a 5% decrease in annual thermal energy when compared to the NF-PVT. This could be due to the significantly higher a_3 coefficient of the NF-PVT compared to the F-PVT. However, when comparing the overall coefficients in this case, it can be seen that the absorbers of the PVTs are very similar in terms of their thermal performance. This should be the case as when

both the side panels and the roof were present, the impact of wind on the absorber has been significantly reduced, leading to the fins not having an impact on the thermal performance of the absorber.

4.2.3.1 Impact of Irradiance and Wind Speed

For the back and side panel installation, a 200 W/m^2 increase in irradiance at the NF-PVT resulted in a 98 W/m^2 increase in specific thermal power of the regression irrespective of the temperature difference between the ambient and the mean brine temperatures. For the F-PVT, this increase was calculated to be 108 W/m^2 . This can be seen in Figure C11 in Appendix C where the regression lines of the two PVTs are compared at different irradiance levels.

In terms of the impact of wind, at zero-irradiance, the NF-PVT experienced a 30% increase in specific thermal power of the regression when the wind speed increased from 0.5 m/s to 3 m/s. For the F-PVT this increase was 22%. At an irradiance level of 400 W/m^2 and a temperature difference of $4 \text{ }^\circ\text{C}$, this increase in specific thermal power was only 4% for the NF-PVT, while the F-PVT experienced a negligible increase. This is shown in Figure C12 in Appendix C where the NF-PVT regression is compared the F-PVT regression at different wind speeds considering two irradiance levels.

4.3 Medium Flow Rate

The data set corresponding to the medium flow rate consisted of 2,656 data points, or approximately 44 hours of operational time. Figures C13 and C14 in Appendix C show the data points grouped by irradiance level. The ambient conditions over this operational period can be seen in Appendix A. The KPIs of the medium flow rate data set can be seen in Table 15.

Table 15: KPIs of the NF-PVT and F-PVT with a medium flow rate.

KPI	NF-PVT	F-PVT
Annual Thermal Energy	2427	2685
η_0	0.470	0.523
a_1	29.206	27.032
a_3	9.951	12.304
a_6	0.062	0.064
R^2	0.9	0.9

In the case of the medium flow rate, the F-PVT provided 11% more annual thermal energy than the NF-PVT. Similarly to the overall coefficients found for the low flow rate, the a_1 of the NF-PVT is higher at the medium flow rate while the a_3 is lower than those of the F-PVT. A more detailed comparison between the results of the low flow rate and the medium flow rate are provided in the Discussion section.

4.3.1 Impact of Irradiance

When looking at the impact of irradiance for the medium flow rate, the trend observed for the individual PVTs was the same as for the baseline. It was calculated that a 200 W/m^2 increase in irradiance resulted in an 82 W/m^2 increase in specific thermal power of the regression for the NF-PVT, irrespective of the temperature difference between the ambient and the mean brine temperatures. For the F-PVT, this increase was calculated to be 92 W/m^2 .

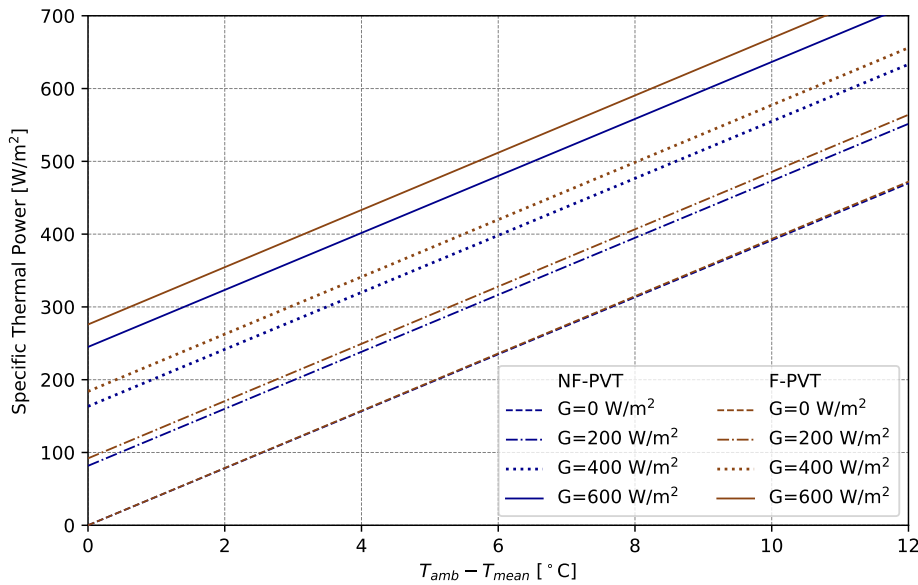


Figure 19: Comparison between NF-PVT and F-PVT at different irradiance levels for the medium flow rate.

When comparing the NF-PVT to the F-PVT at the medium flow rate, see Figure 19, it was observed that at zero irradiance, and wind speed of 1 m/s , the F-PVT marginally outperforms the NF-PVT by 0.5% . This is because of the higher a_6 coefficient of the F-PVT compared to the NF-PVT. While the difference between the two PVTs is not statistically significant, because this result varies from the low flow rate case where the NF-PVT significantly outperforms the F-PVT, an observation regarding the increasing flow rate can still be made. This observation is that the higher flow rate improves the F-PVT's thermal performance compared to the NF-PVT. As irradiance increases, the F-PVT's regression results in increasingly higher specific thermal power outputs than the NF-PVT. This is because of the higher zero-loss efficiency of the F-PVT.

4.3.2 Impact of Wind Speeds

Similarly to the analysis in of different wind speeds at the low flow rate, at the medium flow rate the same trends were observed. This can be seen in Figure 20. In terms of the specific impact of wind, at zero-irradiance, the NF-PVT experienced a 73%

increase in specific thermal power of the regression when the wind speed increased from 0.5 m/s to 3 m/s. For the F-PVT this increase was 93%. At an irradiance level of 400 W/m^2 and a temperature difference of $4 \text{ }^\circ\text{C}$, this increase in specific thermal power was only 12% for the NF-PVT, and 18% for the F-PVT.

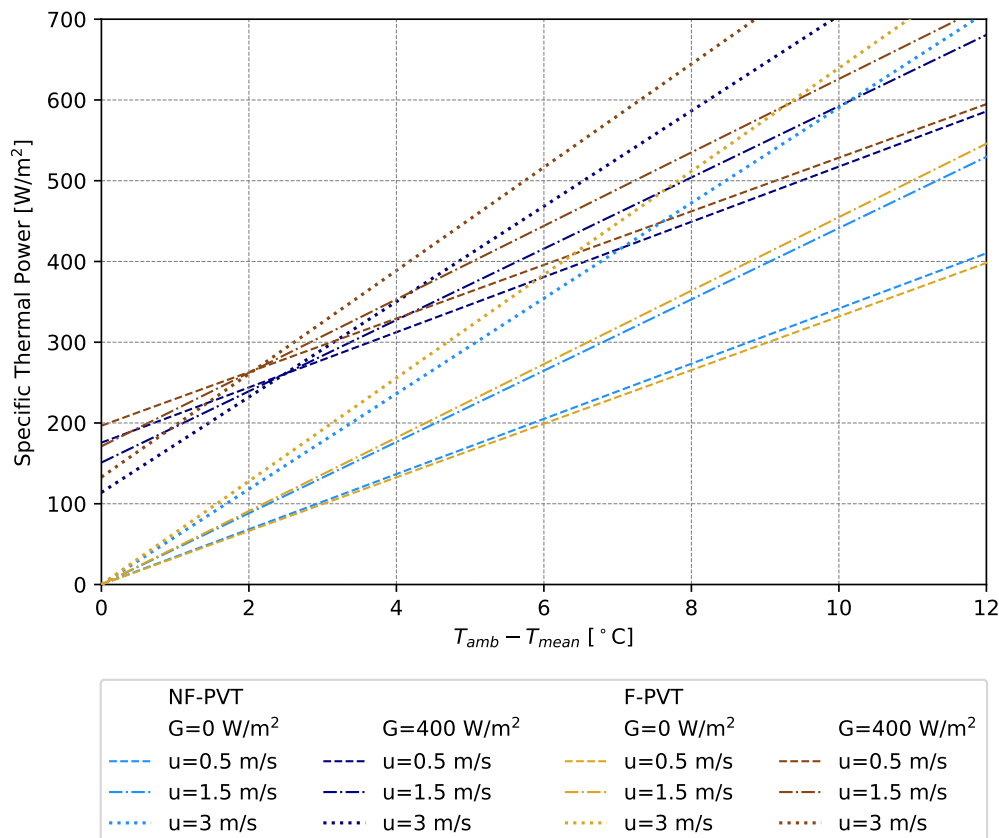


Figure 20: The impact of different wind speed on the specific thermal power output of the NF-PVT at the medium flow rate and two different irradiance levels.

At the medium flow rate the increase in specific thermal power output with increasing wind is much larger than observed for the low flow rate. This fact can be explained by the relative velocity of the ambient air and the brine in the absorber. As flow rate increases, the heat absorbed from the PV is taken away faster allowing for the brine to absorb more heat from the ambient. At the higher wind velocity, the wind is also replacing the cold air with warm air more rapidly, allowing for efficient heat transfer.

Unlike in the low flow rate case, for the medium flow rate, the NF-PVT only thermally outperforms the F-PVT at zero-irradiance and low wind speeds. Under all other conditions the F-PVT outperforms the NF-PVT, with higher wind speeds resulting in higher improvements to the specific thermal power output. Like with the irradiance at the medium flow rate, the faster flow rate serves to improve the thermal performance of the F-PVT compared to the NF-PVT.

4.3.3 Impact of Wind Direction

To study the impact of wind direction, the medium flow rate data set was divided based on wind direction. The calculated coefficients can be found in Table 16.

Table 16: Wind dependence coefficients of the NF-PVT and F-PVT with a medium flow rate.

Wind Direction	NF-PVT			F-PVT		
	a_1	a_3	a_6	a_1	a_3	a_6
North	39.689	6.006	0.102	38.911	6.036	0.109
East	33.984	8.885	0.054	28.402	11.931	0.069
South	25.080	12.884	0.080	21.829	17.273	0.098
West	28.604	2.343	0.171	30.379	2.694	0.148

In the case of the medium flow rate, when the wind was blowing to the north, the a_1 coefficient was higher for both PVTs than in the other wind directions. This could be because here the wind is blowing directly towards the front of the PVT and so the wind will push air up along the back of the absorber. This means the air is moving in the same direction as the brine resulting in a lower apparent wind velocity compared to when the wind is blowing in the south direction. In these cases, the wind is moving opposite to the brine and so the apparent wind velocity is much higher leading to the high a_3 coefficients observed. At this medium flow rate, the higher apparent wind speeds might begin to hinder heat transfer with the ambient as there is not enough time for the heat to be absorbed by the brine. This suggests that there is a maximum desired wind velocity for optimal heat exchange with ambient, depending on the flow rate.

The difference between the results for the east and west directions of the two PVTs can be explained by the different levels of shelter provided by the test rig and the differences in the ambient conditions during those times, as seen in Appendix A.

4.4 High Flow Rate

There were 4662 data point recorded at the high flow rate. This is equivalent to roughly 77 hours of operational time. Figures C15 and C16 in Appendix C show the measured data points. The ambient conditions over these 77 hours can be found in Appendix A. The KPIs obtained at the high flow rate can be seen in Table 17.

The annual thermal energy output of the F-PVT is 16% higher than that of the NF-PVT. Similarly to both previously tested flow rates, the trends of the coefficients are the same. The zero-loss and a_3 of the F-PVT are higher than the NF-PVT and the a_1 of the NF-PVT is higher than the F-PVT.

At this flow rate however, the difference between the a_1 coefficients of the NF-PVT and the F-PVT are very small, meaning the two results are within statistical error of each other. This shows that at a high flow rate the impact of the fins is larger as the a_1 coefficients are comparable.

Table 17: KPIs of the NF-PVT and F-PVT with a high flow rate.

KPI	NF-PVT	F-PVT
Annual Thermal Energy	2033	2360
η_0	0.267	0.326
a_1	45.979	45.419
a_3	1.939	4.313
a_6	0.000	0.000
R^2	0.87	0.86

4.4.1 Impact of Irradiance

As with the two previous flow rates, it was found that an increasing irradiance level led to higher specific thermal power outputs for both PVTs as seen in Figure 21. At the high flow rate, a 200 W/m^2 increase in irradiance resulted in a 53 W/m^2 increase in specific thermal power output of the regression for the NF-PVT, while for the F-PVT the increase was 65 W/m^2 .

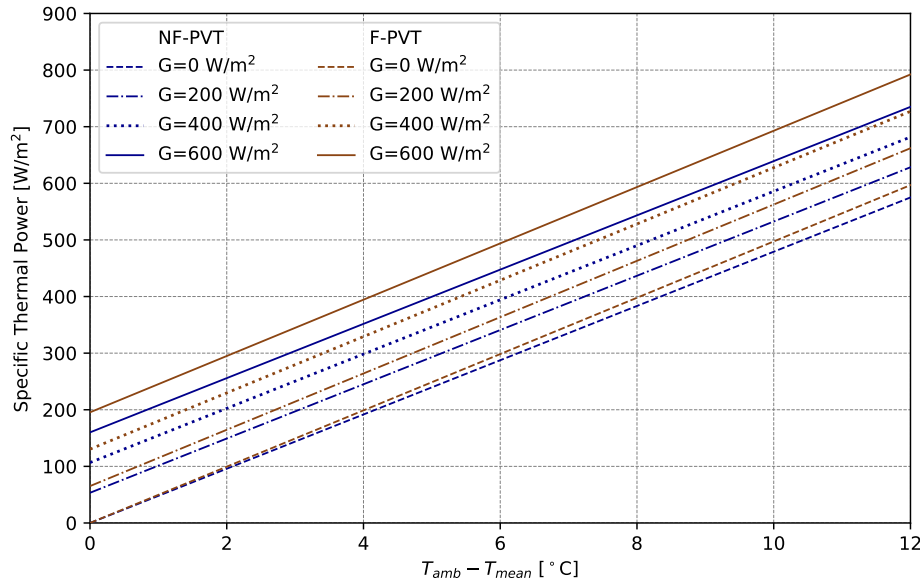


Figure 21: Comparison between NF-PVT and F-PVT at different irradiance levels for the high flow rate.

Like for the medium flow rate, at the high flow rate the F-PVT always thermally outperforms the NF-PVT. Unlike for the other flow rates, the regression line of the two PVT's at non-zero irradiances are almost parallel as the a_1 coefficients are very similar. This means that they will intersect at a very high temperature difference, one that is not achieved in standard operation. Therefore at the high flow rate, the F-PVT

will always thermally outperform the NF-PVT in standard operation.

4.4.2 Impact of Wind Speed

As in the analysis of different wind speeds at the low and medium flow rate, at the high flow rate the same trends in the individual PVTs were observed. This can be seen in Figure 22, showing that as wind speed increases or the temperature difference increases, the thermal performance of both PVTs increases. In terms of the specific impact of wind, at zero-irradiance the NF-PVT experienced a 10% increase in the specific thermal power of the regression when the wind speed increased from 0.5 m/s to 3 m/s. For the F-PVT this increase was 23%. At an irradiance level of 400 W/m² and a temperature difference of 4 °C, this increase was 7% for the NF-PVT, while the F-PVT experiences an 13% increase.

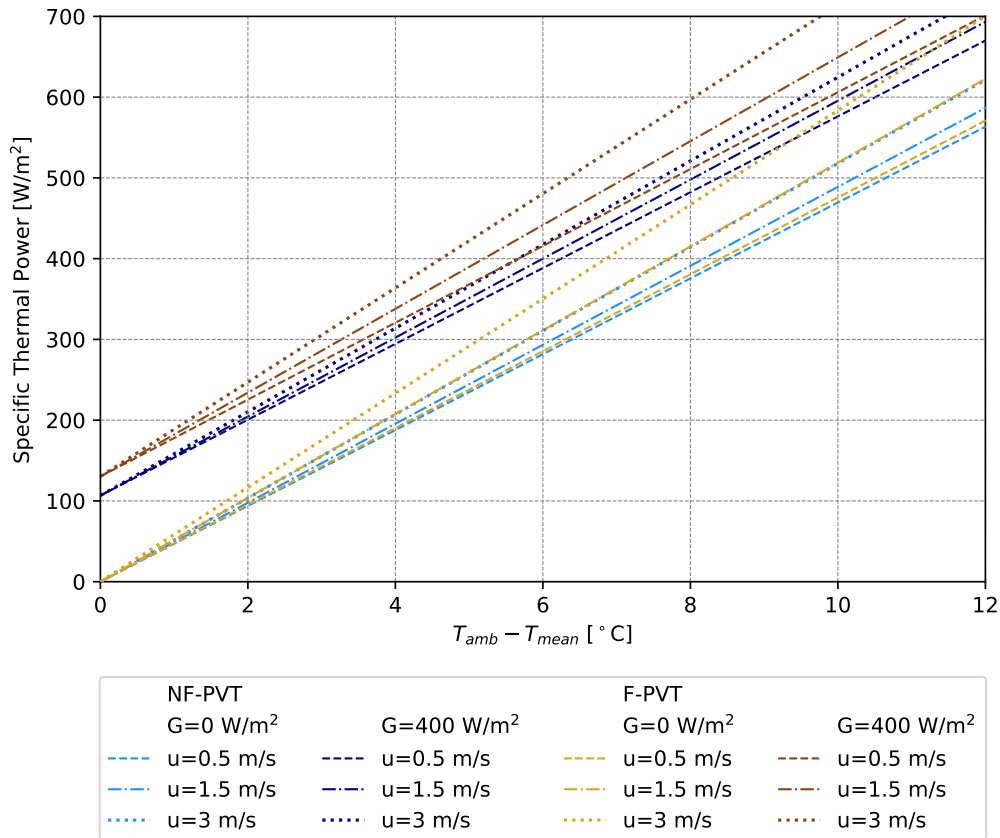


Figure 22: Comparison between NF-PVT and F-PVT at different wind levels for the high flow rate.

At the high flow rate the increase in specific thermal power output with increasing wind is much lower than observed for the medium flow rate. This shows that there is an optimum operational conditions between wind speed and flow rate, as higher wind speeds are more beneficial at certain flow rates. At the high flow rate, the velocity

of the fluid is too fast to fully take advantage of the increased wind speed. This is because there is insufficient time for the fluid to absorb heat from the ambient.

In the case of the high flow rate, as observed with the irradiance levels, the F-PVT thermally outperforms the NF-PVT at all wind levels. This again shows that the higher flow rate benefits the thermal performance of the F-PVT more than that of the NF-PVT.

4.4.3 Impact of Wind Direction

The coefficients for the wind separated data of the high flow rate can be found in Table 18. At the high flow rate, the a_1 of the west direction is the largest for both PVTs, this can be explained by the significantly higher wind speed experienced at this wind direction that for the others, see Appendix A. Discounting this result due to the very different ambient conditions for this data set, the north and south wind directions have the highest a_1 coefficients. This shows that the wind blowing parallel to the fins aids heat transfer. Furthermore, at the high flow rate, the a_1 coefficient for all wind directions is higher for the F-PVT than the NF-PVT. This shows that at higher flow rate the fins have a larger positive impact on the ability of the PVT to exchange heat with the ambient.

Table 18: Coefficients of the NF-PVT and F-PVT for different wind directions at a high flow rate.

Wind Direction	NF-PVT			F-PVT		
	a_1	a_3	a_6	a_1	a_3	a_6
North	40.967	2.688	0.000	44.475	4.486	0.000
East	37.887	6.879	0.014	40.348	8.209	0.020
South	40.880	4.925	0.000	41.571	7.279	0.000
West	47.119	1.342	0.000	54.596	2.365	0.000

Like before, the overall higher a_3 of the F-PVT compared to the NF-PVT shows that the fins increase the wind dependence of heat transfer. However, when comparing the a_3 coefficients of different wind directions, the greater shelter from south and east blowing winds results in overestimated a_3 values by the regression. This happens because of the discrepancy between the measured wind speed by the weather station and the wind speed experienced by the PVTs.

4.5 Model Results

To see if the model accurately described the experimental results a comparison of the specific power was made between the numerical model and the calculated NF-PVT baseline regression. This comparison can be seen in Table 19. At zero-irradiance, the modelled specific thermal power does not match the experimentally measured specific thermal power of the NF-PVT. This could be due to the way the model calculates the heat transfer between the ambient air and the aluminium micro-channel, as at zero irradiance heat from the ambient is the only heat gained by the fluid. At non-zero

irradiance, the numerical model more closely calculates the specific thermal power expected from the experimental regression.

Table 19: Comparison of the numerically modelled and NF-PVT regression of specific thermal power output under different ambient conditions.

Irradiance	$T_{amb} - T_{mean}$	Experimental	Modelled
W/m ²	°C	W/m ²	W/m ²
0	14.7	554	87
0	9.7	373	49
0	4.9	188	21
500	12.1	676	403
500	7.5	499	351
500	2.8	319	303
1000	9.6	792	751
1000	4.9	611	704
1000	0.2	431	662

4.5.1 Convective Heat Transfer Coefficients

When obtaining the convective heat transfer coefficient for different flow rate of the micro-channel, the effect of different ambient conditions such as irradiance and the temperature difference between ambient and the mean fluid temperature was studied. However, as in the model the mean fluid temperature could not be set, instead the temperature difference between ambient and the intel fluid temperature is used to give a representative temperature difference. It should be noted that the largest difference between all the presented results of the convective heat transfer coefficient is relatively small, only 548 W/(m²)K.

It was observed that under any given set boundary conditions, an increase in flow rate resulted in an increase in the convective heat transfer coefficient. This can be seen in both Figures 23 and 24. These results shows that for the flow rates tested, around the baseline flow rate of 100 l/h, the lower flow rates were too low to efficiently transfer the heat from the aluminium to the fluid.

From Figure 23 it can be seen that the largest change in the convective heat transfer coefficient for increasing flow rate occurred at zero irradiance. This is because the only available heat for transfer comes from the heat the aluminium gains from the ambient. Therefore the faster the heat is taken away by the fluid, the faster the fluid can absorb heat from the aluminium and in turn the faster the aluminium can absorb heat from the ambient.

As irradiance increases, increasing the flow rate results in diminishing returns. This is because as irradiance increases there is a significantly higher amount of heat available for heat transfer between the aluminium and the fluid. This heat is the heat the aluminium absorbs from the PV panel as it heats up due to increased irradiance.

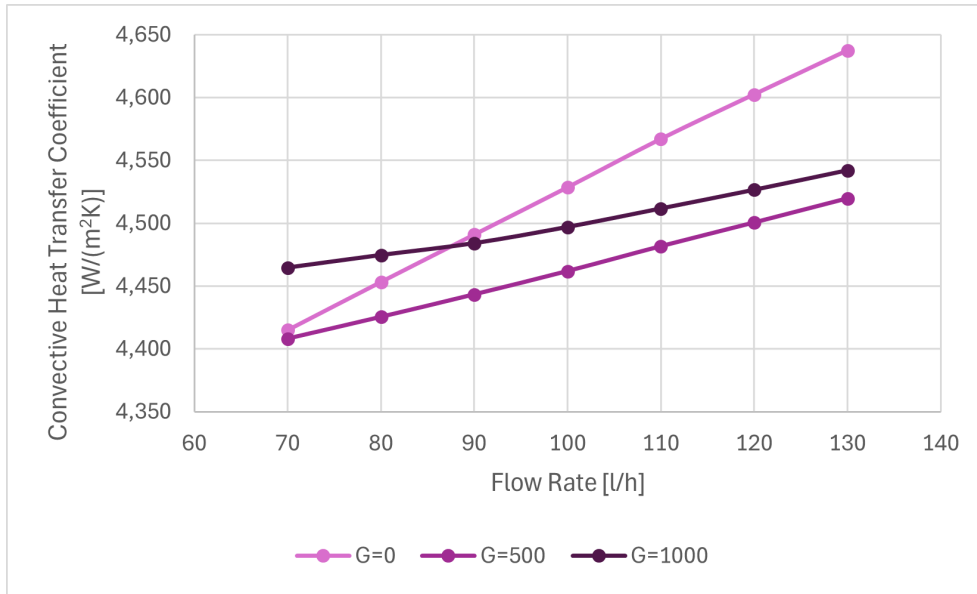


Figure 23: The impact of changing flow rates on the convective heat transfer coefficient of the micro-channel at three different irradiance levels and a constant temperature difference of 10 °C.

With this larger amount of heat available, even larger flow rates would be needed to take away the heat so that faster heat transfer can occur.

Nevertheless, when irradiance is present, higher irradiance levels will result in higher heat transfer coefficients due to the higher temperature gradients observed. However, this effect has a maximum as eventually the diminishing returns at higher irradiance prevail against the benefit of the higher temperature difference.

As the temperature difference between the ambient and the inlet increases, the heat transfer coefficient decreases, as seen in Figure 24. However, as mentioned above this is a very small change and there are many different parameters which affect the convective heat transfer coefficient.

4.5.2 Thermal Power Degradation

The specific thermal power output was calculated for each non-uniform flow scenario under all tested ambient conditions. The results presented in this section are absolute decrease in specific thermal power of each scenario to the baseline of a uniform mass flow. Like with the convective heat transfer coefficient, the absolute decrease for the scenarios is studied at different irradiance levels as well as different fluid inlet temperatures.

Figures 25, 26 and 27 shows how the different scenarios compared to the baseline at three different temperature differences between the ambient and the fluid inlet temperature. For the zero irradiance case, Figure 25, the difference between the baseline specific thermal power and the specific thermal power of the six scenarios, at all inlet temperatures, is relatively small compared to the other non-zero irradiance

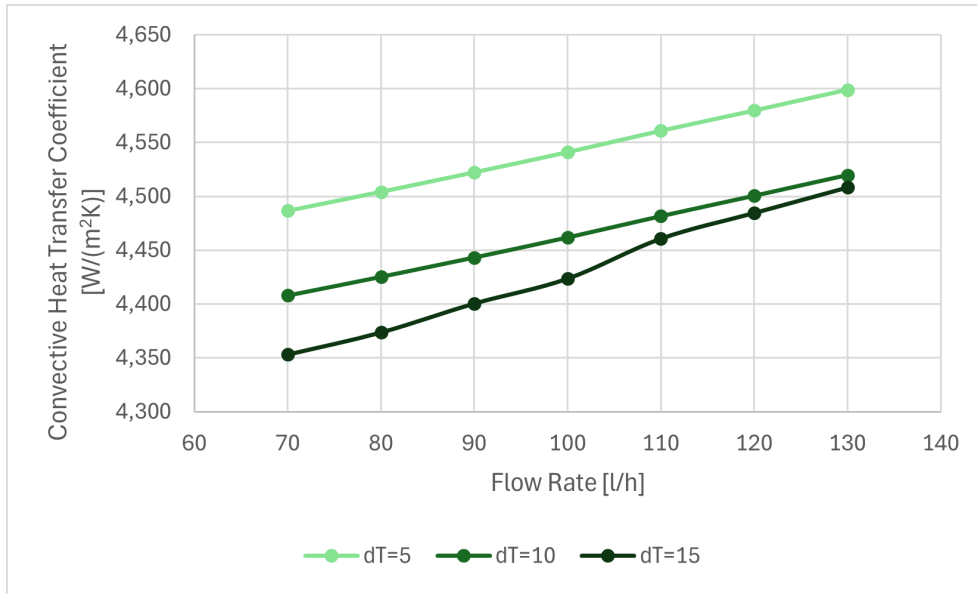


Figure 24: The impact of changing flow rates on the convective heat transfer coefficient of the micro-channel at three different temperature differences and a constant irradiance level of 500 W/m^2 .

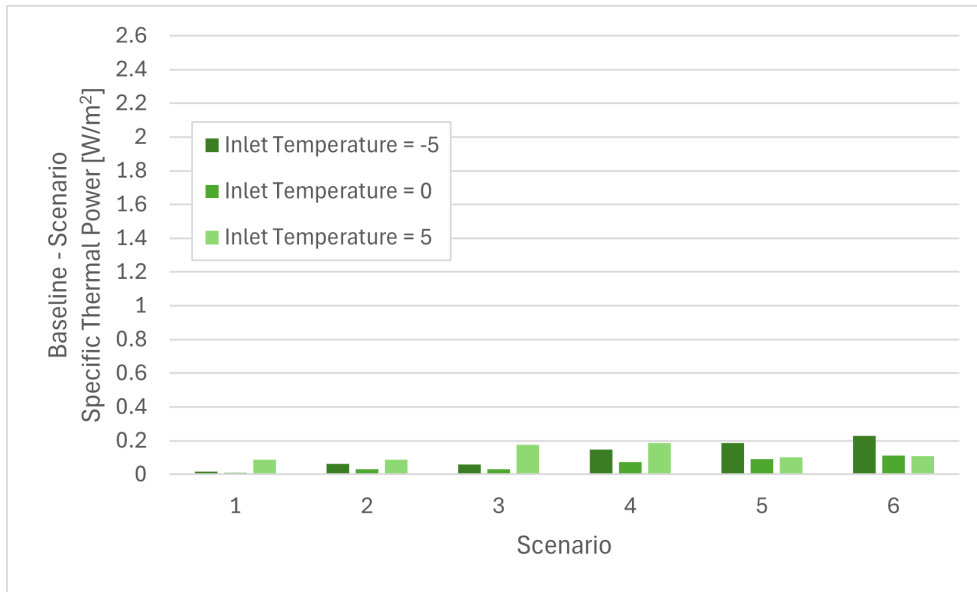


Figure 25: Comparison of the power degradation for the six scenarios at zero irradiance, for three difference temperature differences between ambient and fluid inlet temperature.

cases. At an irradiance level of 1000 W/m^2 , Figure 27, the difference between the baseline and the scenarios is the largest.

For all irradiance levels, the more uniform the flow rate distribution, the smaller the decrease in the specific thermal power. This can be seen by comparing Scenario 1

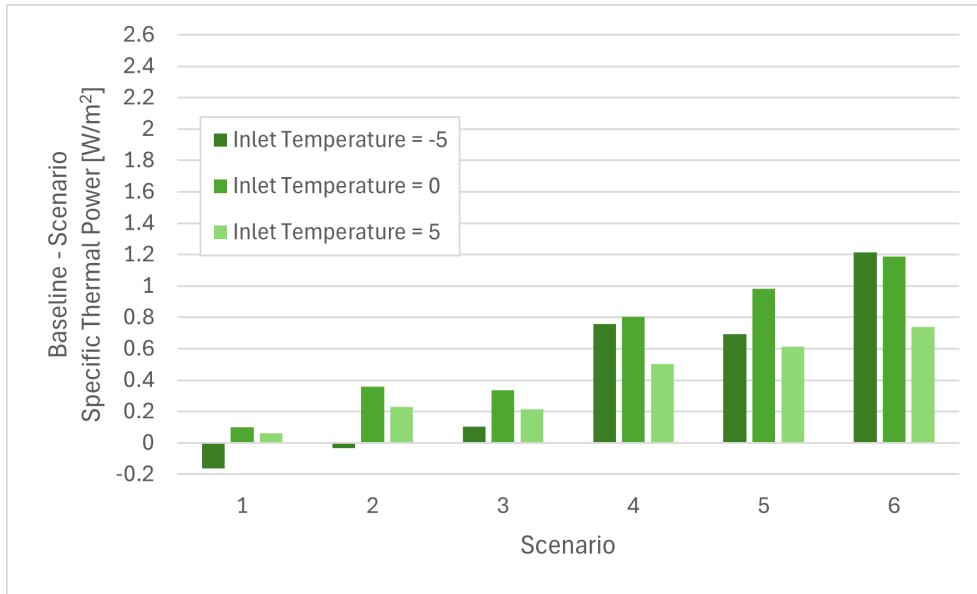


Figure 26: Comparison of the power degradation for the six scenarios at an irradiance of 500 W/m^2 , for three difference temperature differences between ambient and fluid inlet temperature.

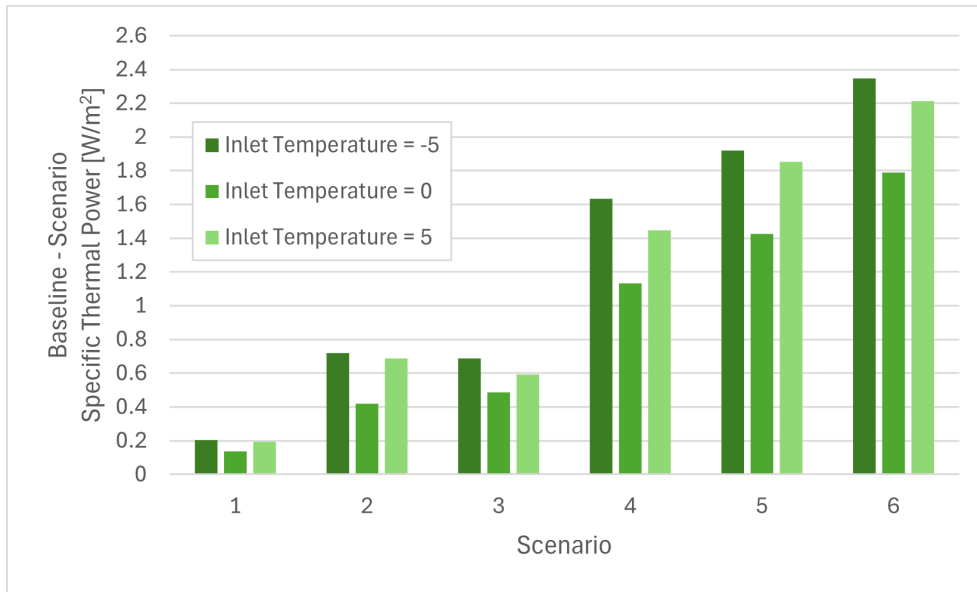


Figure 27: Comparison of the power degradation for the six scenarios at an irradiance of 1000 W/m^2 , for three difference temperature differences between ambient and fluid inlet temperature.

to Scenario 6 as well as Scenarios 2 and 3 to Scenarios 4 and 5. When comparing Scenarios 4 and 5 to Scenario 6, it can be seen that larger variation in flow rate from the baseline in any given channel the larger the negative impact will be on the final specific thermal output of scenario.

5 Discussions

In the following section, the thermal performance of the two PVTs will be compared between the different flow rates and the different roof installations. This will answer Research Questions 2 and 3, respectively. These comparisons will also be made at different ambient conditions to add to the already presented results for Research Question 1. Additionally, at the end of the section the limitations identified will be discussed.

5.1 Comparison of the PVT Collectors

One of the most consistent findings throughout this study was that the F-PVT displayed a higher zero-loss efficiency while the NF-PVT had higher values of the heat transfer coefficient, a_1 . These results are contrary to the expectation as the zero-loss efficiency was expected to be the same while the a_1 of the F-PVT was expected to be higher due to the addition of the fins.

To try and explain these results the two PVT collectors were examined. It was observed that the contact between the PV panel and the absorber on the F-PVT was better than that of the NF-PVT. This was then further verified with thermal images of the two PVTs. As can be seen in Figure 28, the NF-PVT on the left has a hot spot in the upper part of the PV panel. This means that in this area, the channels of the absorber are not in contact with the PV panel creating an air gap. This air can serve to decrease the thermal contact between the PV panel and the absorber, decreasing the zero-loss efficiency, and also expose more of the absorber surface area to ambient air, increasing a_1 . The F-PVT, on the right of Figure 28, also has a hot spot, but it is not as hot as that of the NF-PVT, meaning that there is less of a gap between the absorber and the PV panel leading to better thermal contact.

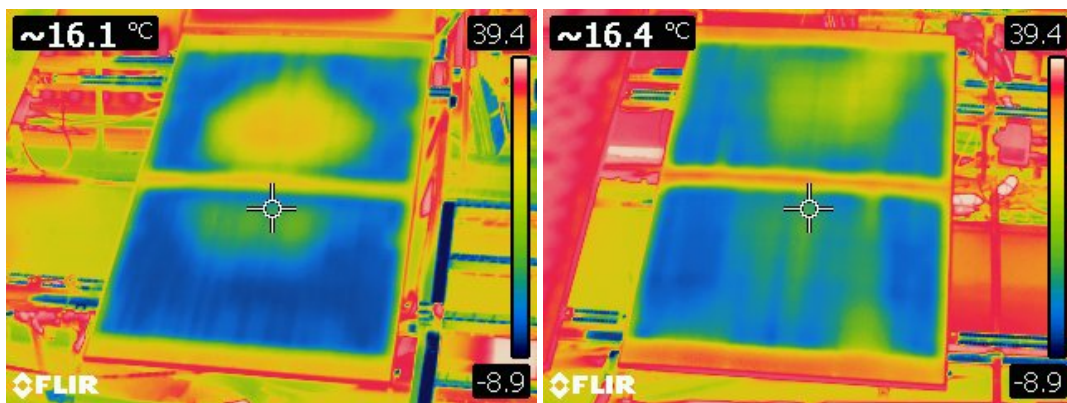


Figure 28: Left) Thermal image of the NF-PVT. Right) Thermal Image of the F-PVT.

The thermal images in Figure 28 also show that when there is good thermal contact between the absorber and the PV panel, the absorber is effective at extracting heat from the PV. This is seen by the predominantly blue colour of the PV panel. The yellow/red horizontal line in the middle of the PV panels indicates the location where

the absorber is purposefully not in contact with the panel to allow for space of the electrical equipment of the PV panel, and the colour shows that here the PV panel is not being cooled.

5.2 Different Operating Conditions

As was expected, ambient conditions have an impact on the thermal performance of the PVT. For all the tested scenarios on both PVTs, an increase in both irradiance and wind speed resulted in an increased specific thermal power output.

5.2.1 Changing Flow Rates

Figure 29 shows how an increase in irradiance affected the different tested flow rates for both the NF-PVT. At zero-irradiance the medium flow rate performs thermally the worst out of all the tested flow rates. It was expected that as flow rate increases, so does the thermal performance of the PVT up to a certain high flow rate. This was because as flow rate increases the rate at which heat can be absorbed from the ambient increases. The reason that the low flow rate appears to perform better might be due to the different average conditions of the data sets used to calculate the coefficients. For the low flow rate the average irradiance of the data set is significantly higher than that of the medium and low flow rate. This will result in an artificially high zero-loss efficiency as the regression is skewed towards describing the behaviour of the PVT at the predominant ambient conditions. Higher irradiances result in higher zero-loss

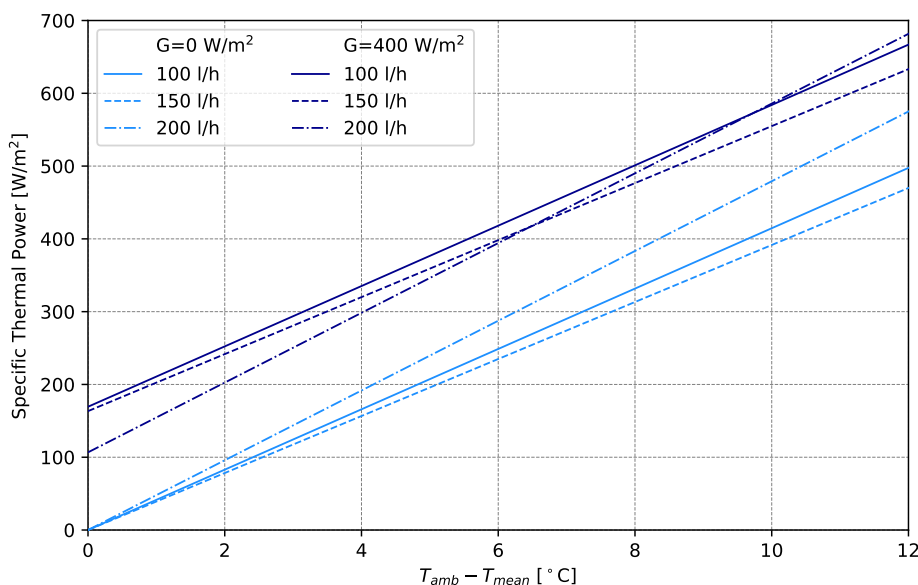


Figure 29: The regression lines of the NF-PVT at the three tested flow rates, comparing the impact of changing irradiance.

efficiencies as there is more heat available to be extracted from the PV panel. This means that the regression will give artificially higher specific thermal power outputs for the low flow rate. However, despite this discrepancy in the ambient conditions, the high flow rate performed thermally better than both the lower flow rates.

At an irradiance level of 400 W/m^2 , the lowest flow rate appears to perform better than both the higher flow rates until a high temperature difference between the ambient and mean fluid temperature. However, it is believed that this result is not comparable to the other two due to the differing ambient conditions of the data sets. When comparing the medium and high flow rate, it can be seen that the medium flow rate thermally outperforms the high flow rate at lower temperature differences, while the opposite is true for high temperature differences. This could be because at low temperature differences, the higher zero-loss efficiency of the medium flow rate dominates the regression while at higher temperature differences the higher a_1 of the high flow rate dominates.

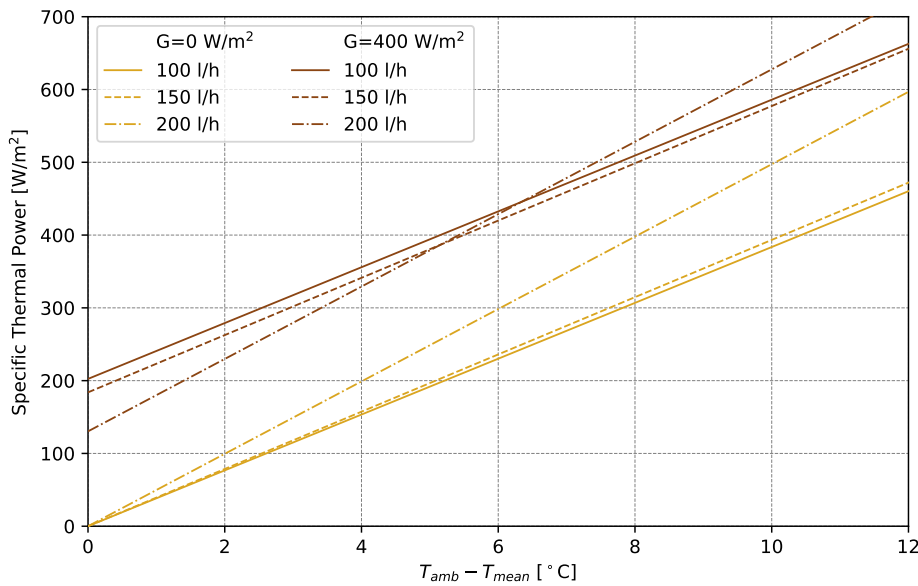


Figure 30: The regression lines of the F-PVT at the three tested flow rates, comparing the impact of changing irradiance level.

In Figure 30, the comparison of the different flow rates for the F-PVT can be seen. As expected at zero-irradiance, the higher the flow rate, the higher the specific thermal power output of the regression. This difference to the NF-PVT could be the result of the of the slightly higher a_3 of the F-PVT at the medium flow rate, while the other coefficients are comparable to the low flow rate because of the differing ambient conditions. Similarly to the NF-PVT, the high flow rate thermally outperforms the two lower flow rates. At an irradiance level of 400 W/m^2 , the same trend as for the NF-PVT, of the lower flow rates displaying higher specific thermal power output at low temperature differences is observed. However, unlike the NF-PVT, the temperature

difference at which the higher flow rates result in higher specific thermal powers is lower for the F-PVT than the NF-PVT.

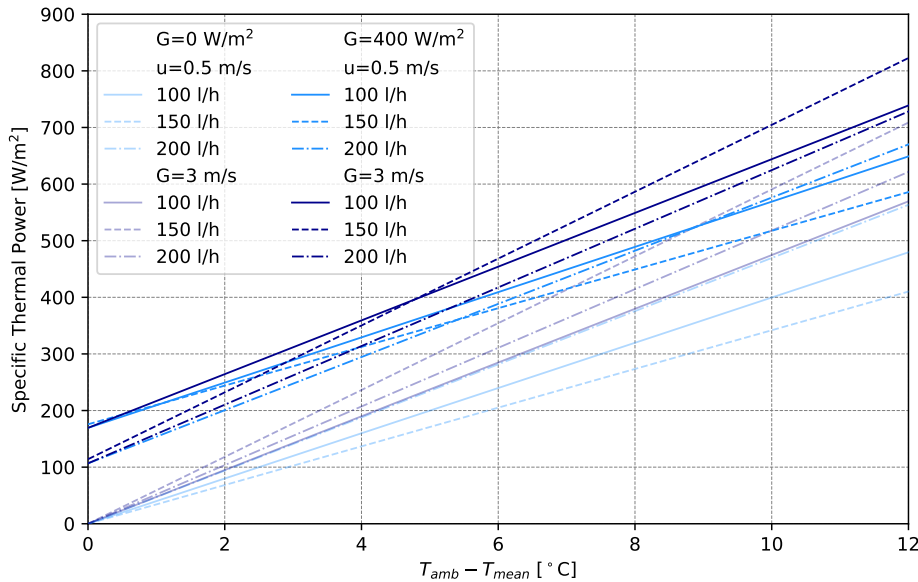


Figure 31: The regression lines of the NF-PVT at the three tested flow rates, comparing the impact of changing wind speed.

When comparing the impact of changing wind speeds, in Figure 31 it can be seen that at zero-irradiance the impact of increasing the wind speed from 0.5 m/s to 3 m/s resulted in the largest increase for the medium flow rate. The smallest increase was experienced at the highest flow rate. This shows that as you increase the flow rate, the impact of the wind speed on the specific thermal output decreases. This is because at a higher flow rate, the heat is already being taken away by the brine at a higher rate, so the effect of the wind replacing the colder air is not as important. In line with the first observation, the medium flow rate performs the worst at the lowest wind speed, while it outperforms both the other flow rates at higher wind speeds. At low wind speeds, the high flow rate performs the best while at high wind speeds, the low flow rate has the lowest specific thermal energy.

At an irradiance level of 400 W/m², the same trend can be seen of higher flow rates being less affected by increasing wind speeds. Furthermore, the positive impact of the higher wind speeds is smaller for each given flow rate compared to the impact at zero-irradiance. For the non-zero irradiance level and the low wind speed, at low temperature differences the high flow rate has the lowest specific thermal power output while the two lower flow rates perform equally. However at high temperature differences, the medium flow rate performs the worst. At a high wind speed however, the medium flow rate performs the best at the high temperature differences while the high flow rate still has the lowest specific thermal power output at low temperature differences. The same trends were observed for the F-PVT, see Figure C17 in Appendix C.

As seen above, different ambient conditions impact the NF-PVT and F-PVT slightly differently at the different flow rates. To compare the overall performance of the two PVTs at the different flow rates, Table 20 compares the annual thermal energy output of the different flow rates to the low flow rate of the respective PVT. The last column in the Table then compares the annual thermal energy output of the F-PVT to that of the NF-PVT for that flow rate. This result has already been presented but now a comparison can be made of the impact of fins on the annual thermal energy output at the different flow rates.

Table 20: The first two columns present a comparison of the annual thermal energy output of the NF-PVT and F-PVT at different flow rates to the low flow rate, respectively. The last column compares the F-PVT to the NF-PVT as the respective flow rate.

Flow rate	NF-PVT	F-PVT	F vs NF
Low	-	-	0.4%
Medium	17%	24%	11%
High	-0.2%	0.9%	16%

Here it is possible to see that the medium flow rate has the largest annual thermal energy output for both PVTs. This shows that over a typical meteorological year in Stockholm the medium flow rate is fast enough to take away the energy absorbed by the brine to enable effective heat transfer, but not fast enough to result in higher wind speeds hindering heat transfer. This conclusion highlights that each system needs to be optimised for its location. For example, a location with lower wind speeds might benefit from higher flow rates, while a location with higher wind speeds might benefit from lower flow rates.

When comparing the two PVTs at each flow rate, it is possible to see that the F-PVT provides more thermal energy annually than the NF-PVT. This is a result of the positive impact of the fins, allowing for increased heat gains at higher wind speeds.

5.2.2 Different Roof Installations

As with the different flow rates, the different roof installations will be compared. In Table 21 the coefficients calculated for both the baseline and the three roof installation types can be seen. The addition of the roof installations served to increase the zero-loss efficiency of the PVTs, while the heat loss coefficient, a_1 , was decreased due to the restriction of the airflow around the absorber. This restriction prevented the replacement of the cold air with warm air for continued heat exchange between the ambient and the brine in the absorber. The wind dependence of the heat loss coefficient, a_3 , increased for the side panel installation compared to the baseline. This is due to the south facing wind channel created by the side panels. The other two roof installations caused a decrease in a_3 compared to the baseline as they created greater shelter from wind for the PVTs. It can be seen that as the value a_1 decreases, the value of a_6 increases. This shows that as the heat exchange between the ambient becomes less dominant in the specific thermal power equation, the wind dependence of the zero-loss efficiency becomes more dominant.

Table 21: Comparison of the baseline coefficients to those of the three different roof installations for both the NF-PVT and the F-PVT.

Coefficients	NF-PVT				F-PVT			
	Baseline	Side	Back	Side & Back	Baseline	Side	Back	Side & Back
η_0	0.423	0.478	0.488	0.507	0.506	0.562	0.554	0.560
a_1	38.460	26.708	29.857	21.899	34.105	21.626	28.197	21.382
a_3	3.001	4.773	2.041	2.786	4.251	6.493	3.224	1.943
a_6	0.000	0.012	0.004	0.015	0.000	0.016	0.014	0.019
R^2	0.94	0.97	0.96	0.97	0.92	0.97	0.96	0.97

Figure 32 shows how a changing irradiance affects the specific thermal power output when different roof installations are considered for the NF-PVT. At zero irradiance, all three roof installations performed worse than the baseline. The discrepancy between the regression lines increased with increasing temperature difference. Out of the three roof installation types, when only the roof was present, the NF-PVT had the highest specific thermal power output while the combination of the roof and side panels had the lowest. This shows that the more restricted the airflow was around the absorber the worse the absorber performed.

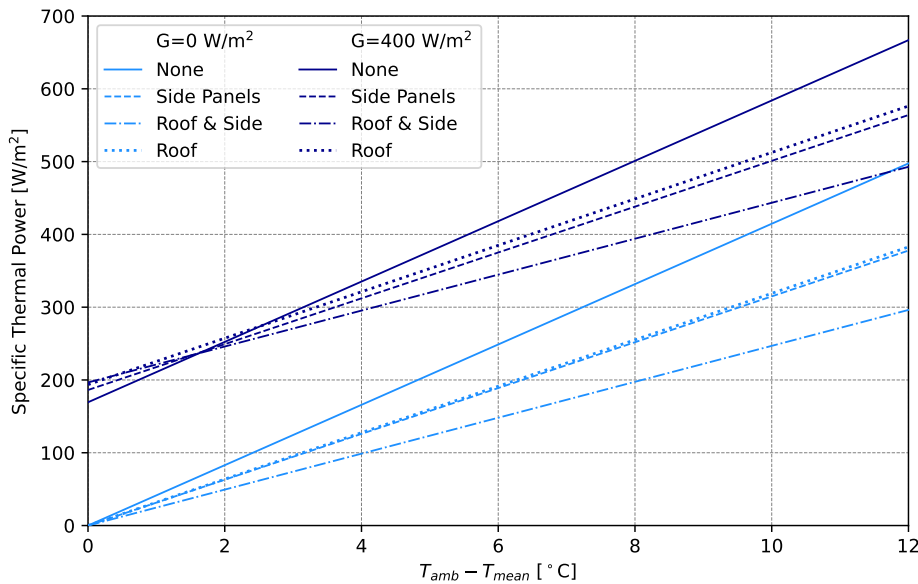


Figure 32: The regression lines of the NF-PVT with the different roof installations, comparing the impact of changing irradiance level.

When irradiance is considered, at very low temperature differences between the ambient and the mean fluid temperature, the roof and side panel configuration had the best thermal performance while the baseline has the worst. However at higher flow rates, this trend reversed to match the observed results of the zero-irradiance case.

Comparing the zero irradiance regression lines to the ones at irradiance, at the same temperature difference the variation between the different roof installations and the baseline was larger for the zero irradiance case. This shows that a non-zero irradiance level leads to an improved performance of the PVT with the roof installations compared to the baseline.

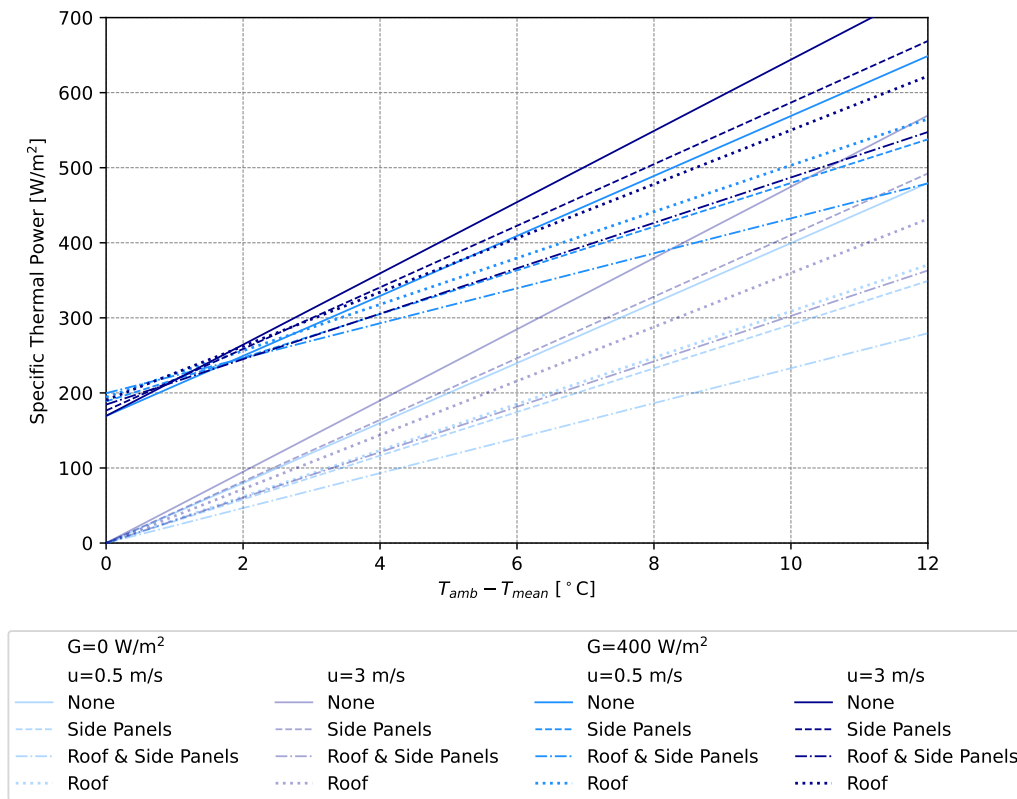


Figure 33: The regression lines of the NF-PVT with the different roof installations, comparing the impact of changing wind speed.

The impact of wind on the NF-PVT with the different roof installations showed similar trends to those observed for the impact of irradiance, see Figure 33. The main difference comes when looking at the impact of increasing wind speed when only the side panels were present. For this roof installation, the increase of wind speed has a much bigger impact on the specific power than for all other roof installations. This is because at the high wind speed, the side panel structure outperforms the back panel structure. This is because when evaluating the different roof installations, the predominant wind direction was south. This means that the wind is blowing directly at the back of the PVT (parallel to the fins in the case of the F-PVT), creating a wind channel behind the absorber. Therefore, at increased wind speeds this configuration has a better airflow behind the NF-PVT than the other roof installations. However, the baseline still thermally outperforms this side panel configuration, even at high wind speeds.

For both the impact of irradiance and wind speed on the roof installations, the F-PVT displayed the same trends as discussed above for the NF-PVT. Figures C18 and C19 in Appendix C show the regression lines for the different roof installations under different irradiance and wind speed conditions.

Table 22: The first two columns present a comparison of the annual thermal energy output of the NF-PVT and F-PVT with different roof installation types to the low flow rate baseline, respectively. The last column compares the F-PVT to the NF-PVT as the respective roof installations.

Roof Type	NF-PVT	F-PVT	F vs NF
Side	-8%	-7%	6%
Roof	-18%	-15%	7%
Side & Back	-26%	-33%	-5%

As with the analysis of the impact of irradiance and wind speed on the different types of roof installation, the annual thermal energy output reflects that any roof installation negatively impacts thermal performance of both PVTs. The worst annual thermal energy output is by the roof installation consisting of both the back and side panels. This is because for this roof installation type the airflow around the PVTs is the most severely restricted.

In all three roof installation types, the F-PVT performed better than the NF-PVT in terms of annual energy output. This suggests that when the PVT is installed on a slanted roof, the addition of fins is beneficial to the PVTs thermal efficiency.

5.3 Finned vs. Non-Finned

As seen in both Tables 20 and 22, in all the cases, except the side and back panel, the F-PVT has a higher annual thermal energy output compared to the NF-PVT. This shows that the fins to improve the thermal efficiency of the PVT, as more heat is being collected. However, the largest improvement the fins provide is 16% and when roof installations are added the improvement drops down to between 6 and 7%. Therefore, it is important to conduct an economical analysis of the two PVT prototypes to ensure that the improvement in thermal performance validates the increase in material and manufacturing cost.

It is also important to note that the fins have a bigger impact on the thermal performance of the PVT depending on the ambient conditions as well as the flow rate used. For example, the fins have a much larger impact at zero irradiance, higher wind speed and higher flow rate. Therefore, it is also important to consider the location of the PVT and under what conditions, both ambient and operational, it will be utilised to decide if the increase in thermal output provided by the fins justifies the increase in cost. For example, in the north of Sweden the increase in thermal output gained by the fins might be sufficient to justify the increased cost, while in the south of Spain this might not be the case.

5.4 Non-Uniform Flow Rate Distribution

In the majority of the non-uniform flow rate scenarios evaluated, the non-uniformity in the flow rate resulted in the losses to the specific thermal power output. In general, the more non-uniform the flow rate, the larger the losses in specific thermal power output. Larger losses also occur at larger irradiance levels.

However, the largest loss measured was just under 2.4 W/m^2 , which was under 1% of the specific power output of the baseline uniform flow rate. Therefore, more scenarios with larger flow rate variations need to be evaluated in order to see if they result in more losses. It would also be beneficial to validate these findings experimentally, as the model use to generate the numerical results showed some discrepancies when compared to the experimentally found regressions of the specific power output.

5.5 Comparability of Results

To obtain the coefficients presented in this study, a simplified version of the ISO 9806:2017 equation for the thermal power output of a solar thermal collector was used. The simplifications have been justified in Section 3, with the majority of them being due to the limitations presented by the testing facilities measuring equipment. Therefore, the results obtained in this study cannot be directly compared to certified databases, such as Solar Keymark.

Additionally to the use of a simplified model for the specific thermal power output, instead of the recommended reduced wind speed, the actual measured wind speed was used. This is because for the majority of the testing period the wind speeds were observed to be less than 3 m/s. Therefore the use of the reduced wind speed would result in both negative and positive wind speeds being used to calculate the regression, causing contradictory effects on the a_3 and a_6 coefficients.

Furthermore, because this study has been conducted in low operating temperatures, the heat loss coefficient is actually measuring gains instead of losses as expected by the ISO standard equation. It is assumed that the heat transfer rate is equal in both directions, however slight differences might result in the inaccurate calculation of the coefficients, introducing uncertainty.

5.6 Uncertainties

As mentioned throughout the Result and Discussion Sections, there were some limitations and sources of uncertainty identified in the experimental testing of the NF-PVT and F-PVT. The nature of outdoor testing of heat exchange means that there can be rapidly changing ambient conditions that do not have time to have an impact the thermal output of the PVT measured. This introduces uncertainty into the results calculated. Through the use of moving averages and data filtering this uncertainty has been minimised but it is still be present to some degree in the results.

Another source of uncertainty comes from the measuring equipment. For example, the flow rate recorded was truncated at two decimal points, meaning that despite

filtering the results for the low flow rate of 0.1 m³/h, flow rates of 0.05 to 0.14 m³/h are included. This change in flow rate will impact the overall calculated power output, as it relies on the flow rate. However, this will happen in normal operation of a PVT collector and so the results are representative. Another limitation with the measuring equipment is that the rain bucket had a sensitivity of 0.2 mm of rain per minute. This meant that light rain was not recorded and so included in the data points despite the desire to not include the impact of rain in the analysis.

A third source of uncertainty came from the location of the PVT collectors in the test rig. This is because the equipment around the two PVTs provided them with different amounts of shelter from the wind, as well as the sun. This means that the weather conditions measured by the weather station might not be the weather conditions experienced by both of the PVTs.

Another identified limitation comes in the form of each data set having different average ambient conditions, as seen in Appendix A. This happened due to the changing weather conditions over the testing period, from March to May, and limited time to conduct the experiments. Having different ambient conditions in the data set results in skewing the calculated coefficients towards those conditions. This means that direct comparisons between data sets may not accurately reflect the true relationship between them. This was especially relevant when calculating the coefficients to study the impact of wind direction.

An additional source of came from the operation of the HP, which was used to supply the cold brine to the PVTs. The intermittent operation of the HP resulted in a fluctuating brine inlet temperature to the PVTs. This happened as when the desired brine inlet temperature was reached the HP shut down and the inlet temperature slowly increased in temperature. After the required stand-by time, around 17 min, the HP would resume operation and cool the inlet brine again. These fluctuations can be seen in Figure 16. The cause of the uncertainty is that these fluctuations in the inlet temperature were often not reflected in the outlet temperature, because of the time dependant nature of heat transfer, again seen in Figure 16. Like with the rapidly changing ambient conditions, moving averages were used to try and minimise the impact of this phenomenon. Furthermore, due to the way the collected heat was dissipated, during periods of high irradiance the PVTs collected more heat that the facility's hot storage tank could store which resulted in the HP turning off for extended periods of time allowing the inlet temperature to warm up significantly. This meant that at high irradiance levels, data points with large temperature differences between ambient temperature and mean brine temperature could not be collected.

The uncertainty in the results was measured through the use of the coefficient of determination of the regression, R². This coefficient provided a value, on a scale of 0 to 1, of how well the regression fit the measured data. The lowest R² measured was 0.81, corresponding to the data set of the north wind direction at a low flow rate for the F-PVT. While larger quantities of data will increase the R², this shows that all the regressions calculated have a good statistical fit and so the results obtained are significant.

6 Conclusions

The aim of this study has been to analyse the thermal performance of a PVT collector under different operating and ambient conditions. These include variable ambient conditions such as irradiance and wind speed. The impact of these was analysed under three flow rates as well as three different roof installation types. Additionally, two PVT collector prototypes were compared to quantify the impact the addition of fins to the absorber has on the thermal performance of the PVT.

In order to fulfil this aim, the two PVT collector prototypes, the NF-PVT and the F-PVT, were evaluated on an outdoor test rig subject to the ambient weather conditions throughout the months of March to May in Stockholm. While this allowed for the collection of data at a range of ambient weather conditions, it also introduced uncertainty into the results because of the mismatch between the rapidly varying ambient weather conditions and slow heat transfer phenomenon. Nevertheless, once a full data set for each operating condition was collected, a multivariable regression was used to calculate the coefficients corresponding to that data set. The coefficients come from the simplified ISO 9806:2017 standard equation for modelled thermal power of solar thermal collectors, Equation 5. These coefficients were used to then calculate the annual thermal energy output, using a typical meteorological year for Stockholm and the monthly average mean fluid temperature following Beltran et. al. (2024) [27]. These calculated outputs formed the key performance indicators used to compare the different data sets and answer the set research questions.

1. How do varying ambient conditions, such as wind and solar irradiance, affect the thermal output of the finned and non-finned designs?

It was found that increasing solar irradiance of 200 W/m^2 resulted in an increase in specific thermal power output for both PVTs, in a range of 80 to 110 W/m^2 depending on the case studied. The same increase in irradiance, resulted in a higher specific thermal power increase for the F-PVT than the NF-PVT due to its higher zero-loss efficiency. Because of this, the F-PVT generally thermally outperformed the NF-PVT. An exception was at zero-irradiance for the low flow rate. This was because the NF-PVT generally displayed a higher heat transfer coefficient, a_1 , due to differences in the manufacturing of the two prototypes.

An increasing wind speed also resulted in an increased specific thermal power output for both PVTs. The increase in the specific thermal power output varied drastically between the difference scenarios evaluated, showing the high sensitivity of heat transfer with the ambient to both ambient and operating conditions. Similarly to the case of increasing irradiance, the same increase in wind speed resulted in a higher power increase for the F-PVT than the NF-PVT. These results support previously published findings.

2. How do varying mass flow rates of the working fluid impact the thermal performance of the finned and non-finned designs?

To quantify the impact of changing flow rates, the annual thermal energy output of the two PVT collectors was compared to the baseline flow rate of 100 l/h. It was found that at a medium flow rate of 150 l/h, both PVTs generated the highest annual thermal energy output, with a 17% and 24% increase over the baseline for the NF-PVT and F-PVT respectively. The high flow rate of 200 l/h was statistically equivalent to the baseline. This shows that there is an optimal flow rate for operation. This result agrees with previously published literature. However, smaller increments in flow rate need to be evaluated to find the true optimum, or in an optimal range of flow rates exists.

It was found that at each flow rate, the F-PVT generated more thermal energy annually than the NF-PVT, with the difference between the two increasing as flow rate increased. This shows that the addition of fins enables larger flow rates through the collector to be used. It also means that the optimum flow rate may not be the same for the two collectors. The use of smaller increments would help determine if both PVTs have the same optimum flow rate.

It should also be noted that the optimal flow rate may change under different ambient conditions, such as average irradiance and wind speed. Therefore, the ambient weather conditions of a location should be evaluated in order to determine the local optimal flow rate.

To further study the impact of a varying mass flow rate, a numerical model of the NF-PVT collector was built in COMSOL Multiphysics and the effect of a non-uniform flow rate through the absorber was studied. It was found that a non-uniform flow rate does decrease the specific thermal power output of the PVT, however the losses observed were all under 1% of the total. A more in-depth study of the non-uniform flow rate distribution is needed to fully quantify the impact of this phenomenon.

3. How does different types of roof installations affect the performance of the finned and non-finned designs?

The overall impact of the different types of roof installations was to decrease the annual thermal energy output of the PVTs compared to the baseline with no roof installation. This was because the roof installations restricted the airflow around the PVTs, reducing the amount of heat exchange with the ambient as expected from existing literature. The addition of a roof presented a larger decrease in energy output than the addition of side panels. The addition of both resulted in a reduction of annual thermal energy of over 25% for both PVTs, with the reduction being larger for the F-PVT than the NF-PVT. This trend was observed for all the roof installations.

After the conclusion of this study, further research topics were identified. To improve the results of this study a longer data collection period could be used. This would result in more data point at different ambient conditions, generating a more representative set of coefficients for thermal performance of the PVT collectors. As mentioned above, to find the true optimum flow rate of the NF-PVT and the F-PVT, a more in-depth study of different flow rates can be conducted. Because this study has focused on only the impacts of irradiance and wind, a more comprehensive study of the impacts of different weather conditions is needed for a fully representative picture of the operation of the PVT. This includes the study of the impacts of condensation, frost

and rain, especially in a location like Stockholm where these phenomena routinely occur during late autumn, winter and early spring.

References

- [1] N. Aste, C. del Pero, and F. Leonforte, “Water flat plate pv–thermal collectors: A review,” *Solar Energy*, vol. 102, pp. 98–115, 2014. [Online]. Available: <https://www.sciencedirect.com/science/article/pii/S0038092X14000437>
- [2] F. Beltran, N. Sommerfeldt, C. Reichl, and H. Mandani, “Techno-economic analysis of photovoltaic/thermal collector designs for intergation with ground source heat hump systems,” 2023, pre-print.
- [3] Intergovernmental Panel on Climate Change (IPCC), *Global Warming of 1.5°C: IPCC Special Report on Impacts of Global Warming of 1.5°C above Pre-industrial Levels in Context of Strengthening Response to Climate Change, Sustainable Development, and Efforts to Eradicate Poverty*. Cambridge University Press, 2022.
- [4] Net Zero Tracker, “Net Zero Tracker: Data Explorer,” Available at <https://zerotracker.net/>. Date Accessed (19 Feb 2024).
- [5] IRENA, *World Energy Transitions Outlook 2023: 1.5°C Pathway*. Abu Dhabi: International Renewable Energy Agency, 2023.
- [6] IEA, “Renewables 2022,” Paris, Tech. Rep., 2022.
- [7] European Commission, Directorate-General for Energy, F. Gerard, T. Smit, K. Rademaekers, S. Braungardt, M. Monejar Montagud, and L. Guevara Opinska, *Policy support for heating and cooling decarbonisation – Roadmap*. Publications Office of the European Union, 2022.
- [8] IEA, “Heating,” Available at <https://www.iea.org/energy-system/buildings/heating>. Date Accessed (20 Feb 2024), 2023.
- [9] European Commission, “COM(2022) 230: RePowerEU Plan,” Brussels, 2022, Available at <https://eur-lex.europa.eu/legal-content/EN/TXT/?uri=COM:2022:230:FIN&qid=1653033742483>.
- [10] M. H. Abbasi, B. Abdullah, M. W. Ahmad, A. Rostami, and J. Cullen, “Heat transition in the european building sector: Overview of the heat decarbonisation practices through heat pump technology,” *Sustainable Energy Technologies and Assessments*, vol. 48, p. 101630, 2021. [Online]. Available: <https://www.sciencedirect.com/science/article/pii/S2213138821006445>
- [11] M. Formolli, T. Kleiven, and G. Lobaccaro, “Assessing solar energy accessibility at high latitudes: A systematic review of urban spatial domains, metrics, and parameters,” *Renewable and Sustainable Energy Reviews*, vol. 177, p. 113231, 2023. [Online]. Available: <https://www.sciencedirect.com/science/article/pii/S1364032123000874>

- [12] N. Sommerfeldt and H. Madani, “A Techno-Economic Comparison between PV and PVT Integrated Ground Source Heat Pumps for Multi-Family Houses,” in *Proceedings of the ISES EuroSun 2018 Conference*, 2018, pp. 901–910. [Online]. Available: [10.18086/eurosun2018.02.19](https://doi.org/10.18086/eurosun2018.02.19)
- [13] A. Herez, H. El Hage, T. Lemenand, M. Ramadan, and M. Khaled, “Review on photovoltaic/thermal hybrid solar collectors: Classifications, applications and new systems,” *Solar Energy*, vol. 207, pp. 1321–1347, 2020. [Online]. Available: <https://www.sciencedirect.com/science/article/pii/S0038092X20307945>
- [14] P. Charalambous, G. Maidment, S. Kalogirou, and K. Yiakoumetti, “Photovoltaic thermal (pv/t) collectors: A review,” *Applied Thermal Engineering*, vol. 27, no. 2, pp. 275–286, 2007. [Online]. Available: <https://www.sciencedirect.com/science/article/pii/S1359431106002316>
- [15] European Council, “Infographic - Fit for 55: making buildings in the EU greener,” Available at <https://www.consilium.europa.eu/en/infographics/fit-for-55-making-buildings-in-the-eu-greener/>. Date Accessed (21 Feb 2024).
- [16] T. Chow, “A review on photovoltaic/thermal hybrid solar technology,” *Applied Energy*, vol. 87, no. 2, pp. 365–379, 2010. [Online]. Available: <https://www.sciencedirect.com/science/article/pii/S0306261909002761>
- [17] S. Diwania, S. Agrawal, A. S. Siddiqui, and S. Singh, “Photovoltaic-thermal (PV/T) technology: a comprehensive review on applications and its advancement,” *International Journal of Energy and Environmental Engineering*, vol. 11, pp. 33–54, 2020, Available: [10.1007/s40095-019-00327-y](https://doi.org/10.1007/s40095-019-00327-y).
- [18] M. Herrando, A. Ramos, I. Zabalza, and C. N. Markides, “A comprehensive assessment of alternative absorber-exchanger designs for hybrid pvt-water collectors,” *Applied Energy*, vol. 235, pp. 1583–1602, 2019. [Online]. Available: <https://www.sciencedirect.com/science/article/pii/S0306261918317318>
- [19] P. Bombarda, G. Di Marcoberardino, A. Lucchini, S. Leva, G. Manzolini, L. Molinaroli, F. Pedranzini, and R. Simonetti, “Thermal and electric performances of roll-bond flat plate applied to conventional pv modules for heat recovery,” *Applied Thermal Engineering*, vol. 105, pp. 304–313, 2016. [Online]. Available: <https://www.sciencedirect.com/science/article/pii/S1359431116308511>
- [20] F. Bava and S. Furbo, “A numerical model for pressure drop and flow distribution in a solar collector with u-connected absorber pipes,” *Solar Energy*, vol. 134, pp. 264–272, 2016. [Online]. Available: <https://www.sciencedirect.com/science/article/pii/S0038092X16301074>
- [21] A. Kazemian, M. Hosseinzadeh, M. Sardarabadi, and M. Passandideh-Fard, “Effect of glass cover and working fluid on the performance of photovoltaic thermal (pvt) system: An experimental study,” *Solar*

- Energy*, vol. 173, pp. 1002–1010, 2018. [Online]. Available: <https://www.sciencedirect.com/science/article/pii/S0038092X18307151>
- [22] I. Guarracino, J. Freeman, A. Ramos, S. A. Kalogirou, N. J. Ekins-Daukes, and C. N. Markides, “Systematic testing of hybrid pv-thermal (pvt) solar collectors in steady-state and dynamic outdoor conditions,” *Applied Energy*, vol. 240, pp. 1014–1030, 2019. [Online]. Available: <https://www.sciencedirect.com/science/article/pii/S0306261918318634>
- [23] T. Chow, G. Pei, K. Fong, Z. Lin, A. Chan, and J. Ji, “Energy and exergy analysis of photovoltaic–thermal collector with and without glass cover,” *Applied Energy*, vol. 86, no. 3, pp. 310–316, 2009. [Online]. Available: <https://www.sciencedirect.com/science/article/pii/S0306261908001220>
- [24] M. Lämmle, T. Kroyer, S. Fortuin, M. Wiese, and M. Hermann, “Development and modelling of highly-efficient pvt collectors with low-emissivity coatings,” *Solar Energy*, vol. 130, pp. 161–173, 2016. [Online]. Available: <https://www.sciencedirect.com/science/article/pii/S0038092X1600102X>
- [25] E. Bertram, J. Glembin, and G. Rockendorf, “Unglazed pvt collectors as additional heat source in heat pump systems with borehole heat exchanger,” *Energy Procedia*, vol. 30, pp. 414–423, 2012, 1st International Conference on Solar Heating and Cooling for Buildings and Industry (SHC 2012). [Online]. Available: <https://www.sciencedirect.com/science/article/pii/S1876610212015652>
- [26] N. Sommerfeldt, F. Beltran, and H. Madani, “Solar PVT for heat pumps: Collector development, systems integration, and market potential ,” in *Proceedings of the BuildSIM-Nordic 2020 Conference*, 2020, pp. 221–228, Available: <https://hdl.handle.net/11250/2684040>.
- [27] F. Beltrán, N. Sommerfeldt, J. Eskola, and H. Madani, “Empirical investigation of solar photovoltaic-thermal collectors for heat pump integration,” *Applied Thermal Engineering*, vol. 248, p. 123175, 2024. [Online]. Available: <https://www.sciencedirect.com/science/article/pii/S1359431124008433>
- [28] F. Giovannetti, C. Lampe, M. Krichner, M. Littwin, S. Asenbeck, and S. Fischer, “Experimental Investigations on Photovoltaic-Thermal Arrays Designed for the Use as Heat Pump Source,” in *ISES Solar World COngress 2019*, 2019, Available: <https://proceedings.ises.org/paper/swc2019/swc2019-0020-Giovannetti.pdf>.
- [29] M. Lämmle and G. Munz, “Performance of heat pump systems with pvt collectors with optimized finned heat exchangers integrated as single heat source,” in *EuroSun 2022 Proceedings*, 2022, Available: [10.18086/eurosun.2022.07.06](https://doi.org/10.18086/eurosun.2022.07.06).
- [30] ISO, “ISO9806: Solar energy - Solar thermal collectors - Test methods,” International Organization for Standardization, Geneva, CH, Standard, 2017.

- [31] S. Abdul-Ganiyu, D. A. Quansah, E. W. Ramde, R. Seidu, and M. S. Adaramola, "Study effect of flow rate on flat-plate water-based photovoltaic-thermal (PVT) system performance by analytical technique," *Journal of Cleaner Production*, vol. 321, p. 128985, 2021. [Online]. Available: <https://www.sciencedirect.com/science/article/pii/S0959652621031760>
- [32] M. Rahou, M. Othman, M. Sohif, and A. Ibrahim, "Performance study of a photovoltaic thermal system with an oscillatory flow design," *Journal of Solar Energy Engineering*, vol. 136, p. 011012, 2013. [Online]. Available: [10.1115/1.4024743](https://doi.org/10.1115/1.4024743)
- [33] J. Eskola, "Experimental Testing of Solar Photovoltaic/Thermal Collectors for Low Temperature Heat Pump Integration," 2023, Master Thesis at KTH Royal Institute of Technology. Available: <https://www.diva-portal.org/smash/record.jsf?pid=diva2%3A1777431&dswid=-6211>.
- [34] B. Chhugani, P. Pärish, M. Kirchner, M. Littwin, C. Lampe, and F. Giovannetti, "Model validation and performance assessment of unglazed photovoltaic-thermal collectors with heat pump systems," in *EuroSun 2020 Proceeding*, 2020, Available: [10.18086/eurosun.2020.05.13](https://doi.org/10.18086/eurosun.2020.05.13).
- [35] National Geographic Society, "Condensation," Available at <https://education.nationalgeographic.org/resource/condensation/>. Date Accessed (12 Mar 2024).
- [36] E. Bertram, J. Scheuren, J. Glembin, and G. Rockendorf, "Condensation heat gains on unglazed solar collectors in heat pump systems," in *EuroSun 2010 Proceedings*, 2010, Available: [10.18086/eurosun.2010.07.02](https://doi.org/10.18086/eurosun.2010.07.02).
- [37] M. Bunea, B. Perers, S. Eicher, C. Hildbrand, J. Bony, and S. Citherlet, "Mathematical modelling of unglazed solar collectors under extreme operating conditions," *Solar Energy*, vol. 118, pp. 547–561, 2015. [Online]. Available: <https://www.sciencedirect.com/science/article/pii/S0038092X15003205>
- [38] C. Schmidt, A. Schäfer, and K. Kramer, "Single Source "Solar Thermal" Heat Pump for Residential Heat Supply: Performance with an Array of Unglazed PVT Collectors," in *EuroSun 2018 Proceedings*, 2018. [Online]. Available: <https://proceedings.ises.org/paper/eurosun2018/eurosun2018-0015-Schmidt.pdf>
- [39] N. Sommerfeldt and H. Madani, "In-depth techno-economic analysis of pv/thermal plus ground source heat pump systems for multi-family houses in a heating dominated climate," *Solar Energy*, vol. 190, pp. 44–62, 2019. [Online]. Available: <https://www.sciencedirect.com/science/article/pii/S0038092X19307510>
- [40] B. Chhugani, M. Kirchner, M. Littwin, C. Lampe, F. Giovannetti, and P. Pärish, "Investigation of Photovoltaic-Thermal (PVT) collector for direct coupling with heat pumps: Hardware in the Loop (HIL) and TRNSYS simulations," in *BauSIM 2020*, 2020, pp. 121–128. [Online]. Available: <https://www.researchgate.net/p>

ublication/347033349_INVESTIGATION_OF_PHOTOVOLTAIC-THERMAL_PVT_COLLECTOR_FOR_DIRECT_COUPLING_WITH_HEAT_PUMPS_HARDWARE_IN_THE_LOOP_HIL_AND_TRNSYS_SIMULATIONS

- [41] J. Remund, S. Müller, M. Schmutz, and P. Graf, “Meteonorm Version 8,” 2020, https://meteonorm.com/assets/publications/5BV.3.8_pvsec_2020_mn8.pdf.
- [42] C. Cristofari, G. Notton, and J. L. Canaletti, “Thermal behavior of a copolymer pv/th solar system in low flow rate conditions,” *Solar Energy*, vol. 83, no. 8, pp. 1123–1138, 2009. [Online]. Available: <https://www.sciencedirect.com/science/article/pii/S0038092X09000103>
- [43] E. Sakellariou and P. Axaopoulos, “An experimentally validated, transient model for sheet and tube pvt collector,” *Solar Energy*, vol. 174, pp. 709–718, 2018. [Online]. Available: <https://www.sciencedirect.com/science/article/pii/S0038092X18309538>
- [44] T. Chow, “Performance analysis of photovoltaic-thermal collector by explicit dynamic model,” *Solar Energy*, vol. 75, no. 2, pp. 143–152, 2003. [Online]. Available: <https://www.sciencedirect.com/science/article/pii/S0038092X03002512>

Appendices

A Ambient conditions

In this appendix you can find the ambient conditions for all the different data sets. The heading "All" in the Tables below refers to the data collected for each data set after the basic filtering algorithms have been used.

Table A1: Average ambient and operational conditions for the low flow rate data sets.

Condition	Unit	All	North	East	South	West
G	W/m ²	304	193	355	403	128
u	m/s	1.69	1.43	1.58	1.93	1.52
T_{amb}	°C	10.58	7.75	14.09	11.99	5.64
T_{in}	°C	4.70	2.70	7.49	5.34	1.63

Table A2: Average ambient and operational conditions for side panel data sets.

Condition	Unit	All	Time restricted	East	South	West
G	W/m ²	319	426	416	420	757
u	m/s	1.26	1.25	0.86	1.51	1.73
T_{amb}	°C	13.03	13.09	11.70	13.44	19.10
T_{in}	°C	6.69	6.74	5.44	7.01	10.56

Table A3: Average ambient and operational conditions for roof data sets.

Condition	Unit	All	Time restricted	East	South	West
G	W/m ²	366	512	567	585	387
u	m/s	1.32	1.32	1.06	1.39	1.41
T_{amb}	°C	18.59	18.61	16.51	19.60	18.57
T_{in}	°C	10.88	10.84	7.35	11.50	12.08

Table A4: Average ambient and operational conditions for roof and side panels data sets.

Condition	Unit	All	Time restricted	East	South	West
G	W/m ²	353	464	818	434	168
u	m/s	1.29	1.18	0.98	1.31	1.00
T_{amb}	°C	14.17	14.03	13.10	14.39	13.82
T_{in}	°C	7.59	7.35	3.42	8.03	9.60

Table A5: Average ambient and operational conditions for the medium flow rate data sets.

Condition	Unit	All	North	East	South	West
G	W/m ²	104	141	120	88	50
u	m/s	1.20	1.11	1.15	1.28	0.84
T_{amb}	°C	4.55	6.05	4.06	3.74	5.93
T_{in}	°C	1.03	1.66	0.60	0.63	2.70

Table A6: Average ambient and operational conditions for the high flow rate data sets.

Condition	Unit	All	North	East	South	West
G	W/m ²	152	148	162	159	124
u	m/s	1.72	1.79	1.15	1.33	2.83
T_{amb}	°C	3.49	3.30	1.95	2.87	6.77
T_{in}	°C	-0.07	-0.31	-1.41	-0.33	2.77

B Coefficients

In this appendix you will find all of the regression coefficients calculated, that have not been shown in the main body of the report.

Table B1: Wind dependence coefficients of the NF-PVT and F-PVT with a low flow rate.

Wind Direction	NF-PVT					F-PVT				
	η_0	a_1	a_3	a_6	R^2	η_0	a_1	a_3	a_6	R^2
North	0.290	48.097	0.011	0.022	0.84	0.369	44.143	2.564	0.049	0.81
East	0.511	27.825	3.669	0.000	0.95	0.633	20.233	4.855	0.007	0.94
South	0.494	30.062	3.061	0.004	0.95	0.594	23.999	4.096	0.007	0.94
West	0.273	47.752	0.321	0.000	0.85	0.306	45.470	2.061	0.000	0.82

Table B2: KPIs of the NF-PVT and F-PVT with a low flow rate and side panels for all the data point collected.

KPI	NF-PVT	F-PVT
η_0	0.502	0.589
a_1	20.340	13.758
a_3	9.688	12.224
a_6	0.034	0.039
R^2	0.95	0.94

Table B3: Wind dependence coefficients of the NF-PVT and F-PVT with side panels.

Wind Direction	NF-PVT					F-PVT				
	η_0	a_1	a_3	a_6	R^2	η_0	a_1	a_3	a_6	R^2
East	0.501	25.097	3.815	0.000	0.97	0.603	18.241	4.769	0.000	0.97
South	0.467	28.373	2.979	0.000	0.98	0.543	25.097	4.114	0.000	0.98
West	0.515	20.778	14.690	0.097	0.81	0.558	22.587	14.785	0.107	0.83

Table B4: KPIs of the NF-PVT and F-PVT with a low flow rate and a roof for all the data point collected.

KPI	NF-PVT	F-PVT
η_0	0.558	0.644
a_1	18.884	13.561
a_3	9.195	11.197
a_6	0.039	0.053
R^2	0.94	0.93

Table B5: Wind dependence coefficients of the NF-PVT and F-PVT with a roof.

Wind Direction	NF-PVT					F-PVT				
	η_0	a_1	a_3	a_6	R^2	η_0	a_1	a_3	a_6	R^2
East	0.514	27.919	4.441	0.000	0.93	0.629	21.687	4.194	0.000	0.93
South	0.480	30.418	1.733	0.000	0.97	0.535	29.322	2.355	0.002	0.96
West	0.460	25.710	3.213	0.000	0.98	0.486	25.545	3.676	0.001	0.98

Table B6: KPIs of the NF-PVT and F-PVT with a low flow rate, roof and side panels for all the data point collected.

KPI	NF-PVT	F-PVT
η_0	0.532	0.598
a_1	15.040	11.170
a_3	8.735	8.672
a_6	0.034	0.040
R^2	0.94	0.94

Table B7: Wind dependence coefficients of the NF-PVT and F-PVT with a roof and side panels.

Wind Direction	NF-PVT					F-PVT				
	η_0	a_1	a_3	a_6	R^2	η_0	a_1	a_3	a_6	R^2
East	0.600	7.273	10.490	0.061	0.96	0.658	5.554	7.402	0.054	0.95
South	0.487	23.860	2.165	0.006	0.96	0.537	23.926	1.446	0.010	0.96
West	0.482	24.527	0.000	0.017	0.99	0.533	23.926	0.000	0.025	0.98

Table B8: Wind dependence coefficients of the NF-PVT and F-PVT with a medium flow rate.

Wind Direction	NF-PVT					F-PVT				
	η_0	a_1	a_3	a_6	R^2	η_0	a_1	a_3	a_6	R^2
North	0.395	39.689	6.006	0.102	0.85	0.449	38.911	6.036	0.109	0.85
East	0.428	33.984	8.885	0.054	0.90	0.526	28.402	11.931	0.069	0.90
South	0.504	25.080	12.884	0.080	0.91	0.579	21.829	17.273	0.098	0.91
West	0.703	28.604	2.343	0.171	0.94	0.689	30.379	2.694	0.148	0.94

Table B9: Wind dependence coefficients of the NF-PVT and F-PVT with a high flow rate.

Wind Direction	NF-PVT					F-PVT				
	η_0	a_1	a_3	a_6	R^2	η_0	a_1	a_3	a_6	R^2
North	0.350	40.967	2.688	0.000	0.87	0.298	44.475	4.486	0.000	0.85
East	0.367	37.887	6.879	0.014	0.86	0.368	40.348	8.209	0.020	0.86
South	0.359	40.880	4.925	0.000	0.88	0.379	41.571	7.279	0.000	0.88
West	0.331	47.119	1.342	0.000	0.87	0.249	54.596	2.365	0.000	0.86

C Graphs

In this appendix you will find all the graphs that are referred to in the report by have not been shown in the main body to ease readability.

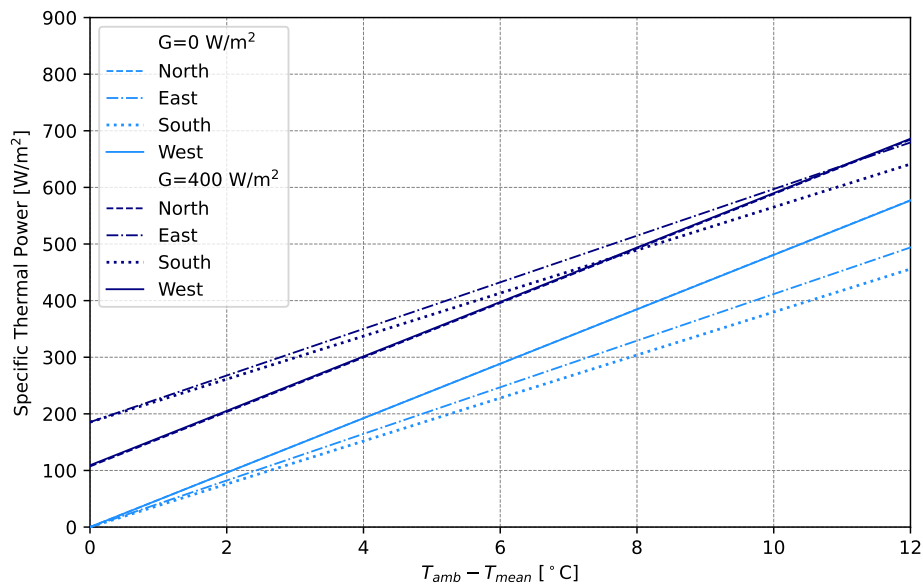


Figure C1: Regression lines for different wind directions at two different irradiance values for the NF-PVT, at a low flow rate.

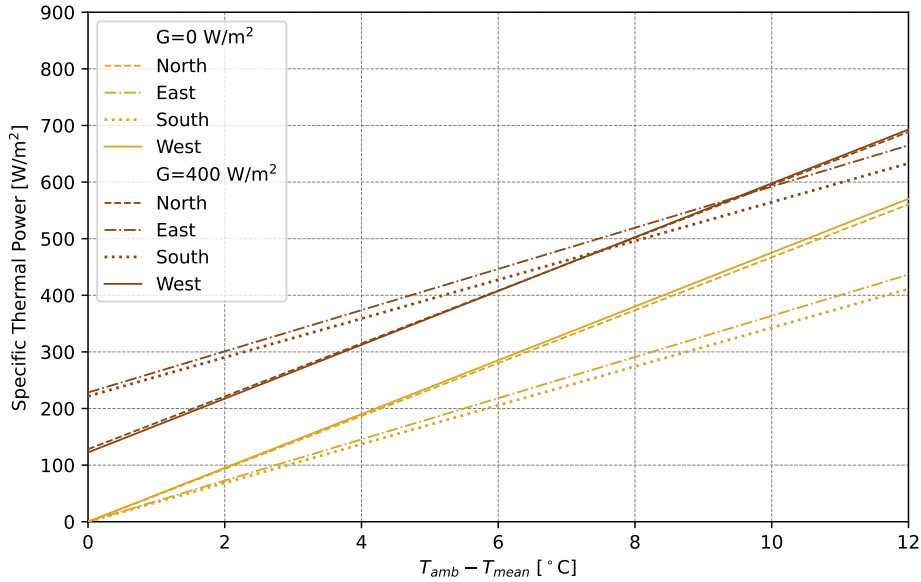


Figure C2: Regression lines for different wind directions at two different irradiance values for the F-PVT, at a low flow rate.

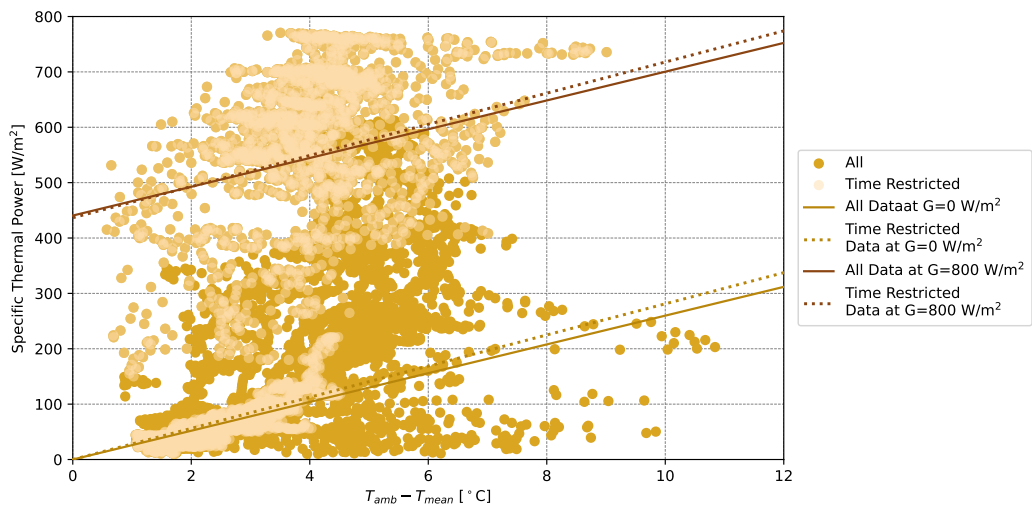


Figure C3: Impact of filtering on the side panels data set for the F-PVT. The coefficients for the regression lines can be found in Tables 10 and B2, for the time restricted and overall regression lines.

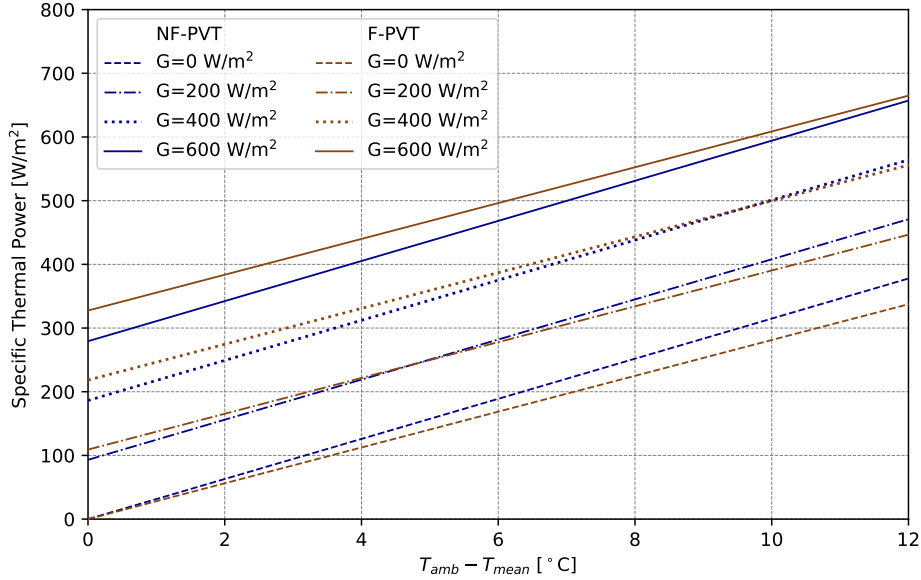


Figure C4: Regressions lines for both the NF-PVT and the F-PVT at different irradiance levels, considering the case when the side panels were attached. The coefficients used for the regressions can be found in Table 10.

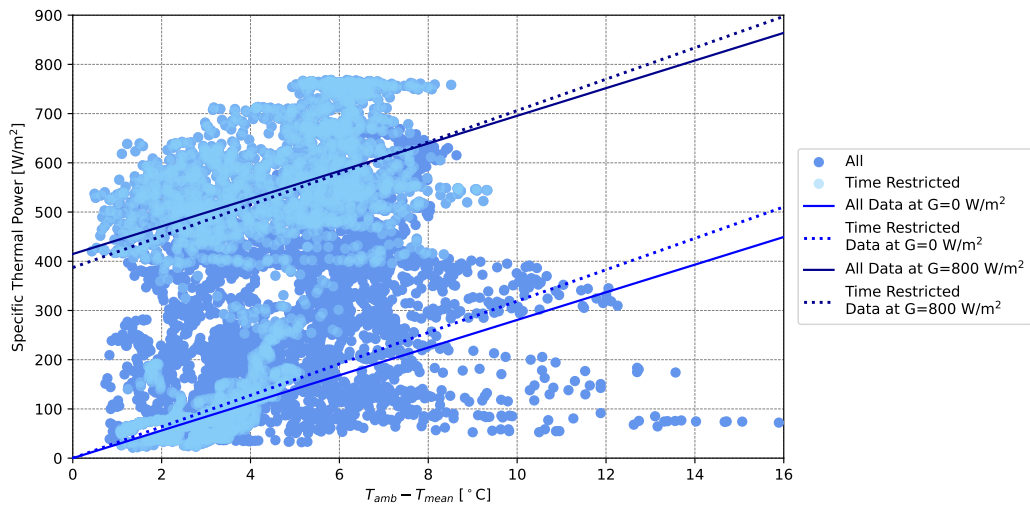


Figure C5: Impact of filtering on the roof data set for the NF-PVT. The coefficients for the regression lines can be found in Tables 12 and B4, for the time restricted and overall regression lines.

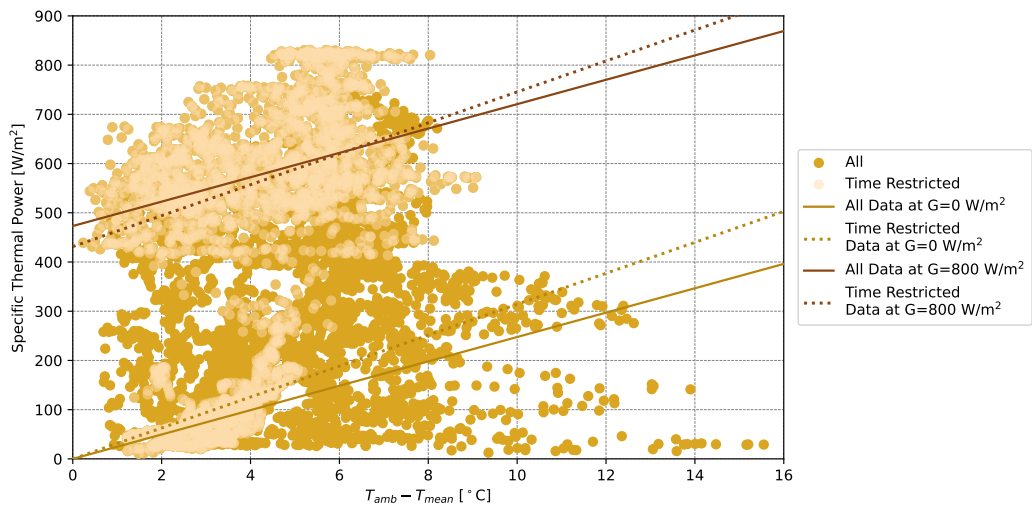


Figure C6: Impact of filtering on the roof data set for the F-PVT. The coefficients for the regression lines can be found in Tables 12 and B4, for the time restricted and overall regression lines.

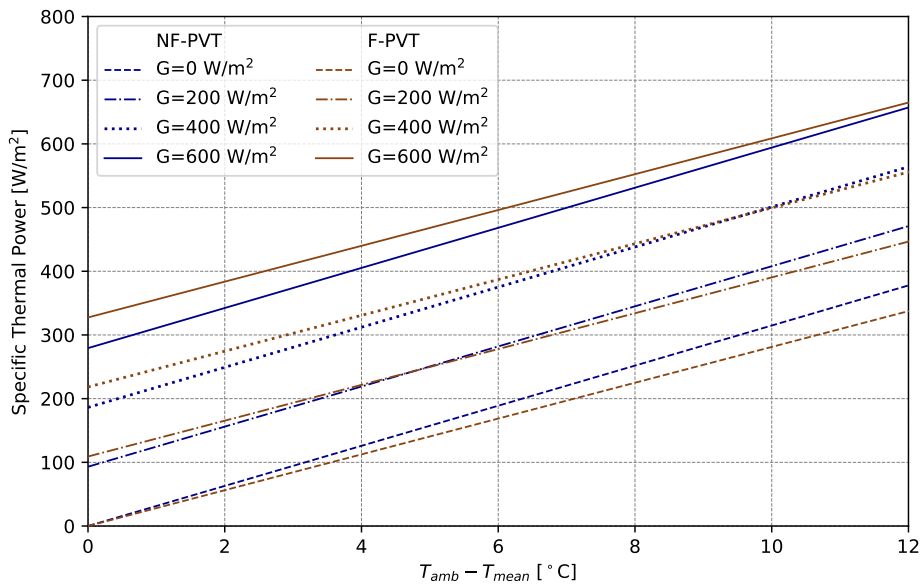


Figure C7: Regressions lines for both the NF-PVT and the F-PVT at different irradiance levels, considering the case when the roof was attached. The coefficients used for the regressions can be found in Table 12.

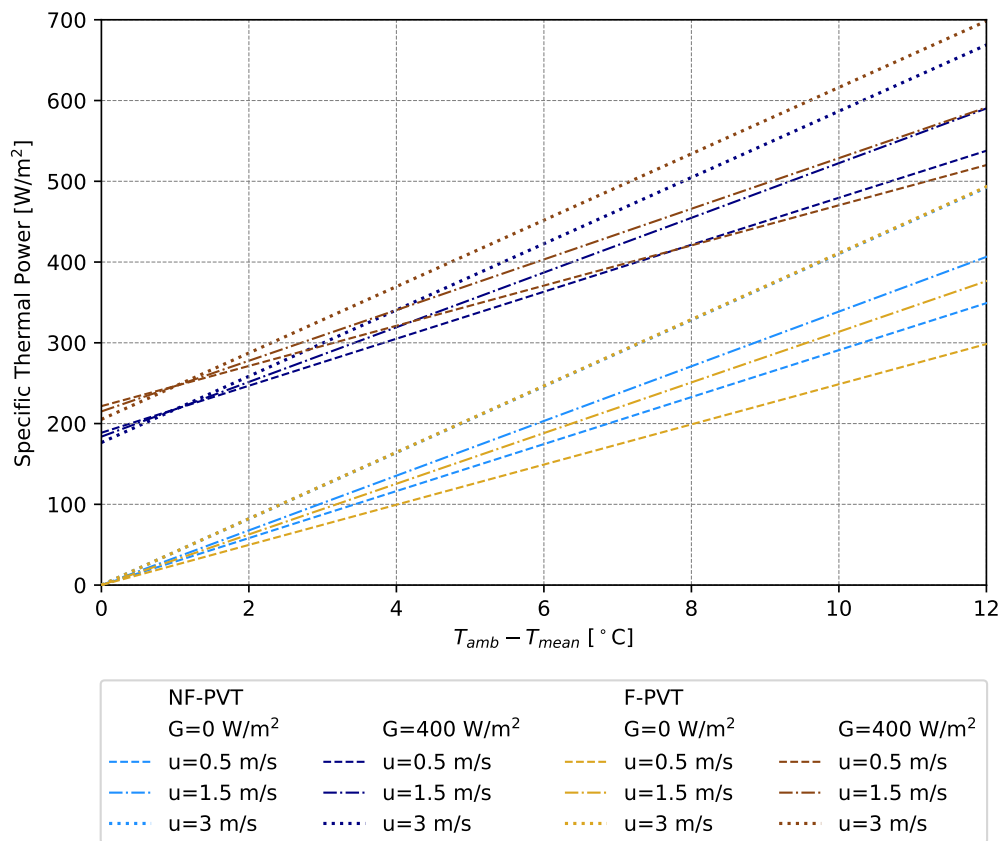


Figure C8: The regression lines for both the NF-PVT and the F-PVT at two different irradiance levels, comparing the impact of wind speed when the roof was attached. The coefficients used for the regression lines can be found in Table 12.

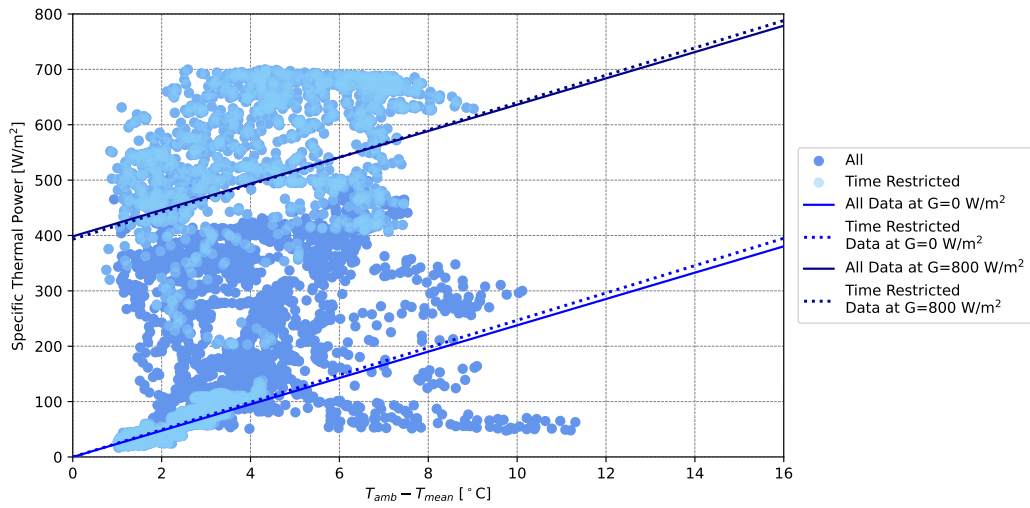


Figure C9: Impact of filtering on the data set with the roof and side panels present for the NF-PVT. The coefficients for the regression lines can be found in Tables 14 and B6, for the time restricted and overall regression lines.

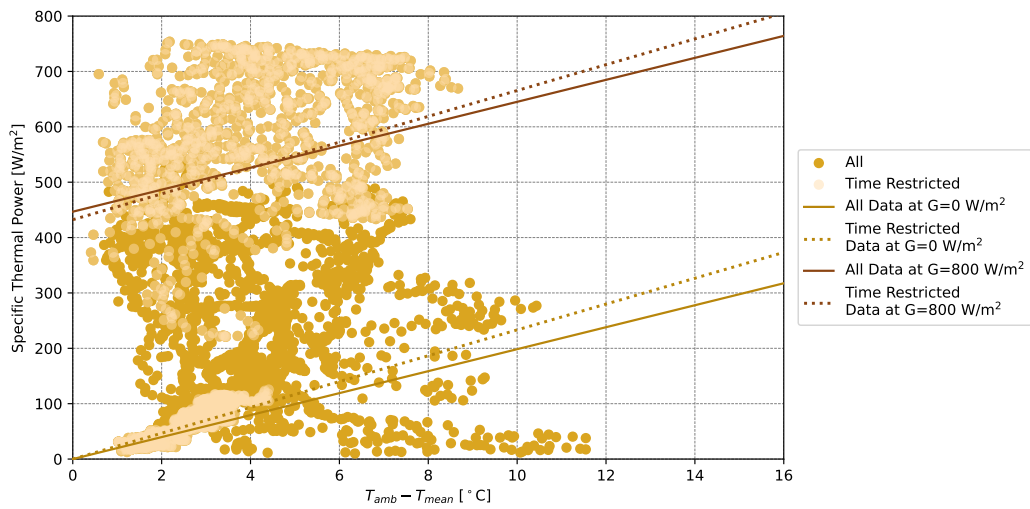


Figure C10: Impact of filtering on the data set with the roof and side panels present for the F-PVT. The coefficients for the regression lines can be found in Tables 14 and B6, for the time restricted and overall regression lines.

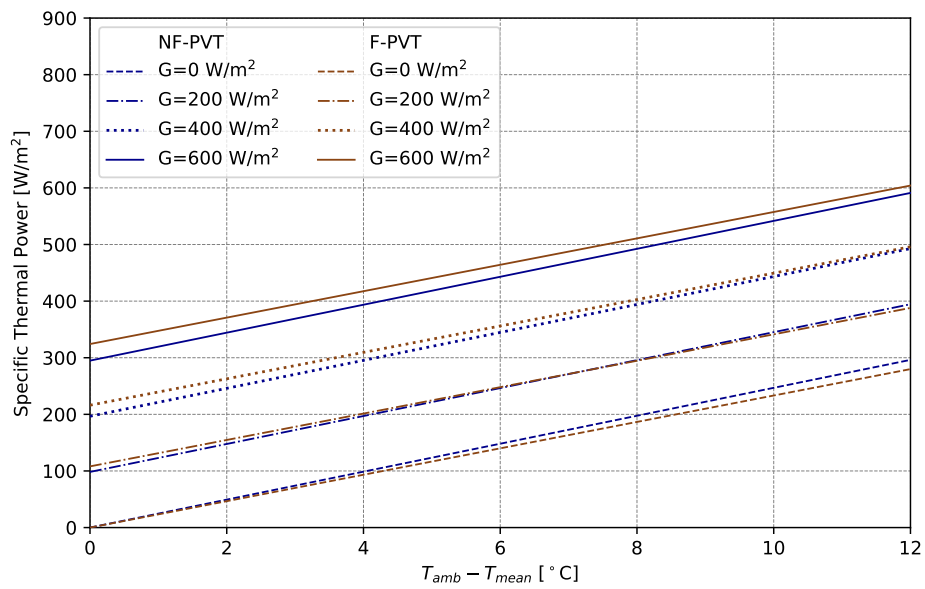


Figure C11: Regressions lines for both the NF-PVT and the F-PVT at different irradiance levels, considering the case when both the side panels and the roof were attached. The coefficients used for the regressions can be found in Table 14.

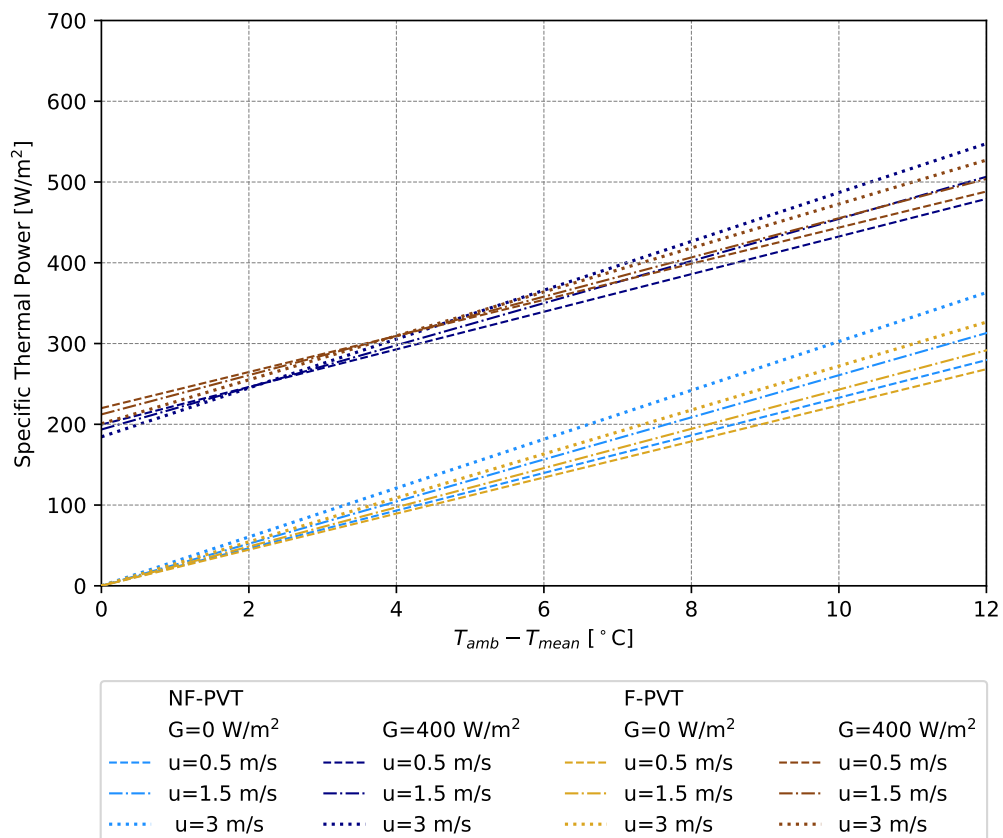


Figure C12: The regression lines for both the NF-PVT and the F-PVT at two different irradiance levels, comparing the impact of wind speed when both the side panels and the roof were attached. The coefficients used for the regression lines can be found in Table 14.

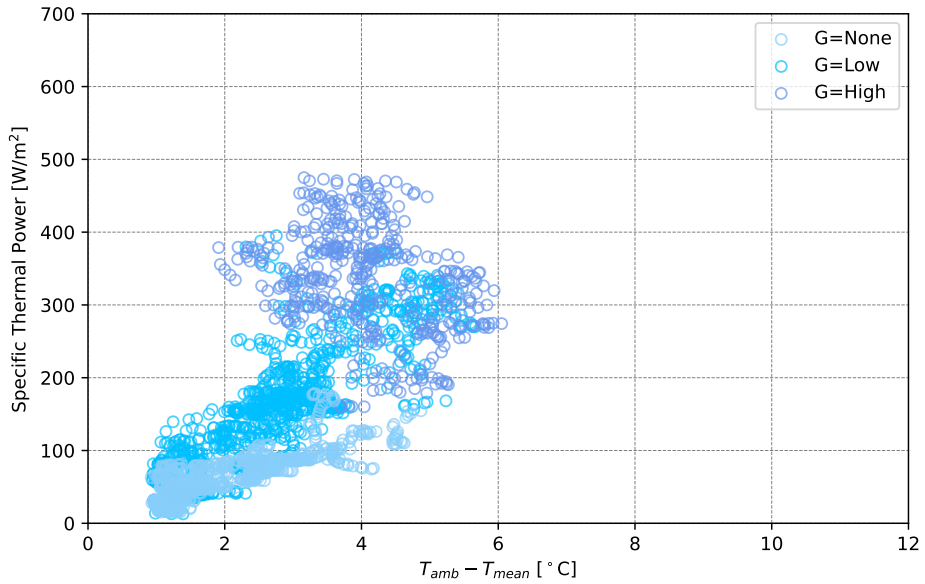


Figure C13: The data collected for NF-PVT at the medium flow rate, colour coded to the irradiance level which they represent.

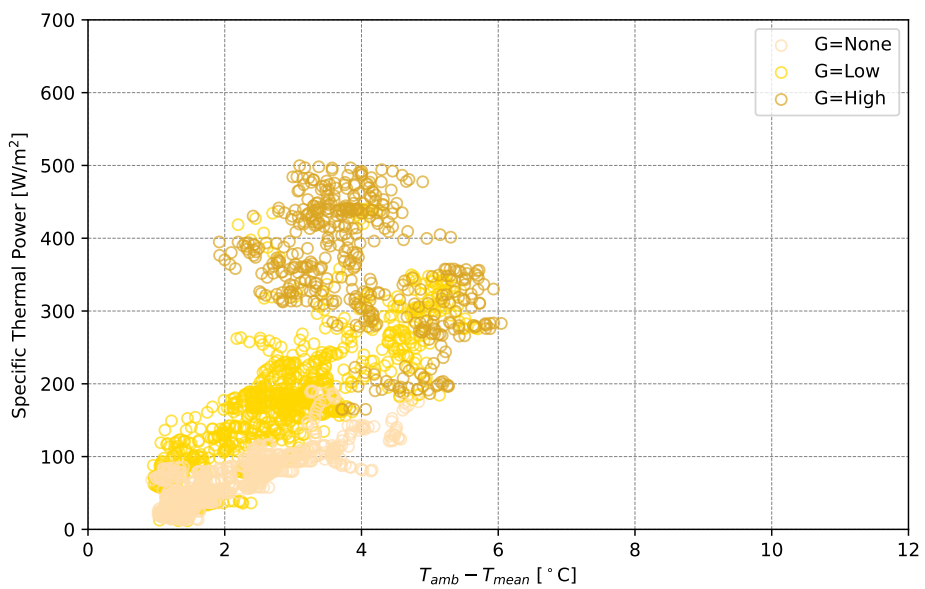


Figure C14: The data collected for F-PVT at the medium flow rate, colour coded to the irradiance level which they represent.

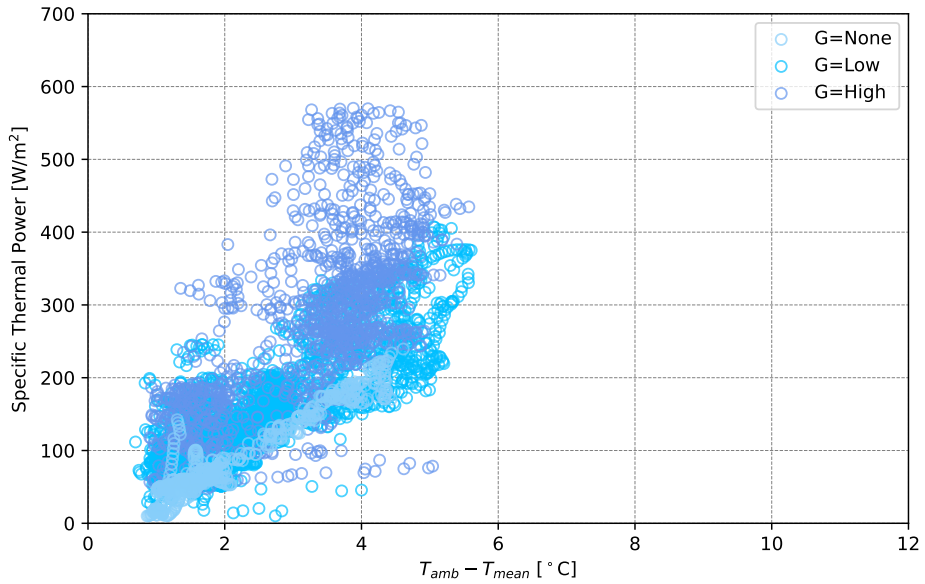


Figure C15: The data collected for NF-PVT at the high flow rate, colour coded to the irradiance level which they represent.

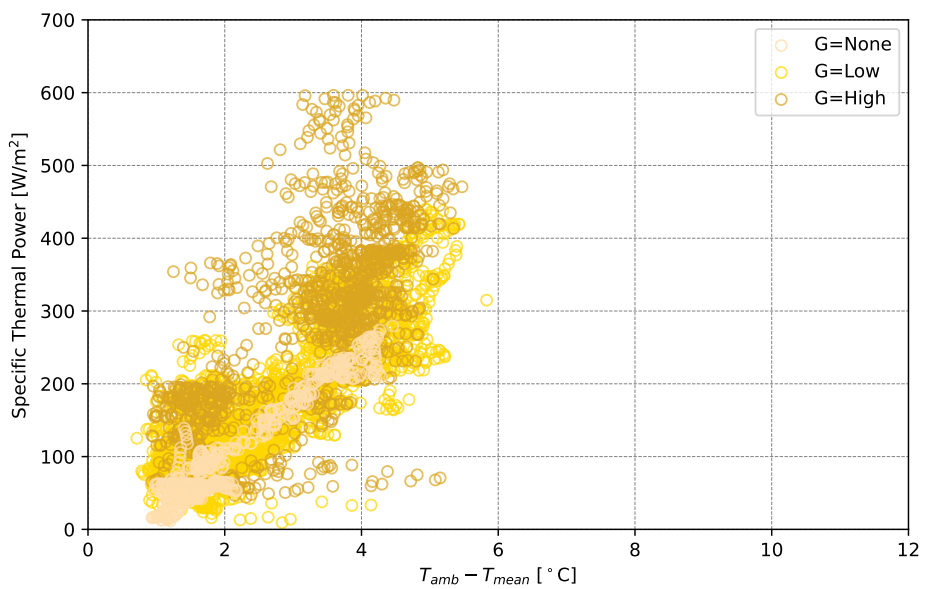


Figure C16: The data collected for F-PVT at the high flow rate, colour coded to the irradiance level which they represent.

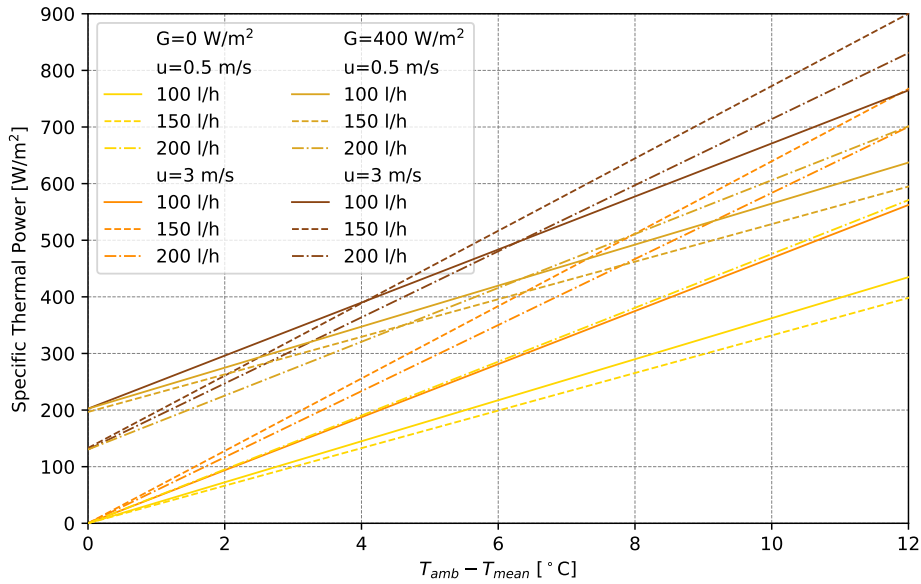


Figure C17: The regression lines of the F-PVT at the three tested flow rates, comparing the impact of changing wind speed.

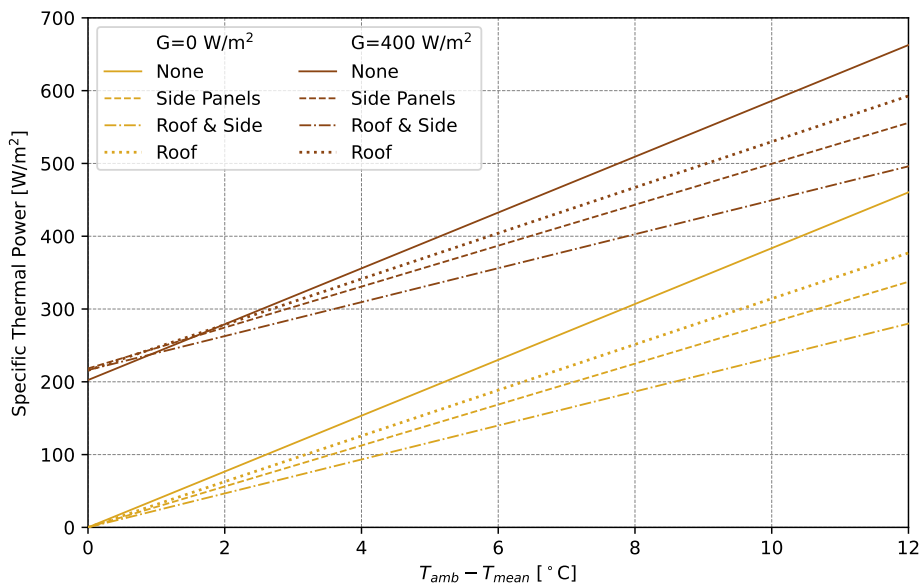


Figure C18: The regression lines of the F-PVT with the different roof installations, comparing the impact of changing irradiance level.

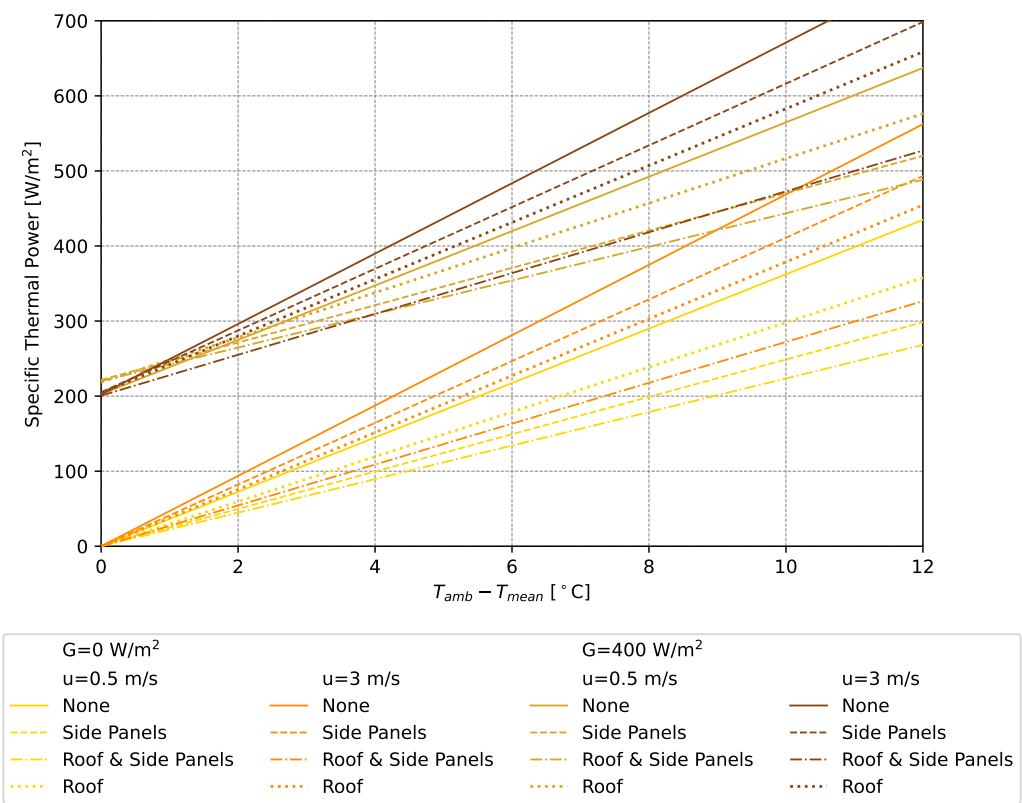


Figure C19: The regression lines of the F-PVT with the different roof installations, comparing the impact of changing wind speed.